

50-250 MHz Pulsar Census with an SKA-Low prototype station: Spectra and Polarization

PRATIK KUMAR,¹ MARCIN SOKOLOWSKI,¹ AND RANDALL WAYTH^{2,1}

¹*International Centre for Radio Astronomy Research, Curtin University, Bentley, WA 6102, Australia*

²*SKAO, Science Operations Centre, CSIRO ARRC, 26 Dick Perry Avenue, Kensington WA 6151, Australia*

ABSTRACT

Low-frequency pulsar observations are crucial for understanding pulsar emission spectra and population physics, as well as for probing the interstellar medium (ISM) and Earth's ionosphere. We report the largest low-frequency pulsar census conducted in the southern hemisphere, covering 50–250 MHz, using the EDA2, an SKA-Low prototype station. In this survey, we detected 120 pulsars, including 23 first-time detections below 150 MHz and 5 below 100 MHz. For each source, we provide integrated pulse profiles and flux-density measurements across five sub-bands spanning 50–250 MHz. We also obtained improved dispersion measure (DM) values for 110 pulsars, with a median absolute DM correction of about 0.1 pc cm^{-3} . We measured significant Faraday rotation for 40 pulsars with improved rotation measure (RM) values for 4 pulsars, as well as phase-resolved RM variation in J1453-6413. Full-polarimetric pulse profiles are provided for all these pulsars, with multi-frequency polarimetric data for 20 of them. These results will enhance future SKA-Low science: refining pulsar population models, informing survey strategies, and advancing characterization of both the ISM and the ionosphere through low-frequency pulsar monitoring.

1. INTRODUCTION

Pulsars are highly magnetized, rotating neutron stars that emit radiation by converting their rotational energy into dipole radiation across the electromagnetic (EM) spectrum, but mainly at radio frequencies. However, even after their discovery at low radio frequencies (81.5 MHz, [A. Hewish et al. 1968](#)) almost six decades ago, their observations have remained elusive at the lowest frequencies, with most discoveries and studies reported around ~ 1 GHz. Even among those discovered, a large fraction remains undetected and poorly understood at low frequencies below ~ 300 MHz. Many factors contribute to this, both technological and observational limitations. While many advancements have been made in the past decade in technology and instrumentation with the addition of new radio frequency observatories like the Low Frequency Array (LOFAR; [M. P. van Haarlem et al. 2013](#)); the Murchison Widefield Array (MWA; [S. J. Tingay et al. 2013](#)); the Long Wavelength Array (LWA; [G. B. Taylor et al. 2012](#)); and NenuFAR ([P. Zarka et al. 2015](#)), most pulsars have not been detected at low frequencies, partly also due to observational constraints.

The ability to detect a source with high signal-to-noise (S/N) ratio also depends on the background noise, given the high Galactic background emission at low frequen-

cies, which follows a power law with an index of -2.6 ([C. G. T. Haslam et al. 1982](#)). Therefore, higher sensitivity is required to detect fainter sources. In general, pulsars are classified as steep spectrum sources, $S_\nu \propto \nu^\alpha$, where S_ν is the flux density at frequency ν and α is the spectral index with a mean value of -1.6 ([F. Jankowski et al. 2018](#)). However, their radio spectra have been extensively studied for decades in order to understand their population as well as their complex emission mechanism (see, e.g., [W. Sieber 1973](#); [I. F. Malov 1979](#); [V. M. Malofeev et al. 2000](#); [D. R. Lorimer et al. 1995a](#)). These studies suggest a turnover in pulsar spectra at low frequencies attributed to synchrotron self-absorption ([W. Sieber 1973](#)) in the pulsar magnetosphere or free-free absorption ([I. F. Malov 1979](#)) in the interstellar medium (ISM). Studies of pulsars at higher frequencies show that flux density spectra follow similar trends among normal and millisecond pulsars (MSPs) ([F. Jankowski et al. 2018](#)). At the same time, some studies of MSPs have shown that the power law behavior continues to the lowest frequencies ([A. D. Kuzmin & B. Y. Losovsky 2001](#)), unlike normal pulsars, although more recent studies indicate a spectral turnover in MSP spectra as well ([R. Sharan et al. 2024](#)). This suggests the need for improving the frequency coverage of MSPs at frequencies below 300 MHz. The combined effect of higher system noise and low flux density due to spectral

arXiv:2603.11553v1 [astro-ph.HE] 12 Mar 2026

turnover makes it difficult to detect more pulsars at low frequencies.

In addition to these, the effects of dispersion ($\propto \nu^{-2}$) and scattering ($\propto \nu^{-4}$) on pulsar emission, which have a very strong frequency dependence, can not be ignored (N. D. R. Bhat et al. 2004). With improvements in computing, dispersion effects can be minimized with the application of coherent de-dispersion techniques, whereas multi-path scattering introduces asymmetric broadening, which is more difficult to correct. Nevertheless, the strong frequency dependence of these effects presents an opportunity to make high-precision measurements of pulsar dispersion and scattering. An application is to improve high-precision pulsar timing array (PTA) experiments, geared towards detecting gravitational waves, whose sensitivity is affected due to variability in the ISM (D. A. Hemberger & D. R. Stinebring 2008). Recent studies have shown that low-frequency observations can provide accurate measurements of pulsar scattering index (K. Bansal et al. 2019; F. Kirsten et al. 2019), measurements of solar wind variability (C. Tiburzi et al. 2021; P. Kumar et al. 2022), and even time-dependent scattering variability (J. Y. Donner et al. 2019; P. Kumar et al. 2025), which could all contribute towards improving the noise modeling, thereby increasing the sensitivity of PTAs. Pulsars also scintillate due to turbulence in the interstellar medium. This causes the measured signal to fluctuate, leading to variations in measured flux density of pulsars. This effect is more pronounced at low frequencies (N. D. R. Bhat et al. 2023).

As pulsars are also highly polarized sources, propagation through the ionized and magnetized ISM also imparts a frequency-dependent distortion to the linearly polarized signal via Faraday Rotation (FR) on the received signal. Again, since this effect is proportional to λ^2 , observations at low frequencies allows for more robust measurements of pulsar Rotation Measure (RM), which is the product of line-of-sight (LOS) magnetic field and the intervening electron density. We can probe the magneto-ionic structure of the ISM, large-scale magnetic field structure of the galaxy (C. Sobey et al. 2019). It is possible to determine the average LOS magnetic field strength of the ISM, using pulsar observations as,

$$\langle B_{\parallel} \rangle = 1.232 \frac{RM}{DM} \mu G \quad (1)$$

where RM in rad m^{-2} and DM (in pc cm^{-3}) is the pulsar dispersion measure (electron density integrated along the LOS). Long-term studies of pulsar RM and its variation also allow us to understand the feasibility of different ionospheric electron density models and their usefulness on different time scales (see, e.g., P. Kumar et al. 2025). Finally, pulsar polarizations are also

important to understand their complex emission characteristics (A. von Hoensbroech et al. 1998).

1.1. Motivations and science goals

Detecting, characterizing and monitoring pulsars is a key science goal for the future Square Kilometre Array (SKA)-Low radio telescope. In addition to studying pulsars themselves, high precision DMs are required for PTAs to detect low frequency gravitational waves (G. Janssen et al. 2015). Pulsars are typically detected at higher frequencies, hence observations of known pulsars at lower frequencies provides high precision DM and RM measurements as well as measurements of any spectral turnover at low frequencies. Additionally, pulsar observations and detections at low frequencies are also affected propagation effects such as scattering and dispersion (N. D. R. Bhat et al. 2004). This wide bandwidth information is required for estimating the number of detections of future pulsar surveys. Low frequency observations between 50-250 MHz also provide very large fractional bandwidth to study the evolution of pulse profiles and the identification of interesting sources. Low-frequency data from the presented survey will provide these information and improve our understanding of pulsar spectra.

2. OBSERVATIONS

The Engineering Development Array2 (EDA2) is a low-frequency aperture array comprising 256 MWA dual polarization bowtie dipoles, with modified low-noise amplifiers (LNAs) that improve the sensitivity down to ~ 50 MHz. The dipoles are distributed in a pseudo-random layout with a diameter of 35 m. This is a second-generation prototype station built as a verification system for low-frequency Square Kilometer Array (SKA-Low) (M. Caiazzo et al. 2017), operating between 50-350 MHz. Details of EDA2 system verification, design, calibration, and performance are presented in R. Wayth et al. (2022). The observing band is split into 512 coarse channels, separated by ~ 0.781 MHz. These coarse channels are oversampled using a polyphase filterbank (PFB) to get a channel width of ~ 0.926 MHz. The station can operate in stand-alone mode, both as an interferometer and as a beamformed array.

Pulsar observations are carried out using the beamformed mode, by coherently summing the complex dipole voltages to form a phase-array beam. The sensitivity of the phase array varies as a function of frequency, pointing direction, and local sidereal time (LST), with the highest sensitivity at zenith. The station beams are electronically steered in a pointing direction, using a digital beamforming method implemented in the firmware

of the Tile Processing Modules (TPMs; G. Naldi et al. 2017), by applying a phase delay to each dipole in the signal chain. A census of pulsars was carried out with an initial system at intermediate frequencies (C. P. Lee et al. 2022) deployed with a maximum time resolution of $1.08 \mu\text{s}$, which could capture one coarse channel. EDA2 was also used to search for Fast Radio Bursts (FRBs) with an improved bandwidth and high time resolution imaging capability providing revised rates at low frequencies (M. Sokolowski et al. 2022a). With improvements to hardware and software, the current work makes use of an upgraded system that can capture up to ~ 100 coarse channels. This improved system was also used to analyze the largest sample of Crab giant pulses at low frequencies (M. Sokolowski et al. 2025). Compared to the MWA at MRO, which is a precursor to SKA-Low, EDA2 has real-time beamforming capability, with more manageable data volumes and turnaround times for processing which includes time required for calibration and beamforming of raw data. Whereas, MWA-Voltage capture system (VCS) performs tied-array off-line beamforming which required storing original complex voltages at a very high data rate of 28 TB h^{-1} (S. E. Tremblay et al. 2015), which makes EDA2 more feasible for data-intensive applications such as pulsar observations across the usable frequency range and high cadence pulsar monitoring campaigns.

2.1. Target selection

The observing capability of EDA2 spans three octaves in frequency, and the sensitivity of the instrument varies with conditions and observing setup. As such, the direction-dependent response of these dipoles results in a system equivalent flux density (SEFD), which is a measure of sensitivity, varying by a factor of ~ 2 between $\sim 1.3\text{-}2.2 \text{ kJy}$ as a function of elevation (at frequency 160 MHz where the array is most sensitive). Furthermore, the frequency-dependent response of the instrument degrades the sensitivity by a factor of $\sim 4\text{-}8$ at 70 MHz and similarly by $\sim 3\text{-}5$ at 300 MHz. These values are for the zenith response of EDA2; at lower elevations, the sensitivity is lower. The dependence of EDA2 SEFD on frequency, LST, and elevation is detailed in (M. Sokolowski et al. 2022b), and a python code³ along with a webpage⁴ has been provided for easy viewing. Since a large fraction of known pulsars are in the galactic plane region, we also note that, due to the high system temperature, the sensitivity in those parts of the sky is lower than

stated above. Based on the sensitivity and using available measurements of pulsar flux density we estimated the expected flux density at 160 MHz using *PULSAR SPECTRA*⁵ (N. A. Swainston et al. 2022), and also by scaling literature values by a spectral index of -1.4 , we limited our target sample to $> 20 \text{ mJy}$ at 160 MHz, to avoid very long on source integration time. Additionally, we put the following constraints: (1) declination limit of $\delta < +30^\circ$, except for a few known bright sources, to avoid loss in sensitivity due to low elevation, and (2) a DM cut-off of 200 pc cm^{-3} to avoid non detections due to smearing caused by scattering at low frequencies. Figure 1 shows the distribution of all observed targets on the sky plane in Galactic coordinates.

2.2. Observations and data reduction

Given the peak sensitivity of the instrument at 160 MHz and system limitations, all observations to confirm pulsar detections were carried out with 80 coarse channels centered around 169 MHz. Observations were carried out for an integration time between 0.5 and 2 hours based on expected flux density, and to limit the size of the raw data files ($\sim 0.45 \text{ TB hr}^{-1}$ for 28 MHz bandwidth). Post detection in this frequency range, we did follow up observations over the EDA2 observing band. Since the goal was to study the evolution of pulsar spectra, their profile, and other features, the 50-250 MHz band was split into 5 separate bands. Due to the presence of radio frequency interference (RFI) in the FM band (88-108 MHz), coarse channels below 88 MHz were combined together to create a single frequency band pulse profile. For frequencies above 108 MHz, and up to 250 MHz, the band was split into 4 frequency chunks of $\sim 45 \text{ MHz}$ centered around 131 MHz, and $\sim 28 \text{ MHz}$ centered around 169, 197, and 225 MHz. The lower frequency was given a wider bandwidth due to the presence of some known satellite downlinks in this band (D. Grigg et al. 2025), increased system temperature, and the potential turnover in pulsar spectra at these frequencies.

All observations were scheduled at respective target transit times to maximize available EDA2 sensitivity. The corresponding observing epochs are indicated under $\text{DM}_{\text{Epoch}}^{\text{EDA2}}$ column in Table A1. The raw beamformed voltage data (dada file) was recorded for each coarse channel on the EDA2 server and was subsequently reduced to folded archives. Each dada file was reduced to 512 phase bins, 256 fine channels coherently de-dispersed, and 30 s averaged archives, using the *DSPSR*

³ https://github.com/marcinsokolowski/station_beam

⁴ <http://skalowsensitivitybackup-env.eba-daehsrjt.ap-southeast-2.elasticbeanstalk.com>

⁵ https://github.com/NickSwainston/pulsar_spectra

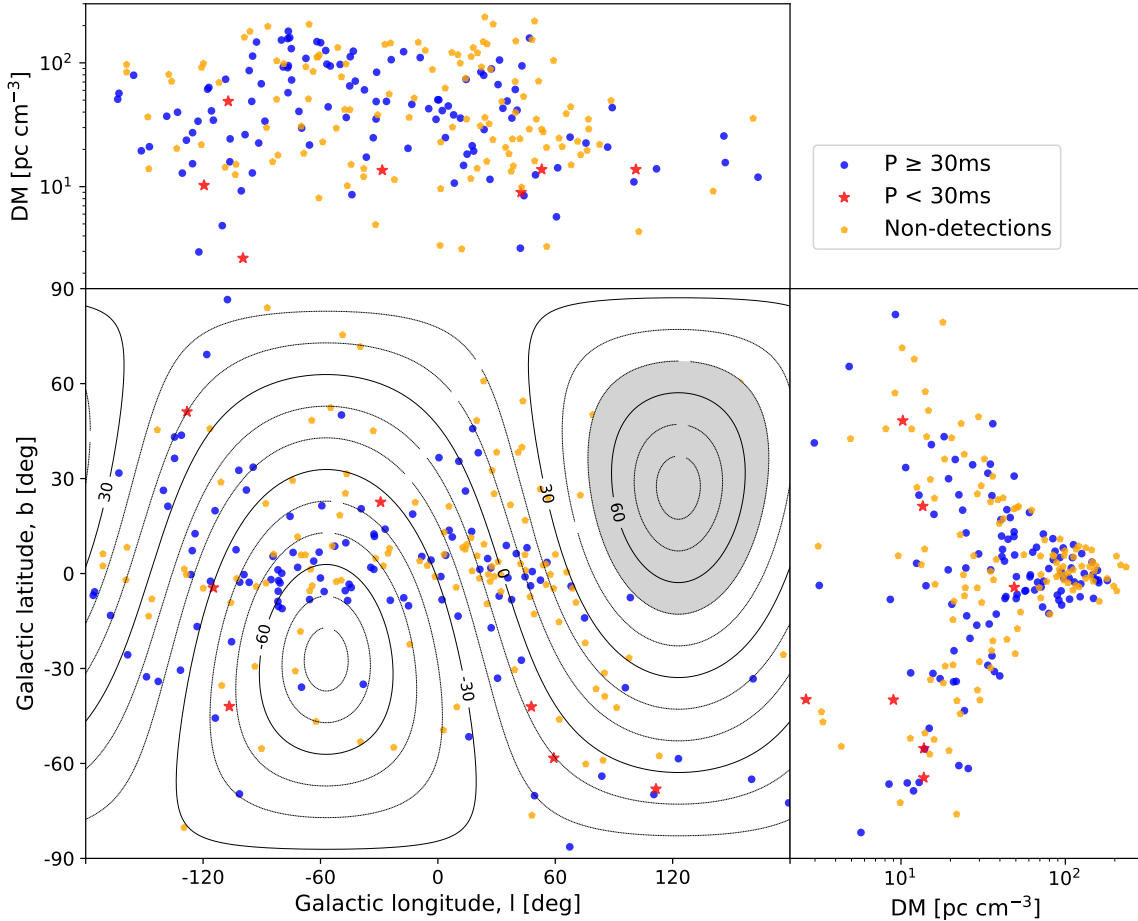


Figure 1. Distribution of census targets in Galactic coordinates. Red and blue indicate the detected targets, with periods below and above 30 ms, respectively, and non-detected targets are shown in yellow. Contours show the line of equal declination, and the shaded region shows the region inaccessible due to low elevation.

package⁶ (W. van Straten & M. Bailes 2011). Since we could not store data files for more than ~ 3.5 hours of observations, data reduction time was estimated, and observations were spaced to get the previous data reduced before the next observation. All of this scheduling and data reduction was automated using a combination of python and bash scripts, which calculates the source transit time and checks the subsystem of the station so that there are no overlapping observations. After data reduction, 36 coarse channels around 169 MHz were combined into a single archive after removing the overlapping frequencies due to oversampled PFB, using a

combination of *psrsh* and *psradd* tools from *PSRCHIVE* software package⁷ (W. van Straten et al. 2012; A. W. Hotan et al. 2004). Bright RFI was excised using python in the combined file, in time and frequency, using median statistics. Detection was made using a combination of visual inspection, comparing against available pulsar profiles in EPN pulsar catalog⁸ and *pdmp* tool from *PSRCHIVE*. In case of marginal detection, the pulsar was reobserved with a larger observing bandwidth to increase the sensitivity and S/N. Among the 240 observed targets, we detected 120 pulsars in our observations. The final list of detected pulsars was then re-observed

⁶ <https://dspsr.sourceforge.net>

⁷ <https://psrchive.sourceforge.net/>

⁸ <https://psrweb.jb.man.ac.uk/epndb/>

in the 50-250 MHz range to study the frequency dependence of the spectrum and profiles.

3. RESULTS AND ANALYSIS

3.1. Average pulse profile

As stated in Section 2.2, observations were performed in five frequency bands, post detection around 160 MHz. Raw voltage data was processed using *DSPSR*, applying pulsar ephemeris and other metadata to create coarse channel archives. These were subsequently combined to create a broadband profile, which was excised for RFI. After the RFI removal, the combined archives were averaged in time and frequency to get the integrated pulse profiles. The same process was applied for each of the five frequency bands, as described in Section 2.2. In some cases, nearby frequency bands were combined to get an improved detection. The average pulse profiles for 120 pulsars with some example pulsars across multiple frequency bands are shown in Figure E1.

3.2. DM correction

We applied the *PSRCHIVE* program *pdmp* to find optimal period and DM to improve the pulsar ephemeris, by maximizing the signal-to-noise of the frequency and time averaged profile. The search was performed in each frequency band of census, and the final period and DM correspond to maximum signal-to-noise (S/N) ratio. Additionally, the diagnostic plots from *pdmp* were also used as a further verification of all detections reported in Section 3.1. We used a DM step size of 0.01 pc cm^{-3} for our search, and pulsars with significant corrections were reprocessed with the updated DM to improve average pulse profiles.

From the current sample, 110 pulsars showed a significant change in DM, with a median absolute value of 0.1 pc cm^{-3} , over a span of 8 to 38 years. Some notable examples which showed a large change in DM are PSR J1711-5350, J1240-4124, J0856-6137, and J1418-3921, where the DM change was -0.85, -0.83, 0.76, and 0.59 pc cm^{-3} respectively. Since pulsar dispersion has an inverse square dependency on observing frequency (D. R. Lorimer & M. Kramer 2004), low frequency observations are generally more sensitive to DM measurements. Hence, we could get a significant change in DM in some cases, compared to those reported in ATNF pulsar catalog (R. N. Manchester et al. 2005), generally from high frequency observations. Although it should be pointed out that the DM estimated using S/N maximization may be biased by the profile frequency evolution, which is more pronounced at low frequencies. Table A1 provides the list of all detected pulsars along with their catalog period, DM, and the corrected DM obtained from this

work. Apart from higher sensitivity to pulsar DMs and profile evolution at low-frequencies, Section 4.4 elaborates on other reasons for observed DM variations in pulsars.

3.3. Calibration and mean flux density

The flux density (S_ν) of a pulsar can be obtained from the radiometer equation in D. R. Lorimer & M. Kramer (2004) below:

$$S_\nu = \gamma \frac{S/N T_{\text{sys}}}{G \sqrt{n_p \Delta\nu T}} \sqrt{\frac{W_{\text{eq}}}{P - W_{\text{eq}}}} \quad (2)$$

where $\gamma=1$ is a correction factor, S/N is the signal to noise ratio of the pulsar average profile, P is the pulse period, T is the total integration time, $\Delta\nu$ is the effective bandwidth of the data, n_p is the number of polarizations, $\frac{G}{T_{\text{sys}}} = \text{SEFD}$, and W_{eq} is the equivalent width of the pulse. Hence, we need to measure the SEFD and profile width for each observation to estimate the pulsar flux density. The SEFD for EDA2 has already been measured using data, for a range of frequencies and observing parameters, and an estimate of the EDA2 SEFD is available from the sensitivity calculator in M. Sokolowski et al. (2022b). These results were further compared against full electromagnetic simulation of the station beam in the commercial simulation package *FEKO*⁹. It is worth pointing out that SEFD estimates for total Stokes I are obtained by taking a quadrature sum of two linear polarizations of the antenna, which is only strictly valid for an unpolarized source and high source elevation, which can lead to mis-estimations at low elevations by $\sim 10 - 20\%$ (A. T. Sutinjo et al. 2021).

The pulse width is measured from the average pulse profiles in Section 3.1, by modeling the profile as a sum of Gaussian components by visually inspecting each profile. The maximum number of Gaussian components used for profile fitting was determined using Bayesian information criteria (BIC, A. R. Liddle 2007). Based on this fitting, we determined the S/N of the profile, along with pulse width at half-maximum (w_{50}) and ten percent of the maximum (w_{10}). The flux density values are estimated using w_{50} measurements. While this entire method may not be the most accurate way to calculate fluxes, but it's likely the only possible one for low-frequency arrays. To account for all errors including SEFD measurements, we assume a total error of 50% in the calculated flux density measurements. Using these measurements along with other catalog measurements, we fit spectra using the *PULSAR SPECTRA* package.

⁹ <https://altair.com/feko>

Table B2 provides the calculated flux density measurements for all detected pulsars at multiple frequencies, along with pulse width measurements and other parameters in equation 2.

3.4. Pulsar Spectra

Since the variation in flux density measurements and calibration from different telescopes can introduce systematic errors in spectral modeling, we adopt the method developed in (F. Jankowski et al. 2018) and use other literature measurements to get a robust fit of spectra using the *PULSAR SPECTRA* package. Details of the implementation of spectral modeling are given by N. A. Swainston et al. (2022). In summary, it uses maximization of a modified Gaussian likelihood function, which downweights outlier data points. We used the five analytical models from (F. Jankowski et al. 2018), simple power-law (PL), broken power-law (BPL), power-law with a low frequency turnover (PLL), power-law with a high frequency cut-off (PLH), and double turnover spectra (DT), where the best fitting model was determined using the Akaike information criteria (AIC). This measures the information retained in the model without overfitting. The model with the lowest AIC is chosen as the best-fitted model. Additionally, we determine the probability, P_{best} , as the inverse sum of likelihoods relative to the best fitting model, that the best fitting model is the true model. Table C3 gives the spectral fitting parameters for all 120 pulsars detected in this census.

Among these pulsars, 20 pulsars show a change in their spectral model, and four pulsars, namely J0038-2501, J0636-4549, J1225-5556, and J1510-4422, had no spectra before the addition of new low-frequency data from EDA2. However, since the model fitting is sensitive to the data, there are cases where the AIC value of best fit model is close to one or more of the other analytical models. Figure F16 shows the flux density spectra for some of these pulsars which showed a changed in spectra with the addition of census data shown in green stars, along with the spectra of other census detected pulsars. It is worth pointing out that we have used the spectral fitting method as described in N. A. Swainston et al. (2022), without any pulsar by pulsar fine tuning, given the large number of pulsars in this census.

Additionally, 13 pulsars show an improvement in their spectral modeling with the addition of EDA2 measurements and are marked with a star in Table C3. Among the EDA2 pulsars, 52 show a turnover in spectra at low frequencies, including five of the seven detected millisecond pulsars. The mean value of low frequency turnover in these pulsars is 115 ± 10 MHz, much better constrained than the value of 130 ± 80 in V. A. Izvekova et al.

(1981). For pulsars with a simple power law behavior, the mean spectral index is -1.78 ± 0.17 , which agrees with the value of -1.6 ± 0.03 in F. Jankowski et al. (2018).

3.5. RM-synthesis

Due to the high level of linear polarization in pulsars (see, e.g, S. Johnston & M. Kerr 2018) and pulsar RM being proportional to λ^2 , makes low frequency observation appealing for precision RM measurement. At the same time, low spatial resolution at these wavelengths can also cause depolarization. Although the simplest approach to measuring RM is by fitting a linear model to the polarization angle as a function of λ^2 , and can be readily done using *rmfit* routine in *PSRCHIVE*, this assumes that there are no additional depolarizing sources along the LOS. This can be resolved using RM-synthesis techniques by B. J. Burn (1966) and further developed by M. A. Brentjens & A. G. de Bruyn (2005). We can describe the complex linear polarization in terms of Stokes parameters (I, Q, U, V) as

$$P = Q + iU = pLe^{i2\psi} = Le^{i2\psi} \quad (3)$$

where I is the total intensity, Q and U are the components of linear polarization, V is the circular polarization, L is the linear polarized intensity, and p and ψ are the fractional degree and polarization angle of linear polarization. While propagating through a magnetized plasma, polarization vector is rotated as a function of observing wavelength squared (λ^2). For a single point source along the LOS, the rotation is linearly proportional to λ^2

$$\psi = \psi_0 + RM\lambda^2 \quad (4)$$

where the proportionality constant RM along the LOS is given by:

$$RM = 1.232 \int n_e(l)B_{\parallel}(l)dl \quad (5)$$

where $n_e(l)$ is the spatial electron number density (cm^{-3}) and $B_{\parallel}(l)$ is the LOS magnetic field (μG), both function of position(l). Although pulsars are Faraday thin sources, application of RM-synthesis methods over the linear approach allows us to discern weakly chromatic noise due to instrumental leakage, from astrophysical RMs. Additionally, theoretical predictions claim that there should not be intrinsic Faraday rotation within pulsar magnetospheres (C. Wang et al. 2011). On the other hand, A. Noutsos et al. (2009) claim to have detected such effects as variations of RM as a function of pulse phase. Our RM measurements can be used to confirm these results. This can help us improve models of the magnetosphere. Hence, following B. J. Burn

(1966), we consider the generalized RM, known as the Faraday depth (ϕ), defined at each point along the LOS to the source. Using equation 3 and 4, we can write,

$$P(\lambda^2) = L e^{2i(\psi_0 + \phi \lambda^2)} \quad (6)$$

Assuming the same ψ_0 at all Faraday depths, we can write the Fourier relation:

$$P(\lambda^2) = \int_{-\infty}^{+\infty} F(\phi) e^{2i\phi \lambda^2} d\phi \quad (7)$$

where $F(\phi)$ is the Faraday dispersion function (FDF) representing intrinsic linear polarization, and will show a peak at an RM given by equation 4 for a single compact source along the LOS. Any deviation from this could be astrophysical or instrumental in nature.

Given that $\lambda^2 < 0$ solutions are not physical and that we can only sample the complex linear polarization at discrete values, after inversion, the above equation can be written as a discrete Fourier transform (DFT):

$$\tilde{F}(\phi) = \frac{1}{N_c} \sum_{j=1}^{N_c} P(\lambda_j^2) e^{-2i\phi(\lambda_j^2 - \lambda_0^2)} \quad (8)$$

where N_c is the number of channels, j is the channel index, λ_j is the channel wavelength, and λ_0 is a reference wavelength following (M. A. Brentjens & A. G. de Bruyn 2005). Since we are only concerned about the RM value and hence the peak of FDF, the choice of λ_0 is arbitrary. M. A. Brentjens & A. G. de Bruyn (2005) also showed that the discrete synthesized FDF in equation 8 is a convolution of the 'real' FDF with the RM spread function (RMSF):

$$\tilde{R}(\phi) = \frac{1}{N_c} \sum_{j=1}^{N_c} e^{-2i\phi(\lambda_j^2 - \lambda_0^2)} \quad (9)$$

which can be deconvolved from the synthesized FDF in equation 8, using RM-CLEAN algorithm implemented by (G. Heald et al. 2009), to obtain the best S/N ratio. This helps reduce confusion due to instrumental leakage, which peaks at $\phi \sim 0$ rad m⁻². This RMSF peak also limits the resolution of the FDF, and is quantified by full width half maximum (FWHM) (D. H. F. M. Schnitzeler et al. 2009) as,

$$\delta\phi \left(\frac{\text{rad}}{\text{m}^2} \right) = \frac{3.8}{\lambda_{max}^2 - \lambda_{min}^2} \quad (10)$$

where λ_{max} and λ_{min} are the span of data wavelength in meters.

3.6. Ionospheric RM

Since the Earth's ionosphere imparts a significant RM (RM_{ion}) to the observed RM (RM_{obs}), it needs to be subtracted to get the 'true' RM and estimate the ISM magnetic field:

$$RM_{ISM} = RM_{obs} - RM_{ion} \quad (11)$$

Ionospheric corrections depend on Earth's magnetic field, which has small variations (P. Alken et al. 2021), and on the total electron content (TEC) of the ionosphere, which changes significantly on all time scales. Previous studies have shown that due to these variations, it is difficult to apply precise correction. Hence, to get most reliable measurements TEC at the telescope site should be measured with a GPS receiver with high time resolution (P. Kumar et al. 2025). However, since this setup is not readily available, we have to rely on global ionospheric models, which interpolate values from a discrete set of receivers to create a map of the ionosphere on hourly timescales. Following this, we employed two methods to measure the ionospheric contribution to the RM: 1) using the method described in P. Kumar et al. (2025) along with IGS and CODE ionospheric maps, which provided the most accurate RM measurements in P. Kumar et al. (2025) on short and long timescales, 2) using the *IonFR* code (C. Sotomayor-Beltran et al. 2013) along with the IGS model. Both models assume a single thin shell of ionospheric plasma for the calculation of RM values. The mean and median of RM_{ISM} from both these methods were compared against literature values, and were found to be the same in each case, hence final values are reported using the *IonFR* method. We also investigated the measurement of ionospheric subtracted RM as a function of observing time and target elevation, to assess the validity of this method and quantify any variation in RM measurements due to instrumental leakages at low elevations. Figure 2 shows the RM_{ISM} for pulsar J0630-2834 as a function of source elevation and observing time in UTC on MJD 60640. We see that all values are consistent within error bars, with the error increasing around UTC=15, which is around sunrise for MRO, during which we expect higher variations in the ionospheric conditions. This pulsar has been previously shown to exhibit no RM variations on long timescales (P. Kumar et al. 2025).

3.7. Pulsar RM and phase resolved RM

We applied the RM-synthesis method to each of our detected pulsars, in each frequency band, to measure the pulsar's highest S/N RM as well as RM as a function of pulse phase, the profiles were downsampled to 64 or 128 bins and < 1000 fine frequency channels to increase the

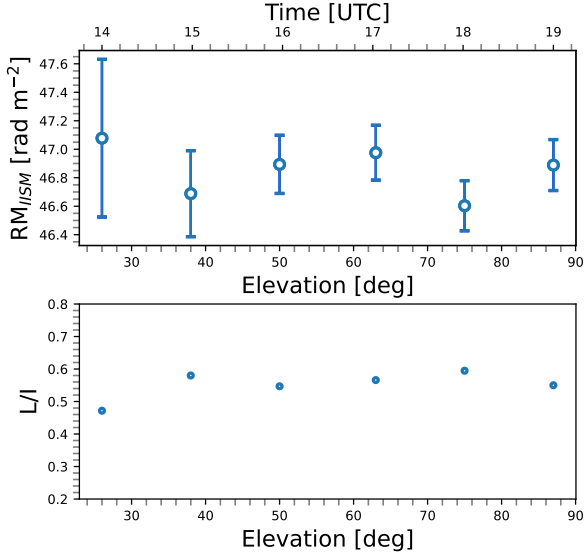


Figure 2. (Top) RM_{ISM} for pulsar J0630-2834 as a function of source elevation and observing time in UTC on MJD 60640. (Bottom) Variation of fractional linear polarization with elevation.

S/N per bin. The RM-synthesis method was then applied to measure the pulsar RM as a function of pulse phase in the Faraday depth range of $-200 < \phi < 200$, which covers the range of expected RM for these pulsars as reported previously in ATNF catalog, with a step size of 0.01 rad m^{-2} , and FDF peaks with $S/N > 6$ were reported for each pulsar. For pulsars with detections across multiple EDA2 frequency bands, the final value is reported using the one that has the highest S/N. In total, we have detected significant pulsar RM in 40 pulsars. Table D4 provides our RM measurements and ionospheric corrections for census pulsars, along with corresponding values reported in the ATNF catalog and at frequencies around 1.3 GHz with the MeerKAT telescope (B. Posselt et al. 2023). Despite the low RM value for many of these pulsars and their FDF peak falling within the FWHM of RMSF peak generated by instrumental polarization at $\phi \sim 0 \text{ rad m}^{-2}$ given by equation 10, 28 of these measurements are unaffected by RMSF peak due to the instrumental leakage.

In Figure 3, we show the difference between ionosphere-corrected RM values for each pulsar between EDA2 and MeerKAT telescopes. We see no particular trend between ΔRM which is the difference between RM_{ISM} from EDA2 and MeerKAT telescopes and RM_{ion} measured for each of the EDA2 observations. Moreover, the mean value of ΔRM is close to zero. Since the contribution of ionospheric RM should be normally distributed around zero across multiple observations, this indicates no systematic trend and that

variations in the ΔRM is mainly due to fluctuation in ionospheric RM correction between these two telescopes.

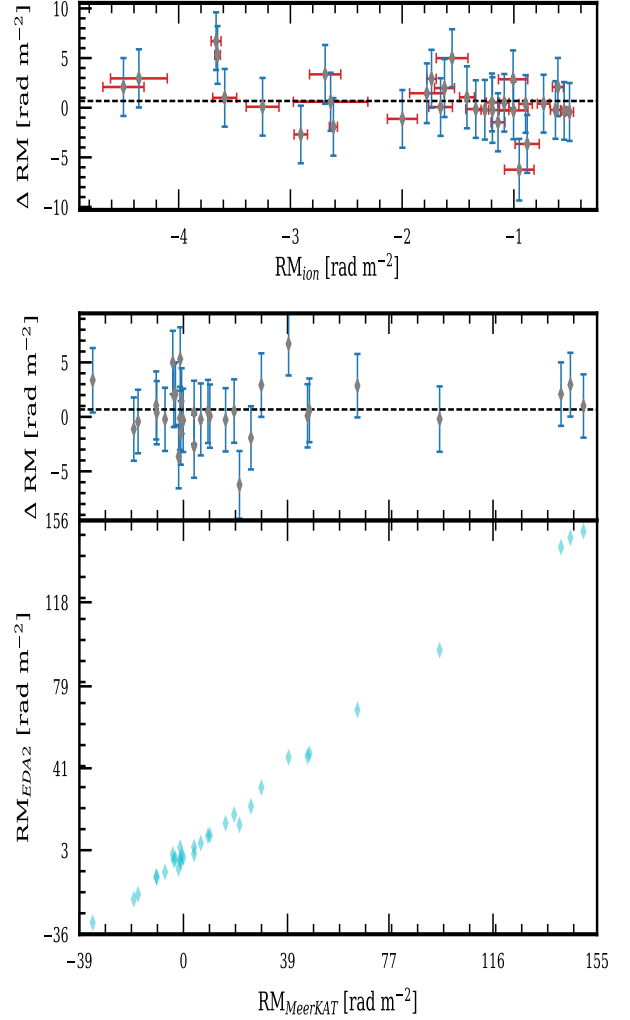


Figure 3. The top panel of the figure shows the difference between RM_{ISM} from EDA2 and MeerKAT telescopes (ΔRM) against the ionospheric RM (RM_{ion}) measured for EDA2 for each of those pulsars. The bottom panel shows the one-to-one RM_{ISM} for pulsars in Table D4 for EDA2 and MeerKAT. The central panel shows ΔRM vs RM_{ISM} for MeerKAT. The dashed line in both the top and central panels indicates the mean value of ΔRM

Since we measure pulsar RM across the pulse phase bin for each pulsar, we are also able to measure a variation in RM over the pulse profile, indicating a magnetospheric origin as explained previously in Section 3.5.

We found phase-resolved RM variations in six pulsars, however in three of those there was only on RM measurement which deviated from the rest and the peak S/N of FDF peak was also low. Figure 4 shows phase-resolved RM variations for the other pulsars. Among these, RM of J0437-4715 falls within the RMSF peak and hence could be biased. We also see a gradual variation in RM for J0742-2622, which has a scattered pulse profile. The most significant variations are seen in J1453-6413 which is far from RMSF peak and where the difference between RM measurements across the pulse phase is larger than the error bars on individual measurements. Moreover, both of these measurements for J1453-6413 FDF peak have a high S/N.

3.8. Polarimetry

Pulsar polarimetry can provide useful insights into the direction-dependent phase stability of the instrument and leakage between orthogonal polarizations of the telescope. This becomes particularly useful for prototype arrays like EDA2 using SKA-Low technologies, which require full validation and verification. Figure G31 shows the full Stokes integrated pulse profiles for 36 best pulsars with RM detections in Table D4.

We compared our polarimetric pulse profiles with those at similar frequencies in the EPN pulsar database¹⁰. We found the degree of linear polarization to be similar in most cases, against those in the EPN database, mainly comparing against the results at ~ 150 MHz and ~ 400 MHz from A. Noutsos et al. (2015) and D. M. Gould & A. G. Lyne (1998) respectively. For EPN pulsars with polarization profiles at 150 MHz, the degree of linear polarization was about 5-10% lower than the EDA2 measurements. This could be due to the large FWHM of the EDA2 beam observations leading to depolarization effects. Additionally, due to uncalibrated polarimetry and variation in dipole response with pointing direction, there could be leakage between the two orthogonal polarizations. To investigate this further, we looked at the variation in fractional linear polarization for J0630-2830 with elevation as shown in the bottom panel of Figure 2, where we get a variation of 2-3% for elevations above 40° , and ~ 4 -7% below that. This indicates the presence of residual errors due to uncalibrated polarimetry, which needs to be investigated further.

For profiles at higher frequencies, a direct comparison of linear polarization fraction with EDA2 measurements is not useful. This is due to the following, assuming radius-to-frequency mapping (RFM, J. M. Cordes

1978), where lower frequencies originate higher in the magnetosphere and curvature radiation framework with two propagating modes (P. F. Wang et al. 2015), higher frequencies are emitted from lower heights where the rotation is weaker and the region of the two modes overlap, leading to depolarization and lower fractional polarization at higher frequencies. This is evident from the higher linear polarization fraction for pulsars J1709-1640, J1935+1616, and J2155-3118 in EDA2 compared to 400 MHz profiles from D. M. Gould & A. G. Lyne (1998) in EPN by a factor of 2. For 20 pulsars, we get multiple detections of pulsar RM across multiple EDA2 bands as shown in Figure H34. However, we see no particular trend in fractional linear polarization, which may suggest that the prediction of (P. F. Wang et al. 2015) do not hold for all pulsars or that we need to compare widely separated frequencies. Another possibility is that it occurs due to the uncalibrated instrumental XY phase.

4. DISCUSSIONS

4.1. Profile evolution

We obtained pulse profiles for 120 pulsars in the frequency range of 50-250 for up to 5 narrow bands, which allows us to study various features of pulsars that evolve with frequency, including the pulse profile. Although many low-frequency pulsar censuses have been reported in the last decade with sensitive instruments like LOFAR and MWA (see, e.g., A. V. Bilous et al. 2016; N. D. R. Bhat et al. 2023), we have been able to obtain 32 new pulse profiles below 150 MHz, especially five below 100 MHz. These detections can help inform future studies of morphological assessment of pulse profiles, which can improve our understanding of pulsar emission (J. M. Rankin 1983). Modeling of these pulse profiles, as stated in Section 3.3, also resulted in the detection of multiple components across pulse profiles. For 72, 36, and 11 pulsars, we detected the presence of 1, 2, and 3 components, respectively, and 4 components in J1057-5226. In a few pulsars, the number of components required to model the pulse profiles changed across our observed band, which could be a result of a change in spectral index and hence S/N of different "core" and "conal" components with frequency (R. Basu et al. 2021). For single-component pulsars, the evolution of pulse width with frequency was generally consistent with the predictions of RFM, decreasing with frequency (J. Kijak et al. 2007), but remained almost constant in some cases. Availability of pulse profiles at multiple frequencies also enabled us to make a qualitative study of pulsar scattering. In our census, 11 pulsars show visible presence

¹⁰ <http://www.jodrellbank.manchester.ac.uk/research/pulsar/Resources/epn/>

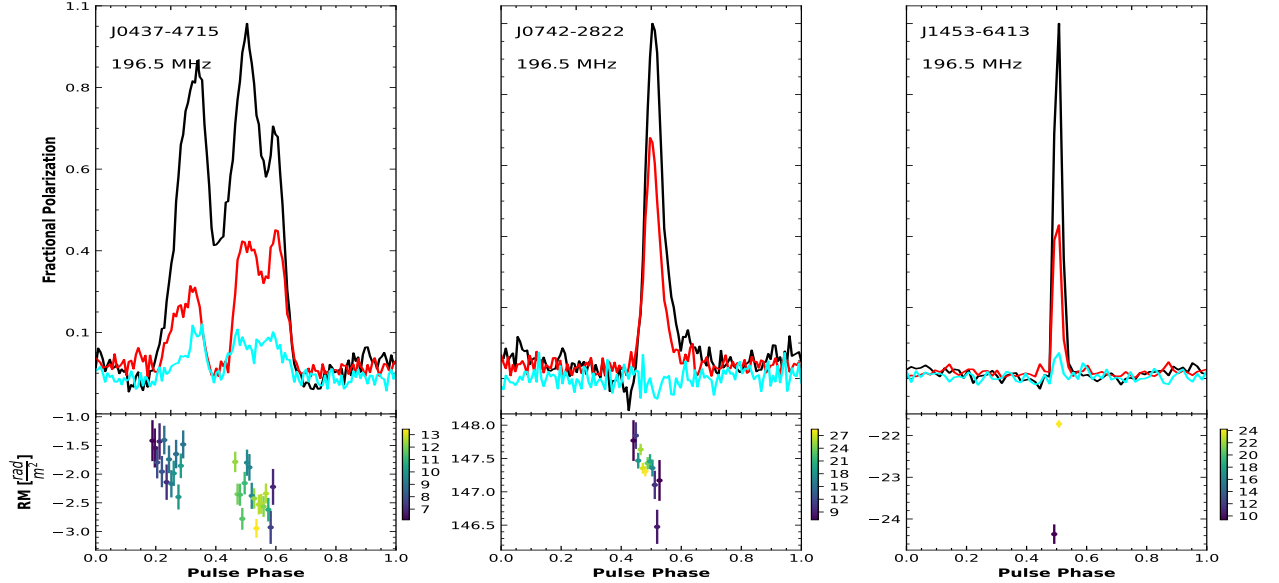


Figure 4. Phase resolved RM variation for three pulsars. The top panel of each subplot shows the total intensity, fractional linear polarization, and fractional circular polarization in black, red, and cyan, respectively. The bottom panel shows RM values measured across the pulse phase, along with a colorbar which indicates the S/N of the FDF peak.

of scattering, among which the most notable are J1820-0427 and J1453-6413, which also show profile evolution.

We observe an inverse correlation between pulse duty cycle (ratio of width and period) and pulsar period, except for the case of J2256-1024. Such broad correlations have been reported for pulsars in the past (D. R. Lorimer et al. 1995a). For normal pulsars with period around 0.5s pulse duty is $\sim 4\text{-}6\%$, however the scatter in duty cycle for normal pulsars is \sim factor of 3 higher than those of MSPs. This impacts the fraction of visible pulsars, since pulsars with wider beams are more likely to intersect the LOS to Earth, increasing their chance of detection. Hence, these measurements have implications for pulsar population studies and pulsar beaming fraction (A. G. Lyne & R. N. Manchester 1988).

T. E. E. Olszanski et al. (2019) showed that there exists a relation between profile width and period and how that evolves with frequency. This is depicted using a Lower boundary line (LBL) of the form $W_B * P^{-d}$, where W_B is the boundary width and P is the period of the pulsar, where they obtained $d \sim -0.5$. This width is thought to correspond to narrowest emission beam and can help estimate the inclination angle. We perform this analysis for our census measurement using quantile regression. Figure 5 shows the result of this analysis along with parametric fits to the above relation. Although the value of d at our highest frequency is $\sim -0.5 \pm 0.1$, consistent with those above, at lower frequency it deviates to $\sim -0.3 \pm 0.1$, suggesting frequency evolution. Similarly, considering the W_{50} case, the value of boundary width

at the highest census frequency is $3.84 \pm 1.15^\circ$, consistent with 327 MHz measurement of 2.37° from A. Skrzypczak et al. (2018); however, it increases at lower frequencies. Assuming a power law evolution of boundary width with frequency, we find the power law index of -0.35 ± 0.03 comparing the value with the value at 327 MHz.

4.2. Flux densities

We measured mean flux density for 120 pulsars at multiple frequencies as described before in Section 3.3, providing several new measurements, including five below 100 MHz and 28 below 150 MHz, where no measurements had been reported before. Additionally, many of these measurements have an overlap with prior low-frequency census measurements at similar frequencies and comparable bandwidths, which can be used for independent verification of our method. Figure 6 shows the comparison of our measurements with other low-frequency catalogs, where we only compared measurements at nearby frequencies. The plot shows detection down to a flux density level of $\sim 15\text{-}20$ mJy, indicative of our sensitivity limit as discussed in Section 2.1. We compared census measurements at ~ 168 MHz with N. D. R. Bhat et al. (2023), A. V. Bilous et al. (2016) and M. E. Bell et al. (2016) at 154, 149 and 154 MHz respectively, census measurements at ~ 131 MHz with 135 MHz in S. Sanidas et al. (2019), census measurements at ~ 198 MHz with 185 MHz in M. Xue et al. (2017), and census measurements at ~ 71 MHz with 79.2 MHz in P. Kumar et al. (2025). For N. D. R. Bhat et al. (2004), M. E. Bell et al. (2016), and M. Xue et al. (2017) ob-

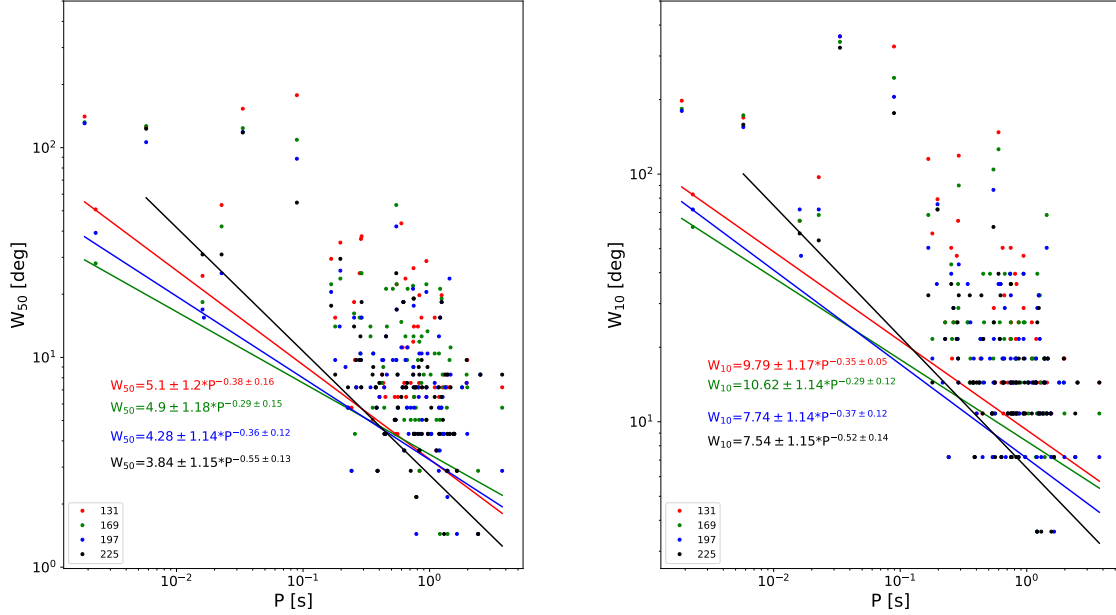


Figure 5. Plot of pulse width versus pulsar period, along with the Lower boundary line in solid lines (Left) using W50 (Right) using W10. The colors represent respective frequencies in the legend.

servations were made with similar bandwidths, whereas census bandwidth was higher compared to P. Kumar et al. (2025), and S. Sanidas et al. (2019), and significantly lower compared to A. V. Bilous et al. (2016). However, in Figure 6 we see that almost all measurements are in agreement within a factor of 2, with large deviations for a few very bright pulsars irrespective of their DMs, which validates our measurements of mean flux densities. However, our measurements are slightly biased towards the higher values around the equality line, which could be due to some of these other census measurements being derived from imaging observations which measure period averaged flux density and are biased towards pulsars with large duty cycle. Five pulsars show a factor of 5 increment in our census flux compared to other catalogs. Among which the variation in J0835-4510 (Vela) and J0534+2200 (Crab) is likely due to highly variables scattering from the associated nebula affecting profile modeling including J0742-2822 which also has a scattered profile. Whereas the variation in J0437-4715, and J2145-0750 both of which are nearby MSPs with a DM of 2.6348 and 9.0008 pc cm⁻³ respectively, is likely due to scintillation. The rms of the relative difference between these flux density measurements from multiple census, except the outlier pulsars, is 118 %. However, the measurements of flux density

are almost equally distributed around the equality line of Figure 6.

4.3. Spectral Analysis

Among the census pulsars 34 follow a simple power law with a mean and median spectral index of -1.78 ± 0.17 and -1.79 ± 0.15 , which is steeper than the empirical value of -1.41 reported by S. D. Bates et al. (2013) near 1 GHz and but closer to the weighted spectral index of -1.6 ± 0.54 of F. Jankowski et al. (2018), however better constrained. Figure 7 shows the spectral index distribution for these pulsars, along with a Gaussian fit to the data with mean and sigma values of -1.78 and 0.49 , respectively. This value is in better agreement with measurements of F. Jankowski et al. (2018). To validate the normality of our Gaussian fit, we perform a Pearson χ^2 test. We find that the null hypothesis is accepted with a p-value of 0.53 with a χ^2 of 1.28, suggesting that the spectral indices are normally distributed. Additionally, we do not find any correlation between spectral index and Galactic latitude or longitude to suggest that the measured spectral indices are affected by the Galactic plane region.

In our sample, 52 pulsars showed a turnover at low frequencies, with 14 and 38 classified as DT and PLL, respectively, with a mean value for $\nu_{peak} = 115 \pm 10$ MHz in agreement with V. A. Izvekova et al. (1981) but higher than the measurements in P. Kumar et al. (2025). Given

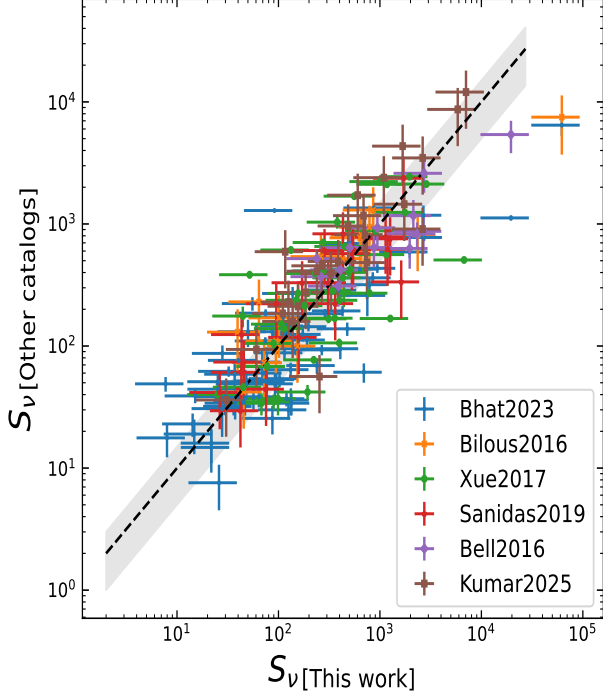


Figure 6. Comparison of our census measurement of mean flux densities with those at similar low frequency observations. Colors in the plot represent the comparison of our census measurement at a frequency close to other catalogs, as indicated in the legend. The dashed line indicates equal flux values, and the shaded grey region represents the 50 and 150 % region of the equal flux value.

the small sample of MSPs in our census, it is difficult to deduce if they show turnover at low frequencies. Since some of these MSPs turnover in agreement with the results of R. Sharan et al. (2024); however, others do not follow and are consistent with the suggestion of A. D. Kuzmin & B. Y. Losovsky (2001). Prior studies of turnover in spectra have also suggested the origin of these turnovers to absorption in the ISM (see, e.g. W. Sieber 1973; I. F. Malov 1979). To investigate this further, we looked for any correlation between the turnover frequency and the Galactic location of the pulsars but found none. Figure 7 shows the Galactic latitude distribution of these 52 census pulsars, indicating an excess in the Galactic plane region, which could be indicative of absorption as stated above. However, this could also be due to selection bias since most of our pulsars are detected at small Galactic latitudes as shown in Figure 1.

For 16 BPL pulsars of our census left panel of Figure 8 shows the plot of spectral index below and above the break, along with the break frequency (ν_{break}), except for J0459-0210 which is an outlier due to the large error-

bar on its spectral index since all except one of its flux density measurements are below 300 MHz. From the figure we can see the general trend where the spectral index flattens below the break frequency as the break frequency moves towards lower frequencies, which could be indicative of low frequency turn over in pulsars with lower ν_{break} and high frequency cut-off in pulsars with higher ν_{break} frequency.

Additionally, 17 census pulsars show a high frequency cut-off ($\nu_{cut-off}$) and are classified as PLH. For these, the right panel of Figure 8 shows the plot of $\nu_{cut-off}$ versus the spectral index, where we see two trends and a couple of outliers. First, pulsars show a cut-off at $\nu \sim 1.5$ GHz due to thermal free-free absorption in the pulsar surrounding (J. Kijak et al. 2007), but with a wide range of spectral index values. Second, we see pulsars with an order of magnitude spread in $\nu_{cut-off}$ above 1.5 GHz but with a spectral index around ~ -1.35 , close to the spectral index value of -1.41 reported by S. D. Bates et al. (2013) at higher frequencies, suggesting that this value may be the correct representative value at these frequencies. However, it is difficult to conclude with any certainty given the small sample of our census pulsars.

4.4. DM variations

Pulsars can have large proper motions and are among the fastest-moving objects in the Galaxy (G. Hobbs et al. 2005). Due to the relative motion of the pulsar in ISM, the pulsar DM along any LOS can change with time depending on ISM variability, proper motion of the pulsar, and span of observations. Hence, long-term pulsar monitoring has resulted in the measurement of DM variability, often linear and with additional periodic or stochastic variations (see, e.g. W. A. Coles et al. 2015; P. Kumar et al. 2025). Sometimes these variations arise due to the presence of discrete structures like bubbles and nebulae (S. K. Ocker et al. 2021). However, it is possible to detect the stochastic signals due to DM variations if the deterministic signals along the LOS red due to discrete structures can be corrected, although it is often difficult (M. T. Lam et al. 2016). Analysis of these variations can cast light on the nature of turbulent ISM, as shown by J. W. Armstrong et al. (1995), where they showed that DM variation in ISM on long time scales has a steep red spectrum. Due to the inverse square dependence of DM on observation frequency, low-frequency pulsar observations provide high precision DM measurements, useful for investigating these variations. Even though DM monitoring would be most suitable to investigate such effects, comparison of our census measurements to those in pulsar catalogs like ATNF can provide some crude estimates. We define the rate of DM variation

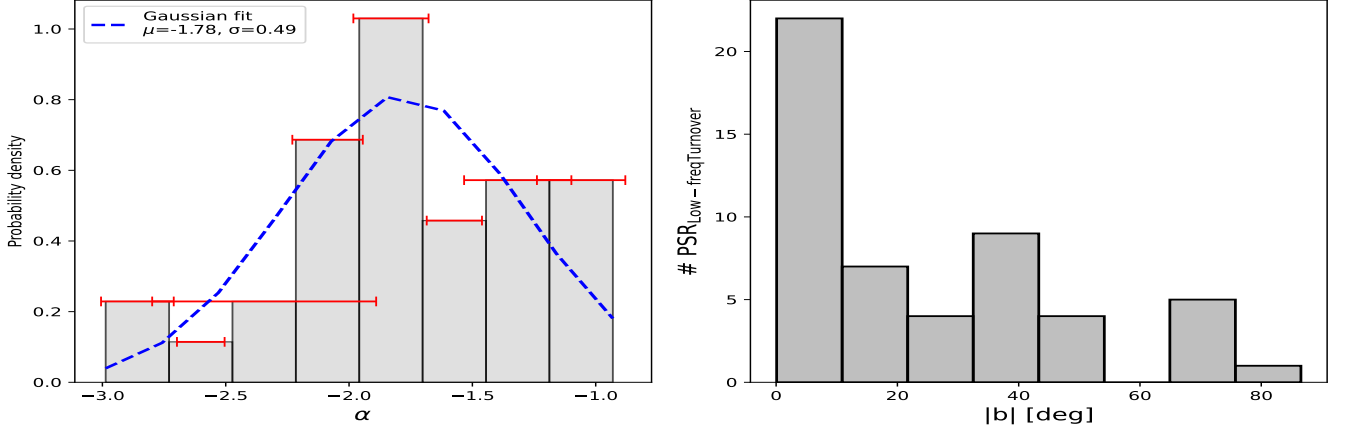


Figure 7. Left: Distribution of spectral index for pulsars classified as PL, along with corresponding error of each bin indicated in red. We also show a Gaussian fit to the data in blue. Right: Distribution of distance from the Galactic plane, as absolute value of Galactic latitude ($|b|$) for pulsars classified as PLL and DT

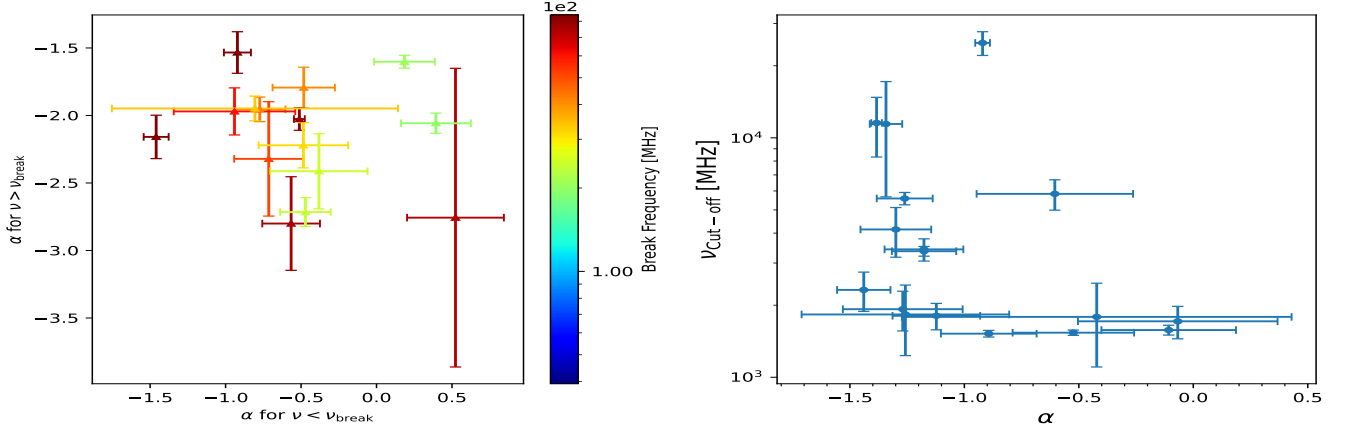


Figure 8. Left: Spectral index below and above the spectral break for 16 pulsars classified as BPL, along with the break frequency indicated by the colorbar, except for outlier pulsar J0459-0210. Right: Plot of spectral index versus high frequency cut-off for 17 PLH pulsars in our census.

and associated error by comparing our measurements as stated in Section 3.2, with those of ATNF catalog values as,

$$\left| \frac{dDM}{dt} \right| = \left| \frac{\Delta DM}{\Delta MJD/365.25} \right| \quad (12)$$

where ΔDM is the change in DM between census and ATNF and ΔMJD is the difference in epochs at which those measurements were taken. Similarly, the error is given by,

$$\epsilon_{\left| \frac{dDM}{dt} \right|} = \left| \frac{\epsilon_{\Delta DM}}{\Delta MJD/365.25} \right| \quad (13)$$

where $\epsilon_{\Delta DM}$ is the quadrature sum of DM errors in the census and ATNF catalogs. Only those pulsars were chosen where both the census and ATNF had a reported uncertainty. Additionally, for final analysis, we rejected the pulsars where the value of $\epsilon_{\Delta DM}$ was bigger than the

value of ΔDM . This gave us a final sample of 43 pulsars with DMs in the range 5-180 pc cm^{-3} , with a time span of 8 to 38 years between the two measurements.

Prior studies on a sample of 13 pulsars (D. C. Backer et al. 1993) with DM in the range 2-200 pc cm^{-3} proposed a wedge model with the relation $\left| \frac{dDM}{dt} \right| \sim \sqrt{DM}$. Similarly, a study of 100 pulsars in the DM range 3-600 pc cm^{-3} spanning 6 to 34 years using pulsar timing method (G. Hobbs et al. 2004) in frequency range of 0.4-1.4 GHz resulted in a relation $\left| \frac{dDM}{dt} \right| = 0.0002 \times DM_{\text{pc cm}^{-3}}^{0.57 \pm 0.09} \text{pc cm}^{-3} \text{yr}^{-1}$. In both of these cases, the spread in $\left| \frac{dDM}{dt} \right|$ was an order of magnitude around the best fit measurements. We compare our measurements against G. Hobbs et al. (2004) indicated by the solid black line with an order of magnitude spread as shown by the shaded region in grey in Figure 9. We fit the function $\left| \frac{dDM}{dt} \right| = A \times DM^B$ to our weighted and unweighted

data, weighted by $|\frac{dDM}{dt}|/\epsilon|\frac{dDM}{dt}|$. For the weighted case, $A \approx 0.0008$ and $B = 0.64 \pm 0.18$, and for the unweighted $A \approx 0.0002$ and $B = 0.41 \pm 0.20$, which is closer to the G. Hobbs et al. (2004) relation, albeit slightly steeper. It is interesting to note that for pulsars with similar DMs, our DM rate is about an order of magnitude higher than that of G. Hobbs et al. (2004) as can also be seen in Figure 9. There can be two explanations, either the turbulence is higher due to the large sampled volume of ISM at low frequencies or due to the possible bias in measurement caused by profile evolution at low frequencies. Parametric values of our unweighted fits are also similar to those reported at low frequencies by A. V. Bilous et al. (2016), but steeper than P. Kumar et al. (2025).

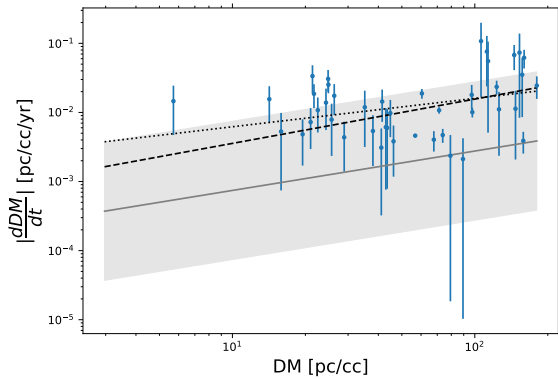


Figure 9. Plot of DM variation versus mean pulsar DMs. Blue points indicate the measured DM rate with error bars, and the dotted and dashed line show the best-fit results, unweighted and weighted by $|\frac{dDM}{dt}|/\epsilon|\frac{dDM}{dt}|$ respectively. The solid black line is the relation from G. Hobbs et al. (2004) with an order of magnitude scatter in the shaded grey region.

4.5. RM and Polarization

Considering 28 pulsars whose RM measurements are unaffected by the instrumental RMSF peak, pulsars with the most significant change in their RM are Vela and J2155-2118. While the former shows variations of $\Delta RM = 6.7$, likely due to the supernova remnant and the Gum Nebula (M. Xue et al. 2019) with an associated ionospheric correction of -3.66 , J2155-3118 has no such associated structure. Since the ΔRM value for this is -6.24 with an ionospheric correction of -0.95 , it is unlikely to be due to ionospheric variation; hence, this is a new, improved RM measurement. Whereas for pulsars J1543-0620, J1825-0935, and J0922+0638, the magnitude of ΔRM is greater than RM_{ion} by one. Since the ionospheric corrections at high frequencies are generally smaller than one, RM measurements for these three pul-

sars are also improved due to the high sensitivity of low-frequency observations to pulsar RMs. For all other pulsars, the magnitude of ΔRM is comparable to RM_{ion} , hence any change is only due to the random fluctuations in ionospheric RMs. The phase-resolved RM variation in J1453-6413 shown in Figure 4 is consistent with the measurements reported in Figure 1 of A. Noutsos et al. (2009). This suggests the presence of magnetospheric RM component in this pulsar, caused the propagation of pulsar radiation through its own plasma. Detection of such RM variations has implications for pulsar emission modeling.

4.6. Census completeness

Out of the 240 observed pulsars, we have detected 120 sources, among which 33 detections were for the first time below 150 MHz, including some below 100 MHz. Additionally, compared to N. D. R. Bhat et al. (2023) and M. Xue et al. (2017), we detected five pulsars undetected by these two MWA censuses at frequencies between 150 and 200 MHz. Even though the detection rate is only 50%, we have to consider the bias due to limited sensitivity and high scattering at low frequencies.

Figure 10 shows the detected and non-detected pulsars in our census against the expected flux density at 160 MHz obtained by scaling literature measurements with a spectral index of -1.4 and using the *PULSAR SPECTRA*, and the expected scattering delay at 160 MHz obtained from the YMW16 model (J. M. Yao et al. 2017) using *PyGEDM* (D. C. Price et al. 2021) normalized by the pulsar period. The two smaller plots in the figure represent the fraction of detected pulsars as a function of flux density and fractional scattering delay. As we can see clearly from the plot, most of our non-detections are from the low flux density regime, where we are sensitivity limited, or from the high fractional scattering. The left panel of Figure 11 shows the correlation between DM and scattering and allows us to estimate the maximum DM at which we can detect pulsars, which is 180 pc cm^{-3} for our census. We can also see two distinct trend lines for normal and millisecond pulsars, where the latter is only detectable up to a slightly lower scattering regime. The right panel of Figure 11 shows the location of our census targets in the Galactic plane, with Earth at the origin. Since DM is a proxy for distance, this allows us to estimate the maximum distance up to which pulsars are detectable, as indicated by the axes of the right panel of Figure 11. We can see that most of our detections come within the DM range of 150 pc cm^{-3} , indicating that low-frequency observations are mostly limited to the nearby pulsar population.

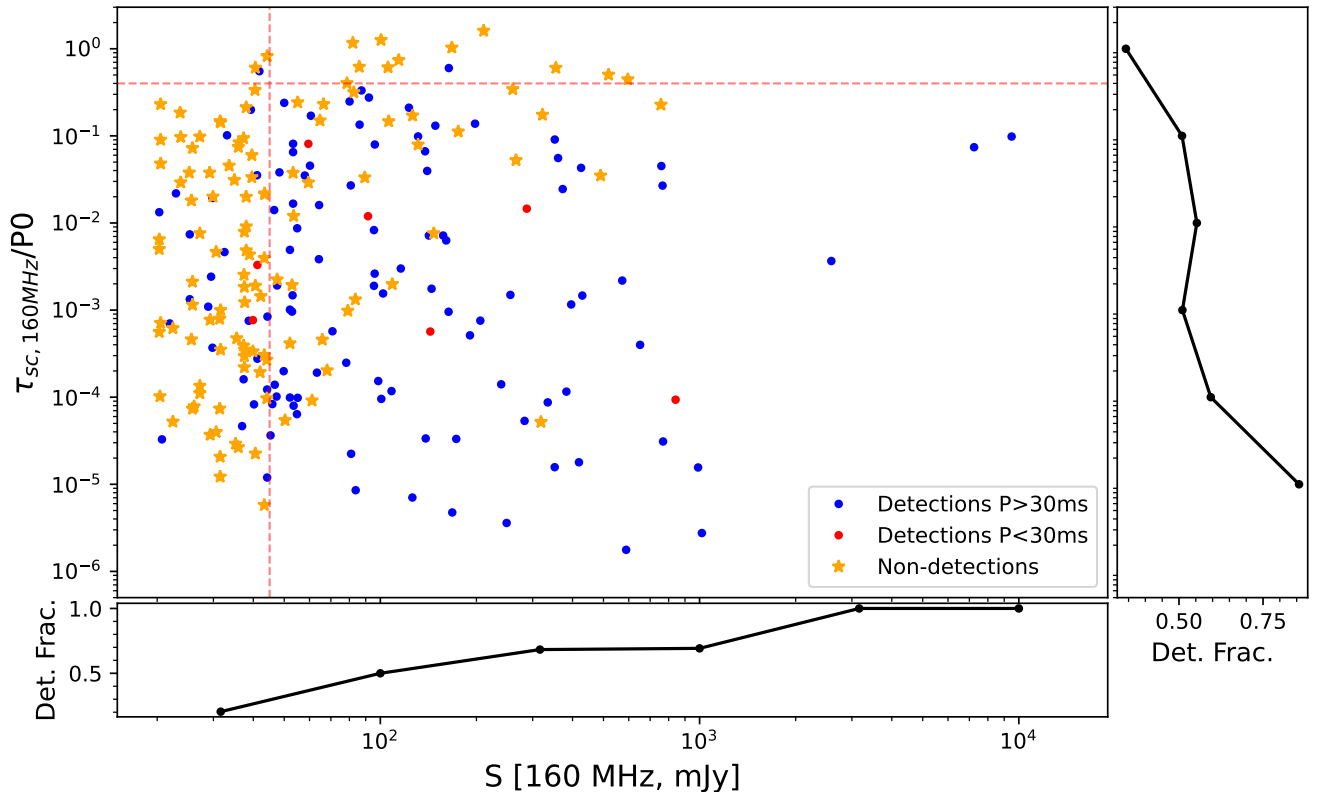


Figure 10. Center: Plot of scattering time at 160 MHz from the YMW16 model (J. M. Yao et al. 2017) normalized by the pulsar period versus the expected pulsar flux density at 160 MHz. Blue and red dots represent the detected pulsars with period above and below 30 ms, and orange stars represent the non-detected pulsars. The dashed vertical and horizontal line represent expected flux density value of 45 mJy and ratio of scattering time to pulsar period of 0.4 both at 160 MHz. The right and bottom panels represent the fraction of detected pulsars as a function of ratio of scattering time to period and expected flux density at 160 MHz respectively.

5. SUMMARY AND FUTURE OUTLOOK

We present the most comprehensive census of pulsars in the southern hemisphere at low frequencies with a SKA-Low prototype station. We have performed an all-sky census of pulsars, mainly southern sky, down to a sensitivity limit of ~ 20 mJy in modest observing times of 0.5-2 hrs. We measured flux densities of pulsars in five sub-bands in the frequency range of 50-250 MHz, allowing us not only to robustly validate the system sensitivity by comparing these measurements against other prior low-frequency pulsar census but also to improve spectral characterization of pulsars at low frequencies, and provide improved DM and RM measurements. Below is a summary of the most important results with concluding remarks.

1. We detected 120 pulsars in the frequency range of 50-250 MHz, many of which were detected in

multiple sub bands centered at $\sim 71, 131, 169, 197,$ and 225 MHz.

2. We report the lowest frequency detection of 29 pulsars, which includes 23 pulsars below 150 MHz, and five pulsars, namely J1057-5226, J1116-4112, J1430-6623, J1456-6843, and J1534-5350, detected below 100 MHz.
3. Multi-band pulse profiles are provided for all census pulsars, where 72 and 36 pulsars show profiles with 1 and 2 components, respectively. Additionally, 11 pulsars have a visible presence of scattering at low frequencies.
4. Analysis of pulsars with PL spectra using our census measurement shows that the mean spectral index is -1.78 ± 0.17 , consistent with the results of F. Jankowski et al. (2018). Moreover, 52 pulsars have a turnover at low frequencies with a mean

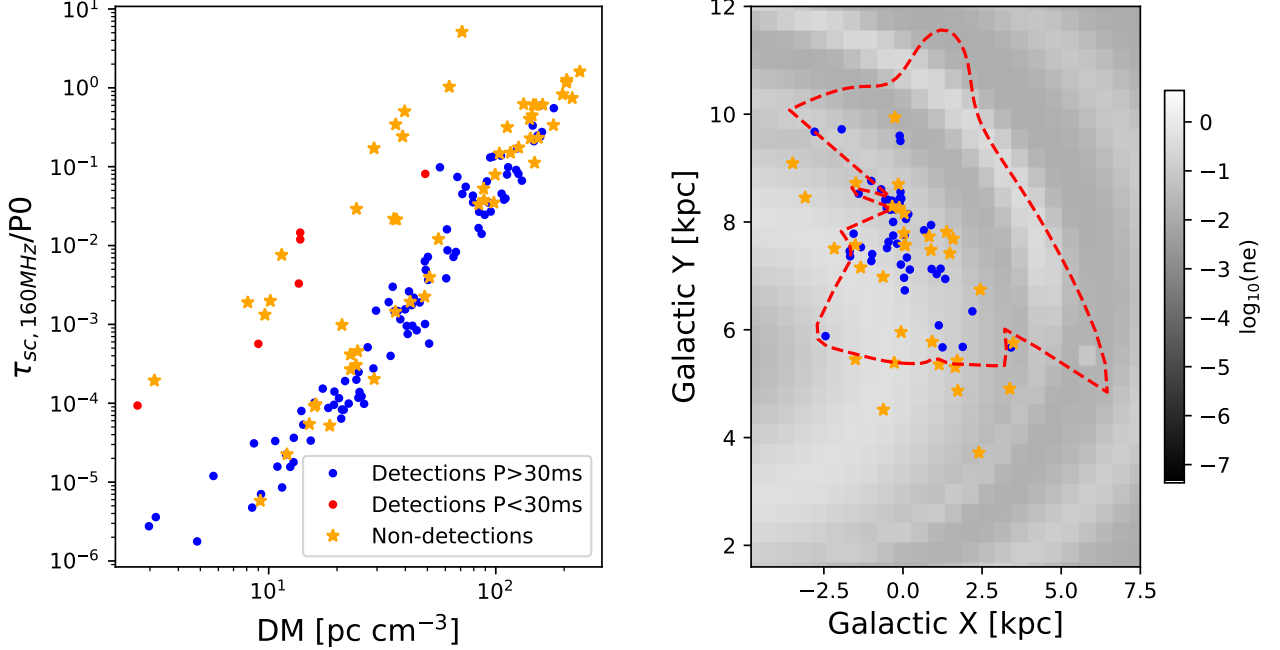


Figure 11. Left: Normalized scattering time in units of pulse period versus the pulsar DM. Right: The grey-scale represent the electron density model of YMW16 in the Galactic plane. Blue points and orange stars represent pulsars distance derived from YMW16 model for the detected and undetected pulsars of census respectively, for pulsars with distance to Galactic plane less than 300 pc. The dotted red line is a contour of DM 150 pc cm^{-3} . Only pulsars with expected flux density $> 40 \text{ mJy}$ at 160 MHz are plotted.

turnover frequency of 115 ± 10 , consistent with results from V. A. Izvekova et al. (1981). For pulsars with PLH, the high-frequency cutoff occurs around 1 GHz, consistent with the predictions of J. Kijak et al. (2007).

5. Due to the high precision and sensitivity of low-frequency observations to pulsar DM and variation due to the change in LOS, we provide improved DM measurement for 110 pulsars with a median absolute offset with respect to ATNF values of 0.1 pc cm^{-3} with the most notable DM change of $-0.85, -0.83, 0.76,$ and 0.59 pc cm^{-3} in PSR J1711-5350, J1240-4124, J0856-6137, and J1418-3921 respectively.
6. Using these DM variation we model the fluctuation of electron density in the ISM, where we obtain the relation $|\frac{dDM}{dt}| = 0.0008 \times DM_{\text{pc cm}^{-3}}^{0.64 \pm 0.18} \text{ pc cm}^{-3} \text{ yr}^{-1}$ which is slightly steeper than the result of (G. Hobbs et al. 2004) but consistent with P. Kumar et al. (2025) obtained below 100 MHz. This may suggest that the turbulence in ISM is higher at low frequencies.
7. We also performed RM-synthesis on our census pulsars, where we obtained RM measurements

for 40 pulsars, mostly consistent with the prior values reported at higher frequencies. However, for PSR J2155-3118, J1543-0630, J1825-0935, and J0922+0638, we obtained improved RM measurements after rejecting the possibility of a change in RM due to variations in ionospheric RMs. For PSR J1453-6413, we also obtained a phase-resolved variation in RM.

This study offers a compelling demonstration of the pulsar and ISM science that will be enabled by the future SKA-Low telescope. Since many of the detections reported here are the first at frequencies below 150 MHz, these data are particularly valuable for exploring spectral turnover behavior in pulsar emission. With the enhanced sensitivity of SKA-Low and observations of a larger sample of pulsars, spectral modeling can be extended across a broader population. This dataset can be used to improve existing pulsar population models, which will be valuable for future pulsar surveys aimed at searching for new pulsars with SKA-Low. Moreover, the variation in pulsar DM due to the ISM and RM due to the ionosphere presented in this work demonstrates how low-frequency monitoring of pulsars can be gainfully employed to study and characterize the ISM and ionosphere. This can easily be achieved by the multi-

beaming and sub-array capabilities of SKA-Low, by taking simultaneous observations of many pulsars.

ACKNOWLEDGMENTS

We thank the referee for constructive suggestions. EDA2 is hosted by the MWA under an agreement via the MWA External Instruments Policy. This scientific work makes use of the Murchison Radio astronomy Observatory, operated by CSIRO. We acknowledge the Wajarri Yamatji people as the traditional owners of the Observa-

tory site. This work was further supported by funding from the Australian Government and the Government of Western Australia. The acquisition system was designed and purchased by INAF/Oxford University and the RX chain was design by INAF, as part of the SKA design and prototyping program.

Software: astropy (Astropy Collaboration et al. 2013, 2018, 2022), numpy ((C. R. Harris et al. 2020)), matplotlib (J. D. Hunter 2007), scipy (P. Virtanen et al. 2020)

REFERENCES

- Alam, M. F., Arzoumanian, Z., Baker, P. T., et al. 2021, ApJS, 252, 4, doi: [10.3847/1538-4365/abc6a0](https://doi.org/10.3847/1538-4365/abc6a0)
- Alken, P., Thébaud, E., Beggan, C. D., et al. 2021, Earth, Planets and Space, 73, doi: [10.1186/s40623-020-01288-x](https://doi.org/10.1186/s40623-020-01288-x)
- Aloisi, R. J., Cruz, A., Daniels, L., et al. 2019, ApJ, 875, 19, doi: [10.3847/1538-4357/ab0d21](https://doi.org/10.3847/1538-4357/ab0d21)
- Armstrong, J. W., Rickett, B. J., & Spangler, S. R. 1995, ApJ, 443, 209, doi: [10.1086/175515](https://doi.org/10.1086/175515)
- Astropy Collaboration, Robitaille, T. P., Tollerud, E. J., et al. 2013, A&A, 558, A33, doi: [10.1051/0004-6361/201322068](https://doi.org/10.1051/0004-6361/201322068)
- Astropy Collaboration, Price-Whelan, A. M., Sipőcz, B. M., et al. 2018, AJ, 156, 123, doi: [10.3847/1538-3881/aabc4f](https://doi.org/10.3847/1538-3881/aabc4f)
- Astropy Collaboration, Price-Whelan, A. M., Lim, P. L., et al. 2022, ApJ, 935, 167, doi: [10.3847/1538-4357/ac7c74](https://doi.org/10.3847/1538-4357/ac7c74)
- Backer, D. C., Hama, S., van Hook, S., & Foster, R. S. 1993, ApJ, 404, 636, doi: [10.1086/172317](https://doi.org/10.1086/172317)
- Bansal, K., Taylor, G. B., Stovall, K., & Dowell, J. 2019, ApJ, 875, 146, doi: [10.3847/1538-4357/ab0d8f](https://doi.org/10.3847/1538-4357/ab0d8f)
- Bartel, N., Sieber, W., & Wielebinski, R. 1978, A&A, 68, 361
- Basu, R., Mitra, D., & Melikidze, G. I. 2021, ApJ, 917, 48, doi: [10.3847/1538-4357/ac0828](https://doi.org/10.3847/1538-4357/ac0828)
- Bates, S. D., Lorimer, D. R., & Verbiest, J. P. W. 2013, MNRAS, 431, 1352, doi: [10.1093/mnras/stt257](https://doi.org/10.1093/mnras/stt257)
- Bell, M. E., Murphy, T., Johnston, S., et al. 2016, Monthly Notices of the Royal Astronomical Society, 461, 908, doi: [10.1093/mnras/stw1293](https://doi.org/10.1093/mnras/stw1293)
- Bhat, N. D. R., Cordes, J. M., Camilo, F., Nice, D. J., & Lorimer, D. R. 2004, ApJ, 605, 759, doi: [10.1086/382680](https://doi.org/10.1086/382680)
- Bhat, N. D. R., Swainston, N. A., McSweeney, S. J., et al. 2023, PASA, 40, e020, doi: [10.1017/pasa.2023.18](https://doi.org/10.1017/pasa.2023.18)
- Bhattacharyya, B., Cooper, S., Malenta, M., et al. 2016, ApJ, 817, 130, doi: [10.3847/0004-637X/817/2/130](https://doi.org/10.3847/0004-637X/817/2/130)
- Bilous, A. V., Kondratiev, V. I., Kramer, M., et al. 2016, A&A, 591, A134, doi: [10.1051/0004-6361/201527702](https://doi.org/10.1051/0004-6361/201527702)
- Bilous, A. V., Bondonno, L., Kondratiev, V. I., et al. 2020, A&A, 635, A75, doi: [10.1051/0004-6361/201936627](https://doi.org/10.1051/0004-6361/201936627)
- Bondonno, L., Griebmeier, J. M., Theureau, G., et al. 2020, A&A, 635, A76, doi: [10.1051/0004-6361/201936829](https://doi.org/10.1051/0004-6361/201936829)
- Bondonno, L., Griebmeier, J. M., Theureau, G., et al. 2021, A&A, 652, A34, doi: [10.1051/0004-6361/202039339](https://doi.org/10.1051/0004-6361/202039339)
- Brentjens, M. A., & de Bruyn, A. G. 2005, A&A, 441, 1217, doi: [10.1051/0004-6361:20052990](https://doi.org/10.1051/0004-6361:20052990)
- Burn, B. J. 1966, MNRAS, 133, 67, doi: [10.1093/mnras/133.1.67](https://doi.org/10.1093/mnras/133.1.67)
- Caiazzo, M., et al. 2017, Tech. rep., Tech. Rep. SKA-TEL-SKO-0000008 (SKA Organisation)
- Chatterjee, S., Goss, W. M., & Brisken, W. F. 2005, ApJL, 634, L101, doi: [10.1086/498822](https://doi.org/10.1086/498822)
- Coles, W. A., Kerr, M., Shannon, R. M., et al. 2015, ApJ, 808, 113, doi: [10.1088/0004-637X/808/2/113](https://doi.org/10.1088/0004-637X/808/2/113)
- Cordes, J. M. 1978, ApJ, 222, 1006, doi: [10.1086/156218](https://doi.org/10.1086/156218)
- Costa, M. E., McCulloch, P. M., & Hamilton, P. A. 1991, MNRAS, 252, 13, doi: [10.1093/mnras/252.1.13](https://doi.org/10.1093/mnras/252.1.13)
- Crowter, K., Stairs, I. H., McPhee, C. A., et al. 2020, MNRAS, 495, 3052, doi: [10.1093/mnras/staa933](https://doi.org/10.1093/mnras/staa933)
- Dai, S., Hobbs, G., Manchester, R. N., et al. 2015, MNRAS, 449, 3223, doi: [10.1093/mnras/stv508](https://doi.org/10.1093/mnras/stv508)
- Deller, A. T., Tingay, S. J., Bailes, M., & Reynolds, J. E. 2009, ApJ, 701, 1243, doi: [10.1088/0004-637X/701/2/1243](https://doi.org/10.1088/0004-637X/701/2/1243)
- Demorest, P. B., Ferdman, R. D., Gonzalez, M. E., et al. 2013, ApJ, 762, 94, doi: [10.1088/0004-637X/762/2/94](https://doi.org/10.1088/0004-637X/762/2/94)
- Dewey, R. J., Taylor, J. H., Weisberg, J. M., & Stokes, G. H. 1985, ApJL, 294, L25, doi: [10.1086/184502](https://doi.org/10.1086/184502)
- Donner, J. Y., Verbiest, J. P. W., Tiburzi, C., et al. 2019, A&A, 624, A22, doi: [10.1051/0004-6361/201834059](https://doi.org/10.1051/0004-6361/201834059)
- Dowell, J., Ray, P. S., Taylor, G. B., et al. 2013, ApJL, 775, L28, doi: [10.1088/2041-8205/775/1/L28](https://doi.org/10.1088/2041-8205/775/1/L28)

- Fomalont, E. B., Goss, W. M., Lyne, A. G., Manchester, R. N., & Justtanont, K. 1992, MNRAS, 258, 497, doi: [10.1093/mnras/258.3.497](https://doi.org/10.1093/mnras/258.3.497)
- Frail, D. A., Jagannathan, P., Mooley, K. P., & Intema, H. T. 2016, ApJ, 829, 119, doi: [10.3847/0004-637X/829/2/119](https://doi.org/10.3847/0004-637X/829/2/119)
- Gentile, P. A., McLaughlin, M. A., Demorest, P. B., et al. 2018, ApJ, 862, 47, doi: [10.3847/1538-4357/aac9c9](https://doi.org/10.3847/1538-4357/aac9c9)
- Gitika, P., Bailes, M., Shannon, R. M., et al. 2023, MNRAS, 526, 3370, doi: [10.1093/mnras/stad2841](https://doi.org/10.1093/mnras/stad2841)
- Gould, D. M., & Lyne, A. G. 1998, MNRAS, 301, 235, doi: [10.1046/j.1365-8711.1998.02018.x](https://doi.org/10.1046/j.1365-8711.1998.02018.x)
- Grigg, D., Tingay, S., Prabu, S., Sokolowski, M., & Indermuehle, B. 2025, PASA, 42, e015, doi: [10.1017/pasa.2024.136](https://doi.org/10.1017/pasa.2024.136)
- Han, J., Wang, C., Xu, J., & Han, J.-L. 2016, Research in Astronomy and Astrophysics, 16, 159, doi: [10.1088/1674-4527/16/10/159](https://doi.org/10.1088/1674-4527/16/10/159)
- Han, J. L., & Tian, W. W. 1999, A&AS, 136, 571, doi: [10.1051/aas:1999234](https://doi.org/10.1051/aas:1999234)
- Harris, C. R., Millman, K. J., van der Walt, S. J., et al. 2020, Nature, 585, 357, doi: [10.1038/s41586-020-2649-2](https://doi.org/10.1038/s41586-020-2649-2)
- Haslam, C. G. T., Salter, C. J., Stoffel, H., & Wilson, W. E. 1982, A&AS, 47, 1
- Heald, G., Braun, R., & Edmonds, R. 2009, A&A, 503, 409, doi: [10.1051/0004-6361/200912240](https://doi.org/10.1051/0004-6361/200912240)
- Hemberger, D. A., & Stinebring, D. R. 2008, ApJL, 674, L37, doi: [10.1086/528985](https://doi.org/10.1086/528985)
- Hewish, A., Bell, S. J., Pilkington, J. D. H., Scott, P. F., & Collins, R. A. 1968, Nature, 217, 709, doi: [10.1038/217709a0](https://doi.org/10.1038/217709a0)
- Hobbs, G., Lorimer, D. R., Lyne, A. G., & Kramer, M. 2005, MNRAS, 360, 974, doi: [10.1111/j.1365-2966.2005.09087.x](https://doi.org/10.1111/j.1365-2966.2005.09087.x)
- Hobbs, G., Lyne, A. G., Kramer, M., Martin, C. E., & Jordan, C. 2004, MNRAS, 353, 1311
- Hotan, A. W., van Straten, W., & Manchester, R. N. 2004, PASA, 21, 302, doi: [10.1071/AS04022](https://doi.org/10.1071/AS04022)
- Hunter, J. D. 2007, Computing in Science & Engineering, 9, 90, doi: [10.1109/MCSE.2007.55](https://doi.org/10.1109/MCSE.2007.55)
- Izvekova, V. A., Kuzmin, A. D., Malofeev, V. M., & Shitov, I. P. 1981, Ap&SS, 45, doi: [10.1007/BF00654022](https://doi.org/10.1007/BF00654022)
- Jankowski, F., van Straten, W., Keane, E. F., et al. 2018, MNRAS, 473, 4436, doi: [10.1093/mnras/stx2476](https://doi.org/10.1093/mnras/stx2476)
- Janssen, G., Hobbs, G., McLaughlin, M., et al. 2015, in Advancing Astrophysics with the Square Kilometre Array (AASKA14), 37, doi: [10.22323/1.215.0037](https://doi.org/10.22323/1.215.0037)
- Johnston, S., Karastergiou, A., & Willett, K. 2006, MNRAS, 369, 1916, doi: [10.1111/j.1365-2966.2006.10440.x](https://doi.org/10.1111/j.1365-2966.2006.10440.x)
- Johnston, S., & Kerr, M. 2018, MNRAS, 474, 4629, doi: [10.1093/mnras/stx3095](https://doi.org/10.1093/mnras/stx3095)
- Johnston, S., Lyne, A. G., Manchester, R. N., et al. 1992, MNRAS, 255, 401, doi: [10.1093/mnras/255.3.401](https://doi.org/10.1093/mnras/255.3.401)
- Johnston, S., Lorimer, D. R., Harrison, P. A., et al. 1993, Nature, 361, 613, doi: [10.1038/361613a0](https://doi.org/10.1038/361613a0)
- Johnston, S., Sobey, C., Dai, S., et al. 2021, MNRAS, 502, 1253, doi: [10.1093/mnras/stab095](https://doi.org/10.1093/mnras/stab095)
- Keith, M. J., Johnston, S., Levin, L., & Bailes, M. 2011, MNRAS, 416, 346, doi: [10.1111/j.1365-2966.2011.19041.x](https://doi.org/10.1111/j.1365-2966.2011.19041.x)
- Kijak, J., Gupta, Y., & Krzeszowski, K. 2007, A&A, 462, 699, doi: [10.1051/0004-6361:20066125](https://doi.org/10.1051/0004-6361:20066125)
- Kijak, J., Kramer, M., Wielebinski, R., & Jessner, A. 1998, A&AS, 127, 153, doi: [10.1051/aas:1998340](https://doi.org/10.1051/aas:1998340)
- Kirsten, F., Bhat, N. D. R., Meyers, B. W., et al. 2019, ApJ, 874, 179, doi: [10.3847/1538-4357/ab0c05](https://doi.org/10.3847/1538-4357/ab0c05)
- Kondratiev, V. I., Verbiest, J. P. W., Hessels, J. W. T., et al. 2016, A&A, 585, A128, doi: [10.1051/0004-6361/201527178](https://doi.org/10.1051/0004-6361/201527178)
- Kouwenhoven, M. L. A. 2000, A&AS, 145, 243, doi: [10.1051/aas:2000240](https://doi.org/10.1051/aas:2000240)
- Kramer, M., Jessner, A., Doroshenko, O., & Wielebinski, R. 1997, ApJ, 488, 364, doi: [10.1086/304706](https://doi.org/10.1086/304706)
- Kramer, M., Lange, C., Lorimer, D. R., et al. 1999, ApJ, 526, 957, doi: [10.1086/308042](https://doi.org/10.1086/308042)
- Kramer, M., Xilouris, K. M., Lorimer, D. R., et al. 1998, ApJ, 501, 270, doi: [10.1086/305790](https://doi.org/10.1086/305790)
- Kravtsov, I. P., Zakharenko, V. V., Ulyanov, O. M., et al. 2022, MNRAS, 512, 4324, doi: [10.1093/mnras/stab3369](https://doi.org/10.1093/mnras/stab3369)
- Kumar, P., Taylor, G. B., Stovall, K., Dowell, J., & White, S. M. 2025, ApJ, 982, 132, doi: [10.3847/1538-4357/adb97a](https://doi.org/10.3847/1538-4357/adb97a)
- Kumar, P., White, S. M., Stovall, K., Dowell, J., & Taylor, G. B. 2022, MNRAS, 511, 3937, doi: [10.1093/mnras/stac316](https://doi.org/10.1093/mnras/stac316)
- Kuniyoshi, M., Verbiest, J. P. W., Lee, K. J., et al. 2015, MNRAS, 453, 828, doi: [10.1093/mnras/stv1604](https://doi.org/10.1093/mnras/stv1604)
- Kuzmin, A. D., & Losovsky, B. Y. 2001, A&A, 368, 230, doi: [10.1051/0004-6361:20000507](https://doi.org/10.1051/0004-6361:20000507)
- Lam, M. T., Cordes, J. M., Chatterjee, S., et al. 2016, ApJ, 821, 66, doi: [10.3847/0004-637X/821/1/66](https://doi.org/10.3847/0004-637X/821/1/66)
- Lazarus, P., Brazier, A., Hessels, J. W. T., et al. 2015, ApJ, 812, 81, doi: [10.1088/0004-637X/812/1/81](https://doi.org/10.1088/0004-637X/812/1/81)
- Lee, C. P., Bhat, N. D. R., Sokolowski, M., et al. 2022, PASA, 39, e042, doi: [10.1017/pasa.2022.40](https://doi.org/10.1017/pasa.2022.40)
- Liddle, A. R. 2007, MNRAS, 377, L74, doi: [10.1111/j.1745-3933.2007.00306.x](https://doi.org/10.1111/j.1745-3933.2007.00306.x)

- Lorimer, D. R., & Kramer, M. 2004, Cambridge Observing Handbooks for Research Astronomers, Vol. 4, Handbook of Pulsar Astronomy (Cambridge University Press).
<https://books.google.com/books?id=OZ8tdN6qJcsC>
- Lorimer, D. R., Yates, J. A., Lyne, A. G., & Gould, D. M. 1995a, MNRAS, 273, 411, doi: [10.1093/mnras/273.2.411](https://doi.org/10.1093/mnras/273.2.411)
- Lorimer, D. R., Nicastro, L., Lyne, A. G., et al. 1995b, ApJ, 439, 933, doi: [10.1086/175230](https://doi.org/10.1086/175230)
- Lorimer, D. R., Xilouris, K. M., Fruchter, A. S., et al. 2005, MNRAS, 359, 1524, doi: [10.1111/j.1365-2966.2005.09005.x](https://doi.org/10.1111/j.1365-2966.2005.09005.x)
- Lyne, A. G., & Manchester, R. N. 1988, Monthly Notices of the Royal Astronomical Society, 234, 477, doi: [10.1093/mnras/234.3.477](https://doi.org/10.1093/mnras/234.3.477)
- Lyne, A. G., Manchester, R. N., Lorimer, D. R., et al. 1998, MNRAS, 295, 743, doi: [10.1046/j.1365-8711.1998.01144.x](https://doi.org/10.1046/j.1365-8711.1998.01144.x)
- Malofeev, V. M. 1993, Astronomy Letters, 19, 138
- Malofeev, V. M., Malov, O. I., & Shchegoleva, N. V. 2000, Astronomy Reports, 44, 436, doi: [10.1134/1.163868](https://doi.org/10.1134/1.163868)
- Malov, I. F. 1979, Soviet Ast., 23, 205
- Manchester, R. N., Hobbs, G. B., Teoh, A., & Hobbs, M. 2005, AJ, 129, 1993, doi: [10.1086/428488](https://doi.org/10.1086/428488)
- Manchester, R. N., & Johnston, S. 1995, ApJL, 441, L65, doi: [10.1086/187791](https://doi.org/10.1086/187791)
- Manchester, R. N., Lyne, A. G., Taylor, J. H., et al. 1978, MNRAS, 185, 409, doi: [10.1093/mnras/185.2.409](https://doi.org/10.1093/mnras/185.2.409)
- Manchester, R. N., Lyne, A. G., D'Amico, N., et al. 1996, MNRAS, 279, 1235, doi: [10.1093/mnras/279.4.1235](https://doi.org/10.1093/mnras/279.4.1235)
- Manchester, R. N., Hobbs, G., Bailes, M., et al. 2013, PASA, 30, e017, doi: [10.1017/pasa.2012.017](https://doi.org/10.1017/pasa.2012.017)
- McEwen, A. E., Spiewak, R., Swiggum, J. K., et al. 2020, ApJ, 892, 76, doi: [10.3847/1538-4357/ab75e2](https://doi.org/10.3847/1538-4357/ab75e2)
- McGary, R. S., Briskin, W. F., Fruchter, A. S., Goss, W. M., & Thorsett, S. E. 2001, AJ, 121, 1192, doi: [10.1086/318739](https://doi.org/10.1086/318739)
- McLean, A. I. O. 1973, MNRAS, 165, 133, doi: [10.1093/mnras/165.2.133](https://doi.org/10.1093/mnras/165.2.133)
- Mignani, R. P., Paladino, R., Rudak, B., et al. 2017, ApJL, 851, L10, doi: [10.3847/2041-8213/aa9c3e](https://doi.org/10.3847/2041-8213/aa9c3e)
- Mikhailov, K., & van Leeuwen, J. 2016, A&A, 593, A21, doi: [10.1051/0004-6361/201628348](https://doi.org/10.1051/0004-6361/201628348)
- Murphy, T., Kaplan, D. L., Bell, M. E., et al. 2017, PASA, 34, e020, doi: [10.1017/pasa.2017.13](https://doi.org/10.1017/pasa.2017.13)
- Naldi, G., Mattana, A., Pastore, S., et al. 2017, Journal of Astronomical Instrumentation, 6, 1641014, doi: [10.1142/S2251171716410142](https://doi.org/10.1142/S2251171716410142)
- Noutsos, A., Karastergiou, A., Kramer, M., Johnston, S., & Stappers, B. W. 2009, MNRAS, 396, 1559, doi: [10.1111/j.1365-2966.2009.14806.x](https://doi.org/10.1111/j.1365-2966.2009.14806.x)
- Noutsos, A., Sobey, C., Kondratiev, V. I., et al. 2015, A&A, 576, A62, doi: [10.1051/0004-6361/201425186](https://doi.org/10.1051/0004-6361/201425186)
- Ocker, S. K., Cordes, J. M., Chatterjee, S., & Dolch, T. 2021, ApJ, 922, 233, doi: [10.3847/1538-4357/ac2b28](https://doi.org/10.3847/1538-4357/ac2b28)
- Olszanski, T. E. E., Mitra, D., & Rankin, J. M. 2019, MNRAS, 489, 1543, doi: [10.1093/mnras/stz2172](https://doi.org/10.1093/mnras/stz2172)
- Posselt, B., Karastergiou, A., Johnston, S., et al. 2023, MNRAS, 520, 4582, doi: [10.1093/mnras/stac3383](https://doi.org/10.1093/mnras/stac3383)
- Price, D. C., Flynn, C., & Deller, A. 2021, PASA, 38, e038, doi: [10.1017/pasa.2021.33](https://doi.org/10.1017/pasa.2021.33)
- Qiao, G., Manchester, R. N., Lyne, A. G., & Gould, D. M. 1995, MNRAS, 274, 572, doi: [10.1093/mnras/274.2.572](https://doi.org/10.1093/mnras/274.2.572)
- Rankin, J. M. 1983, ApJ, 274, 359, doi: [10.1086/161451](https://doi.org/10.1086/161451)
- Sanidas, S., Cooper, S., Bassa, C. G., et al. 2019, A&A, 626, A104, doi: [10.1051/0004-6361/201935609](https://doi.org/10.1051/0004-6361/201935609)
- Sayer, R. W., Nice, D. J., & Taylor, J. H. 1997, ApJ, 474, 426, doi: [10.1086/303446](https://doi.org/10.1086/303446)
- Schnitzeler, D. H. F. M., Katgert, P., & de Bruyn, A. G. 2009, A&A, 494, 611, doi: [10.1051/0004-6361:20078912](https://doi.org/10.1051/0004-6361:20078912)
- Seiradakis, J. H., Gil, J. A., Graham, D. A., et al. 1995, A&AS, 111, 205
- Sharan, R., Bhattacharyya, B., Kumari, S., Roy, J., & Ghosh, A. 2024, ApJ, 971, 174, doi: [10.3847/1538-4357/ad55c8](https://doi.org/10.3847/1538-4357/ad55c8)
- Shrauner, J. A., Taylor, J. H., & Woan, G. 1998, ApJ, 509, 785, doi: [10.1086/306510](https://doi.org/10.1086/306510)
- Sieber, W. 1973, A&A, 28, 237
- Skrzypczak, A., Basu, R., Mitra, D., et al. 2018, ApJ, 854, 162, doi: [10.3847/1538-4357/aaa758](https://doi.org/10.3847/1538-4357/aaa758)
- Sobey, C., Bilous, A. V., Griefmeier, J. M., et al. 2019, MNRAS, 484, 3646, doi: [10.1093/mnras/stz214](https://doi.org/10.1093/mnras/stz214)
- Sokolowski, M., Kumar, P., Dhavali, S., et al. 2025, arXiv e-prints, arXiv:2506.07422, doi: [10.48550/arXiv.2506.07422](https://doi.org/10.48550/arXiv.2506.07422)
- Sokolowski, M., Price, D. C., & Wayth, B., R. 2022a, in 2022 3rd URSI Atlantic and Asia Pacific Radio Science Meeting (AT-AP-RASC, 1, doi: [10.23919/AT-AP-RASC54737.2022.9814380](https://doi.org/10.23919/AT-AP-RASC54737.2022.9814380)
- Sokolowski, M., Tingay, S. J., Davidson, D. B., et al. 2022b, PASA, 39, e015, doi: [10.1017/pasa.2021.63](https://doi.org/10.1017/pasa.2021.63)
- Sotomayor-Beltran, C., Sobey, C., Hessels, J. W. T., et al. 2013, A&A, 552, A58, doi: [10.1051/0004-6361/201220728](https://doi.org/10.1051/0004-6361/201220728)
- Spiewak, R., Bailes, M., Miles, M. T., et al. 2022, PASA, 39, e027, doi: [10.1017/pasa.2022.19](https://doi.org/10.1017/pasa.2022.19)
- Stairs, I. H., Thorsett, S. E., & Camilo, F. 1999, ApJS, 123, 627, doi: [10.1086/313245](https://doi.org/10.1086/313245)

- Stappers, B. W., Karappusamy, R., & Hessels, J. W. T. 2008, in *American Institute of Physics Conference Series*, Vol. 983, *40 Years of Pulsars: Millisecond Pulsars, Magnetars and More*, ed. C. Bassa, Z. Wang, A. Cumming, & V. M. Kaspi (AIP), 593–597, doi: [10.1063/1.2900304](https://doi.org/10.1063/1.2900304)
- Stokes, G. H., Taylor, J. H., Welsberg, J. M., & Dewey, R. J. 1985, *Nature*, 317, 787, doi: [10.1038/317787a0](https://doi.org/10.1038/317787a0)
- Stovall, K., Ray, P. S., Blythe, J., et al. 2015, *ApJ*, 808, 156, doi: [10.1088/0004-637X/808/2/156](https://doi.org/10.1088/0004-637X/808/2/156)
- Sutinjo, A. T., Sokolowski, M., Kovaleva, M., et al. 2021, *A&A*, 646, A143, doi: [10.1051/0004-6361/202039445](https://doi.org/10.1051/0004-6361/202039445)
- Swainston, N. A., Lee, C. P., McSweeney, S. J., & Bhat, N. D. R. 2022, *PASA*, 39, e056, doi: [10.1017/pasa.2022.52](https://doi.org/10.1017/pasa.2022.52)
- Taylor, G. B., Ellingson, S. W., Kassim, N. E., et al. 2012, *Journal of Astronomical Instrumentation*, 1, 1250004, doi: [10.1142/S2251171712500043](https://doi.org/10.1142/S2251171712500043)
- Taylor, J. H., Manchester, R. N., & Lyne, A. G. 1993, *ApJS*, 88, 529, doi: [10.1086/191832](https://doi.org/10.1086/191832)
- Tiburzi, C., Shaifullah, G. M., Bassa, C. G., et al. 2021, *A&A*, 647, A84, doi: [10.1051/0004-6361/202039846](https://doi.org/10.1051/0004-6361/202039846)
- Tingay, S. J., Goetze, R., Bowman, J. D., et al. 2013, *PASA*, 30, e007, doi: [10.1017/pasa.2012.007](https://doi.org/10.1017/pasa.2012.007)
- Toscano, M., Bailes, M., Manchester, R. N., & Sandhu, J. S. 1998, *ApJ*, 506, 863, doi: [10.1086/306282](https://doi.org/10.1086/306282)
- Tremblay, S. E., Ord, S. M., Bhat, N. D. R., et al. 2015, *PASA*, 32, e005, doi: [10.1017/pasa.2015.6](https://doi.org/10.1017/pasa.2015.6)
- Tyul'bashev, S. A., Tyul'bashev, V. S., Oreshko, V. V., & Logvinenko, S. V. 2016, *Astronomy Reports*, 60, 220, doi: [10.1134/S1063772916020128](https://doi.org/10.1134/S1063772916020128)
- van Haarlem, M. P., Wise, M. W., Gunst, A. W., et al. 2013, *A&A*, 556, A2, doi: [10.1051/0004-6361/201220873](https://doi.org/10.1051/0004-6361/201220873)
- van Ommen, T. D., D'Alessandro, F., Hamilton, P. A., & McCulloch, P. M. 1997, *MNRAS*, 287, 307, doi: [10.1093/mnras/287.2.307](https://doi.org/10.1093/mnras/287.2.307)
- van Straten, W., & Bailes, M. 2011, *PASA*, 28, 1, doi: [10.1071/AS10021](https://doi.org/10.1071/AS10021)
- van Straten, W., Demorest, P., & Osłowski, S. 2012, *Astronomical Research and Technology*, 9, 237. <https://arxiv.org/abs/1205.6276>
- Virtanen, P., Gommers, R., Oliphant, T. E., et al. 2020, *Nature Methods*, 17, 261, doi: [10.1038/s41592-019-0686-2](https://doi.org/10.1038/s41592-019-0686-2)
- von Hoensbroech, A., Lesch, H., & Kunzl, T. 1998, *A&A*, 336, 209, doi: [10.48550/arXiv.astro-ph/9804318](https://doi.org/10.48550/arXiv.astro-ph/9804318)
- von Hoensbroech, A., & Xilouris, K. M. 1997, *A&AS*, 126, 121
- Wang, C., Han, J. L., & Lai, D. 2011, *MNRAS*, 417, 1183, doi: [10.1111/j.1365-2966.2011.19333.x](https://doi.org/10.1111/j.1365-2966.2011.19333.x)
- Wang, P. F., Wang, C., & Han, J. L. 2015, *MNRAS*, 448, 771, doi: [10.1093/mnras/stu2765](https://doi.org/10.1093/mnras/stu2765)
- Wayth, R., Sokolowski, M., Broderick, J., et al. 2022, *Journal of Astronomical Telescopes, Instruments, and Systems*, 8, 011010, doi: [10.1117/1.JATIS.8.1.011010](https://doi.org/10.1117/1.JATIS.8.1.011010)
- Weisberg, J. M., Cordes, J. M., Lundgren, S. C., et al. 1999, *ApJS*, 121, 171, doi: [10.1086/313189](https://doi.org/10.1086/313189)
- Xie, Y.-W., Wang, J.-B., Hobbs, G., et al. 2019, *Research in Astronomy and Astrophysics*, 19, 103, doi: [10.1088/1674-4527/19/7/103](https://doi.org/10.1088/1674-4527/19/7/103)
- Xue, M., Ord, S. M., Tremblay, S. E., et al. 2019, *PASA*, 36, e025, doi: [10.1017/pasa.2019.19](https://doi.org/10.1017/pasa.2019.19)
- Xue, M., Bhat, N. D. R., Tremblay, S. E., et al. 2017, *PASA*, 34, e070, doi: [10.1017/pasa.2017.66](https://doi.org/10.1017/pasa.2017.66)
- Yao, J. M., Manchester, R. N., & Wang, N. 2017, *ApJ*, 835, 29, doi: [10.3847/1538-4357/835/1/29](https://doi.org/10.3847/1538-4357/835/1/29)
- Zakharenko, V. V., Vasylieva, I. Y., Konovalenko, A. A., et al. 2013, *MNRAS*, 431, 3624, doi: [10.1093/mnras/stt470](https://doi.org/10.1093/mnras/stt470)
- Zarka, P., Tagger, M., Denis, L., et al. 2015, in *2015 International Conference on Antenna Theory and Techniques (ICATT)*, 1–6, doi: [10.1109/ICATT.2015.7136773](https://doi.org/10.1109/ICATT.2015.7136773)
- Zhao, R.-S., Wu, X.-J., Yan, Z., et al. 2017, *ApJ*, 845, 156, doi: [10.3847/1538-4357/aa8170](https://doi.org/10.3847/1538-4357/aa8170)
- Zhao, R.-S., Yan, Z., Wu, X.-J., et al. 2019, *ApJ*, 874, 64, doi: [10.3847/1538-4357/ab05de](https://doi.org/10.3847/1538-4357/ab05de)

APPENDIX

A. PERIOD AND DISPERSION MEASURE OF PULSARS DETECTED BY EDA2

Table A1. Period and Dispersion measure of Pulsars detected by the EDA2

Name	Period (s)	DM _{ATNF} (pc cm ⁻³)	DM _{Epoch} ^{ATNF} (MJD)	DM _{EDA2} (pc cm ⁻³)	DM _{Epoch} ^{EDA2} (MJD)	S/N _{pdmf}	DM _{corr} (pc cm ⁻³)
J0034-0534*	0.00188	13.7652(0)	55000	13.7652(0)	60507	—	—
J0034-0721	0.94295	10.922(6)	56843	10.852(87)	60455	54.5	-0.07
J0038-2501	0.25693	5.71(0)	57474	5.59(8)	60482	10.8	-0.12
J0051+0423	0.35473	13.9(0)	49800	13.9(1)	60469	10.8	-0.03
J0151-0635	1.46466	25.7(0)	49347	25.9(1)	60494	15.4	0.24
J0152-1637	0.83274	11.9258(0)	56955	11.9758(805)	60518	88.4	0.05
J0206-4028	0.63055	12.9(120)	57600	12.98(9)	60522	32.0	0.08
J0304+1932	1.38758	15.6568(3)	56703	15.3768(13630)	60503	8.2	-0.28
J0401-7608	0.54525	21.7(10)	55000	21.98(3)	60507	12.7	0.28
J0418-4154	0.75712	24.325(9)	57600	24.435(65)	60503	18.4	0.11
J0437-4715*	0.00576	2.6448(0)	54500	2.6348(0)	60439	—	—
J0450-1248	0.43801	37.041(10)	49338	37.021(32)	60517	21.5	-0.02
J0452-1759	0.54894	39.903(3)	49289	39.873(49)	60526	37.9	-0.03
J0459-0210	1.13308	21.02(3)	50845	20.83(10)	60432	20.0	-0.19
J0520-2553	0.24164	33.77(3)	51216	33.79(2)	60503	10.7	0.02
J0525+1115	0.35444	79.418(13)	56703	79.348(152)	60507	8.7	-0.07
J0528+2200	3.74554	50.8695(13)	56747	50.7195(2285)	60517	15.3	-0.15
J0534+2200	0.03339	56.7712(2)	56703	56.7212(22)	60660	168.9	-0.05
J0630-2834	1.24442	34.425(1)	56706	34.225(238)	60422	159.8	-0.2
J0636-4549	1.9846	26.31(15)	52700	25.93(10)	60664	15.1	-0.38
J0729-1836	0.51016	61.293(10)	49720	61.253(136)	60503	9.5	-0.04
J0737-3039A*	0.0227	48.916(2)	58831	48.906(0)	60681	—	—
J0742-2822	0.16676	73.728(1)	55000	73.798(15)	60437	106.2	0.07
J0758-1528	0.68227	63.327(3)	49896	63.257(136)	60523	8.7	-0.07
J0820-1350	1.23813	40.938(3)	48904	40.868(118)	60436	123.3	-0.07
J0820-4114	0.54545	113.4(20)	57600	113.83(33)	60437	13.1	0.43
J0823+0159	0.86487	23.727(6)	49281	23.937(354)	60503	13.4	0.21
J0826+2637	0.53066	19.4763(1)	56747	19.5263(323)	60529	41.0	0.05
J0835-4510	0.08933	67.771(9)	55000	67.711(17)	60432	139.7	-0.06
J0837+0610	1.27377	12.864(0)	56864	12.914(77)	60480	196.5	0.05
J0837-4135	0.75163	147.2(1)	57600	147.29(7)	60506	48.5	0.09
J0855-3331	1.26754	86.635(16)	49886	86.725(186)	60445	16.9	0.09

Table A1 *continued*

Table A1 (*continued*)

Name	Period (s)	DM _{ATNF} (pc cm ⁻³)	DM _{Epoch} ^{ATNF} (MJD)	DM _{EDA2} (pc cm ⁻³)	DM _{Epoch} ^{EDA2} (MJD)	S/N _{pdmf}	DM _{corr} (pc cm ⁻³)
J0856-6137	0.96251	95.0(300)	57600	95.76(9)	60432	30.5	0.76
J0902-6325	0.66031	72.72(6)	43557	72.69(13)	60689	9.8	-0.03
J0905-6019	0.34085	91.4(40)	55191	91.67(4)	60508	9.0	0.27
J0908-1739	0.40163	15.879(2)	56980	15.929(42)	60431	16.1	0.05
J0922+0638	0.43063	27.2986(5)	56285	27.2786(411)	60436	48.3	-0.02
J0924-5302	0.74634	152.9(50)	57600	153.47(7)	60434	28.8	0.57
J0924-5814	0.73951	57.4(30)	57600	57.37(20)	60483	12.5	-0.03
J0942-5552	0.66439	180.16(2)	57600	179.97(6)	60438	25.4	-0.19
J0942-5657	0.80816	159.74(12)	57600	160.22(8)	60433	22.5	0.48
J0946+0951	1.09771	15.3184(9)	56779	15.3085(0)	60506	—	—
J0953+0755	0.25307	2.9693(0)	56285	2.9493(489)	60419	249.8	-0.02
J0955-5304	0.86212	156.9(20)	57600	156.62(6)	60511	13.6	-0.28
J0959-4809	0.67009	92.7(120)	57600	92.42(8)	60437	14.0	-0.28
J1001-5507	1.43663	130.32(17)	57600	130.24(49)	60439	23.1	-0.08
J1012-2337	2.51795	22.51(9)	49874	22.71(41)	60528	15.2	0.2
J1018-1642	1.80469	48.82(7)	49688	49.25(43)	60504	10.5	0.43
J1022+1001*	0.01645	10.255(0)	58968	10.245(0)	60431	—	—
J1041-1942	1.38637	33.777(10)	48738	33.627(748)	60436	9.9	-0.15
J1057-5226	0.19711	29.69(1)	55000	29.66(7)	60433	21.4	-0.03
J1059-5742	1.185	108.7(30)	57600	108.38(27)	60437	15.8	-0.32
J1112-6926	0.82049	148.4(100)	57600	148.47(6)	60504	14.0	0.07
J1116-4122	0.94316	40.53(3)	48383	40.47(5)	60531	37.8	-0.06
J1136+1551	1.18791	4.8407(3)	56687	4.8007(724)	60528	116.0	-0.04
J1202-5820	0.4528	145.41(19)	57600	145.95(9)	60510	17.0	0.54
J1224-6407	0.21648	97.686(4)	55000	97.836(23)	60435	15.6	0.15
J1225-5556	1.01845	125.835(7)	48660	126.195(283)	60507	8.3	0.36
J1239+2453	1.38245	9.2516(5)	56689	9.1716(1322)	60434	31.9	-0.08
J1239-6832	1.30192	94.3(30)	57600	94.01(12)	60436	12.4	-0.29
J1240-4124	0.51224	44.1(120)	43564	43.27(2)	60669	26.6	-0.83
J1311-1228	0.44752	36.214(8)	49667	36.194(44)	60510	17.7	-0.02
J1320-5359	0.27974	97.1(10)	55000	97.37(3)	60494	18.4	0.27
J1355-5153	0.6443	112.1(40)	57600	111.51(6)	60437	34.5	-0.59
J1418-3921	1.09681	60.49(1)	49014	61.08(9)	60467	18.5	0.59
J1430-6623	0.78544	65.102(4)	57600	65.062(76)	60495	36.6	-0.04
J1440-6344	0.45961	124.2(50)	57600	123.88(6)	60529	11.4	-0.32
J1453-6413	0.17949	71.248(2)	55000	71.088(17)	60433	131.4	-0.16
J1455-3330*	0.00799	13.5697(2)	58813	13.5697(0)	60510	—	—
J1456-6843	0.26338	8.613(4)	55000	8.603(0)	60450	—	—
J1507-4352	0.28676	48.7(50)	57600	49.15(1)	60525	46.5	0.45

Table A1 (*continued*)

Table A1 (*continued*)

Name	Period (s)	DM _{ATNF} (pc cm ⁻³)	DM _{Epoch} ^{ATNF} (MJD)	DM _{EDA2} (pc cm ⁻³)	DM _{Epoch} ^{EDA2} (MJD)	S/N _{pdm}	DM _{corr} (pc cm ⁻³)
J1510-4422	0.94387	84.0(700)	43557	84.32(9)	60527	23.5	0.32
J1527-3931	2.41761	48.8(60)	57600	48.66(23)	60437	17.5	-0.14
J1534-5334	1.36888	24.82(1)	57600	25.06(8)	60467	58.6	0.24
J1543+0929	0.74845	34.9758(16)	56780	35.0058(1135)	60453	22.2	0.03
J1543-0620	0.70906	18.3(20)	56842	18.37(6)	60502	32.2	0.07
J1544-5308	0.17855	35.16(7)	57600	35.06(2)	60671	10.6	-0.1
J1603-2712	0.77831	46.201(16)	49911	46.311(74)	60439	18.1	0.11
J1607-0032	0.42182	10.6823(1)	56843	10.6423(806)	60422	25.1	-0.04
J1614+0737	1.2068	21.3949(2)	56843	21.0649(1427)	60431	9.7	-0.33
J1645-0317	0.38769	35.7555(8)	56842	35.7355(370)	60427	442.5	-0.02
J1703-3241	1.21179	110.306(14)	50005	110.436(230)	60439	19.1	0.13
J1709-1640	0.65305	24.891(1)	56843	25.141(62)	60466	45.5	0.25
J1711-5350	0.89923	106.1(70)	57600	105.25(15)	60483	9.1	-0.85
J1720-1633	1.5656	44.83(3)	49686	45.12(15)	60526	11.6	0.29
J1720-2933	0.62045	42.64(3)	49863	42.54(14)	60506	14.8	-0.1
J1731-4744	0.82983	123.056(4)	55000	123.406(79)	60451	58.6	0.35
J1733-2228	0.87168	41.14(3)	48712	41.24(8)	60521	20.1	0.1
J1735-0724	0.41933	73.512(4)	49887	73.482(92)	60510	10.0	-0.03
J1751-4657	0.74235	20.4(40)	57600	20.58(7)	60430	45.4	0.18
J1752-2806	0.56256	50.372(8)	46483	50.342(53)	60436	239.2	-0.03
J1820-0427	0.59808	84.435(17)	57600	84.415(127)	60530	36.0	-0.02
J1823+0550	0.75291	66.775(3)	48713	66.815(59)	60451	13.9	0.04
J1823-3106	0.28405	50.245(4)	50093	50.265(73)	60523	14.3	0.02
J1825-0935	0.76902	19.3833(9)	56843	19.3233(735)	60427	23.5	-0.06
J1834-0426	0.29011	79.308(8)	49714	79.378(68)	60529	21.6	0.07
J1841+0912	0.38132	49.158(4)	56783	49.108(80)	60527	11.0	-0.05
J1844+1454	0.37546	41.4856(6)	56703	41.6356(738)	60518	12.8	0.15
J1900-2600	0.61221	37.994(5)	48891	37.824(117)	60419	45.0	-0.17
J1901+0156	0.28822	105.394(7)	49298	105.384(0)	60453	—	—
J1913-0440	0.82594	89.385(10)	46634	89.305(78)	60437	62.5	-0.08
J1916+0951	0.27025	60.953(6)	49910	60.923(38)	60511	10.6	-0.03
J1917+1353	0.19463	94.538(4)	49763	94.588(117)	60436	8.8	0.05
J1921+2153	1.3373	12.444(0)	56788	12.374(127)	60433	212.5	-0.07
J1929+00	1.1669	42.95(7)	49717	43.13(14)	60439	9.5	0.18
J1932+1059	0.22652	3.1832(1)	56781	3.1632(216)	60434	41.5	-0.02
J1935+1616	0.35874	158.521(3)	46434	158.671(52)	60522	25.8	0.15
J1943-1237	0.97243	28.918(15)	48717	29.058(94)	60429	23.5	0.14
J2018+2839	0.55795	14.1977(5)	57009	14.0477(805)	60527	42.4	-0.15
J2046-0421	1.54694	35.799(10)	48739	35.899(147)	60436	23.5	0.1

Table A1 *continued*

Table A1 (*continued*)

Name	Period (s)	DM _{ATNF} (pc cm ⁻³)	DM _{Epoch} ^{ATNF} (MJD)	DM _{EDA2} (pc cm ⁻³)	DM _{Epoch} ^{EDA2} (MJD)	S/N _{<i>pdm</i>}	DM _{corr} (pc cm ⁻³)
J2048-1616	1.96157	11.456(5)	46423	11.526(118)	60453	64.1	0.07
J2053-7200	0.34134	17.3(40)	57600	17.62(4)	60508	11.9	0.32
J2113+2754	1.20285	25.1111(1)	56784	25.2211(1162)	60482	11.4	0.11
J2145-0750*	0.01605	9.0008(13)	58751	9.0008(0)	60503	—	—
J2155-3118	1.03	14.8(0)	48714	14.8(0)	60433	34.1	-0.05
J2219+4754	0.53847	43.4975(5)	56842	43.4375(521)	60507	23.3	-0.06
J2256-1024*	0.00229	13.776(0)	55549	13.776(0)	60508	—	—
J2317+2149	1.44465	20.8696(3)	56687	20.7496(1776)	60436	14.0	-0.12
J2330-2005	1.64362	8.456(2)	56979	8.296(237)	60517	33.9	-0.16
J2346-0609	1.18146	22.504(19)	51021	22.784(145)	60502	9.4	0.28

S/N_{*pdm*} is the signal-to-noise ratio found by *pdm* for the optimal DM, DM_{corr} is the correction in dispersion measure obtained using *pdm*

Pulsar with * indicate MSPs.

B. FLUX DENSITY AND PULSE WIDTHS

Table B2. Mean flux density (S_ν) of pulsars detected in this census, along with pulse width measurements.

Name	ν (MHZ)	BW (MHz)	W ₅₀ (phase)	W ₁₀ (phase)	T (s)	S/N	S _{ν} (mJy)
J0034-0534	71.1	33.59	0.465	0.86	3578	579	7055(3527)
J0034-0534	131.6	45.31	0.489	0.69	3119	248	892(446)
J0034-0534	169.1	28.12	0.438	0.63	2790	182	751(375)
J0034-0534	197.3	28.12	0.438	0.63	2639	89	497(248)
J0034-0721	71.1	33.59	0.272	0.42	1743	147	1674(837)
J0034-0721	131.2	44.53	0.199	0.32	1399	168	464(232)
J0034-0721	168.4	28.12	0.162	0.28	1529	188	504(252)
J0034-0721	196.5	28.12	0.162	0.27	1440	114	399(199)
J0034-0721	226.2	31.25	0.161	0.27	1574	89	379(189)
J0038-2501	131.6	45.31	0.027	0.05	2849	34	18(9)
J0038-2501	169.1	28.12	0.12	0.19	2370	16	25(12)
J0038-2501	210.9	57.03	0.099	0.17	2700	25	34(17)
J0051+0423	131.6	45.31	0.078	0.14	2718	30	45(22)
J0051+0423	166.8	25.0	0.079	0.13	1718	15	37(18)
J0051+0423	208.2	51.56	0.092	0.14	2759	12	23(11)

Table B2 *continued*

Table B2 (*continued*)

Name	ν (MHZ)	BW (MHz)	W_{50} (phase)	W_{10} (phase)	T (s)	S/N	S_ν (mJy)
J0151-0635	169.1	28.12	0.06	0.1	2099	19	25(12)
J0151-0635	197.3	28.12	0.059	0.1	2309	31	49(24)
J0151-0635	225.4	28.12	0.051	0.11	2055	18	36(18)
J0152-1637	71.1	33.59	0.034	0.07	3578	48	110(55)
J0152-1637	131.6	45.31	0.03	0.06	1110	68	60(30)
J0152-1637	166.8	25.0	0.034	0.07	1125	76	87(43)
J0152-1637	197.3	28.12	0.044	0.07	1289	188	295(147)
J0152-1637	225.4	28.12	0.044	0.07	1150	96	216(108)
J0206-4028	131.6	45.31	0.021	0.04	959	93	75(37)
J0206-4028	166.8	25.0	0.014	0.02	1109	120	91(45)
J0206-4028	197.3	28.12	0.01	0.02	2310	60	34(17)
J0206-4028	225.4	28.12	0.01	0.02	2535	98	71(35)
J0304+1932	166.8	25.0	0.064	0.1	2547	13	45(22)
J0304+1932	196.5	28.12	0.054	0.09	2760	10	33(16)
J0304+1932	225.4	28.12	0.046	0.08	2894	15	61(30)
J0401-7608	169.1	28.12	0.027	0.05	3135	31	69(34)
J0401-7608	197.3	28.12	0.027	0.04	3176	29	77(38)
J0418-4154	131.6	45.31	0.018	0.03	2322	71	34(17)
J0418-4154	169.1	28.12	0.02	0.04	2925	53	29(14)
J0418-4154	197.3	28.12	0.02	0.04	2370	30	25(12)
J0437-4715	131.6	45.31	0.615	0.77	1499	267	1656(828)
J0437-4715	168.4	28.12	0.56	0.72	1174	343	2684(1342)
J0437-4715	196.5	28.12	0.518	0.68	1796	892	6750(3375)
J0437-4715	225.4	28.12	0.533	0.7	1777	261	2689(1344)
J0450-1248	131.6	45.31	0.086	0.15	2535	37	40(20)
J0450-1248	169.1	28.12	0.094	0.16	2999	39	50(25)
J0450-1248	197.3	28.12	0.069	0.11	3239	28	37(18)
J0450-1248	225.4	28.12	0.14	0.23	3578	20	52(26)
J0452-1759	131.6	45.31	0.161	0.25	2459	45	65(32)
J0452-1759	169.1	28.12	0.137	0.23	3179	53	74(37)
J0452-1759	197.3	28.12	0.197	0.31	2460	31	83(41)
J0452-1759	225.4	28.12	0.123	0.2	2624	43	116(58)
J0459-0210	131.6	45.31	0.041	0.07	1350	33	43(21)
J0459-0210	166.8	25.0	0.064	0.1	975	32	76(38)
J0459-0210	196.5	28.12	0.052	0.09	1735	36	68(34)
J0459-0210	225.4	28.12	0.054	0.1	2024	27	63(31)
J0520-2553	131.6	45.31	0.016	0.02	1515	49	24(12)
J0520-2553	169.1	28.12	0.008	0.02	1048	15	7(3)
J0520-2553	197.3	28.12	0.008	0.02	2550	13	6(3)

Table B2 *continued*

Table B2 (*continued*)

Name	ν (MHZ)	BW (MHz)	W_{50} (phase)	W_{10} (phase)	T (s)	S/N	S_ν (mJy)
J0525+1115	182.8	57.03	0.114	0.2	2805	19	46(23)
J0525+1115	225.4	28.12	0.092	0.18	3420	17	59(29)
J0528+2200	131.6	45.31	0.039	0.07	1690	11	42(21)
J0528+2200	169.1	28.12	0.039	0.06	3135	21	64(32)
J0528+2200	197.3	28.12	0.021	0.05	2910	16	41(20)
J0528+2200	225.4	28.12	0.045	0.09	3134	15	66(33)
J0534+2200	131.6	45.31	0.806	0.93	1559	2532	86026(43013)
J0534+2200	169.1	28.12	0.871	0.94	1489	1602	62050(31025)
J0534+2200	197.3	28.12	0.907	0.97	1508	1203	36414(18207)
J0534+2200	225.4	28.12	0.868	0.94	1308	453	20319(10159)
J0630-2834	70.7	32.81	0.134	0.22	1100	302	2637(1318)
J0630-2834	131.6	45.31	0.136	0.23	859	387	857(428)
J0630-2834	169.1	28.12	0.152	0.26	872	314	872(436)
J0630-2834	196.5	28.12	0.143	0.23	1736	319	789(394)
J0630-2834	224.6	28.12	0.121	0.21	1376	147	517(258)
J0636-4549	131.6	45.31	0.027	0.05	5005	26	13(6)
J0636-4549	168.4	28.12	0.02	0.03	5246	29	14(7)
J0636-4549	196.2	24.22	0.012	0.02	5036	18	9(4)
J0729-1836	185.5	75.0	0.148	0.24	3494	12	14(7)
J0737-3039A	131.6	45.31	0.148	0.27	3578	50	74(37)
J0737-3039A	169.1	28.12	0.273	0.42	1940	34	111(55)
J0737-3039A	197.3	28.12	0.223	0.37	1980	34	122(61)
J0737-3039A	225.4	28.12	0.086	0.15	3578	38	75(37)
J0742-2822	131.6	45.31	0.358	0.54	1181	131	582(291)
J0742-2822	166.8	25.0	0.252	0.4	1380	236	850(425)
J0742-2822	196.5	28.12	0.209	0.34	1436	343	1265(632)
J0742-2822	225.4	28.12	0.144	0.25	1499	156	610(305)
J0758-1528	197.3	28.12	0.012	0.02	3450	17	9(4)
J0820-1350	70.7	32.81	0.018	0.03	1514	70	185(92)
J0820-1350	131.6	45.31	0.062	0.12	1406	152	188(94)
J0820-1350	166.8	25.0	0.049	0.08	1559	212	268(134)
J0820-1350	196.5	28.12	0.05	0.09	1676	199	311(155)
J0820-1350	225.4	28.12	0.05	0.09	1680	157	333(166)
J0820-4114	169.1	28.12	0.293	0.43	2879	37	134(67)
J0820-4114	196.5	28.12	0.255	0.39	1736	38	179(89)
J0820-4114	225.4	28.12	0.177	0.32	3360	18	60(30)
J0823+0159	169.1	28.12	0.035	0.07	2174	36	46(23)
J0823+0159	196.5	28.12	0.029	0.06	1616	54	89(44)
J0823+0159	225.4	28.12	0.027	0.05	3210	33	46(23)

Table B2 *continued*

Table B2 (*continued*)

Name	ν (MHZ)	BW (MHz)	W_{50} (phase)	W_{10} (phase)	T (s)	S/N	S_ν (mJy)
J0826+2637	71.1	33.59	0.02	0.04	1777	24	116(58)
J0826+2637	131.6	45.31	0.018	0.03	1177	88	284(142)
J0826+2637	169.1	28.12	0.014	0.03	1567	136	428(214)
J0826+2637	197.3	28.12	0.014	0.03	1329	124	482(241)
J0826+2637	225.4	28.12	0.014	0.03	1269	75	370(185)
J0835-4510	131.6	45.31	0.886	1.0	1154	263	11724(5862)
J0835-4510	169.1	28.12	0.83	0.94	224	261	19576(9788)
J0835-4510	197.3	28.12	0.795	0.91	446	609	28420(14210)
J0835-4510	225.4	28.12	0.762	0.89	577	533	21774(10887)
J0837+0610	71.1	33.59	0.038	0.06	1615	178	689(344)
J0837+0610	132.0	46.09	0.033	0.05	1532	242	305(152)
J0837+0610	169.1	28.12	0.033	0.06	1515	280	476(238)
J0837+0610	197.3	28.12	0.033	0.06	1527	216	451(225)
J0837+0610	225.4	28.12	0.034	0.06	1379	130	358(179)
J0837-4135	131.6	45.31	0.121	0.2	3195	27	64(32)
J0837-4135	169.1	28.12	0.104	0.17	2370	85	197(98)
J0837-4135	197.3	28.12	0.057	0.12	3014	66	107(53)
J0837-4135	225.4	28.12	0.053	0.09	2009	56	128(64)
J0855-3331	131.6	45.31	0.02	0.04	960	13	14(7)
J0855-3331	169.1	28.12	0.126	0.2	2085	20	40(20)
J0855-3331	196.5	28.12	0.08	0.13	3300	30	45(22)
J0855-3331	222.3	23.44	0.101	0.17	3540	14	31(15)
J0856-6137	168.4	28.12	0.037	0.07	1198	119	267(133)
J0856-6137	196.5	28.12	0.029	0.05	1680	127	247(123)
J0856-6137	225.4	28.12	0.025	0.04	1390	63	156(78)
J0902-6325	169.1	28.12	0.047	0.12	5716	11	14(7)
J0905-6019	169.1	28.12	0.039	0.07	1755	19	36(18)
J0908-1739	131.6	45.31	0.018	0.03	1275	50	31(15)
J0908-1739	168.4	28.12	0.021	0.04	1469	42	32(16)
J0908-1739	196.5	28.12	0.018	0.03	1616	57	52(26)
J0908-1739	225.4	28.12	0.021	0.04	3119	49	48(24)
J0922+0638	71.1	33.59	0.108	0.18	1777	61	388(194)
J0922+0638	131.6	45.31	0.081	0.14	2204	121	213(106)
J0922+0638	166.8	25.0	0.091	0.15	770	63	287(143)
J0922+0638	196.5	28.12	0.089	0.16	1498	118	441(220)
J0922+0638	222.3	23.44	0.105	0.18	1618	81	421(210)
J0924-5302	131.6	45.31	0.074	0.14	2474	52	103(51)
J0924-5302	168.4	28.12	0.035	0.07	1589	76	131(65)
J0924-5302	196.5	28.12	0.025	0.05	1556	125	205(102)

Table B2 *continued*

Table B2 (*continued*)

Name	ν (MHZ)	BW (MHz)	W_{50} (phase)	W_{10} (phase)	T (s)	S/N	S_ν (mJy)
J0924-5302	225.4	28.12	0.02	0.04	1777	40	67(33)
J0924-5814	169.1	28.12	0.061	0.11	3074	71	125(62)
J0924-5814	197.3	28.12	0.059	0.11	2939	49	101(50)
J0942-5552	131.6	45.31	0.124	0.22	2595	17	48(24)
J0942-5552	169.1	28.12	0.103	0.18	1475	34	120(60)
J0942-5552	196.5	28.12	0.067	0.13	1740	43	123(61)
J0942-5552	225.4	28.12	0.021	0.04	1100	47	111(55)
J0942-5657	131.6	45.31	0.165	0.28	2367	34	121(60)
J0942-5657	166.8	25.0	0.027	0.05	1526	80	147(73)
J0942-5657	198.8	28.12	0.02	0.04	716	54	131(65)
J0942-5657	225.4	28.12	0.012	0.03	1449	38	59(29)
J0946+0951	71.1	33.59	0.018	0.03	1467	90	273(136)
J0946+0951	130.5	42.97	0.08	0.13	1047	98	308(154)
J0953+0755	70.3	32.03	0.408	0.59	1496	320	5847(2923)
J0953+0755	131.6	45.31	0.367	0.54	1619	292	1708(854)
J0953+0755	168.4	28.12	0.345	0.51	1395	338	2722(1361)
J0953+0755	197.3	28.12	0.31	0.48	1499	334	2874(1437)
J0953+0755	225.4	28.12	0.321	0.48	1436	213	2355(1177)
J0955-5304	131.6	45.31	0.043	0.07	3000	38	52(26)
J0955-5304	169.1	28.12	0.021	0.04	3059	49	48(24)
J0955-5304	197.3	28.12	0.012	0.02	2939	20	17(8)
J0955-5304	225.4	28.12	0.012	0.02	3179	14	14(7)
J0959-4809	166.8	25.0	0.109	0.2	1601	28	74(37)
J0959-4809	196.5	28.12	0.088	0.16	1616	25	65(32)
J0959-4809	222.3	23.44	0.075	0.1	1616	9	31(15)
J1001-5507	169.1	28.12	0.348	0.52	2129	18	122(61)
J1001-5507	196.5	28.12	0.292	0.44	2756	37	211(105)
J1001-5507	222.3	23.44	0.217	0.35	2459	39	239(119)
J1012-2337	166.8	25.0	0.023	0.04	1469	17	15(7)
J1012-2337	197.3	28.12	0.023	0.04	2635	27	22(11)
J1012-2337	225.4	28.12	0.023	0.04	1366	9	14(7)
J1018-1642	166.8	27.34	0.02	0.04	1354	25	21(10)
J1018-1642	197.3	28.12	0.02	0.04	1268	22	26(13)
J1022+1001	196.5	28.12	0.268	0.39	3480	34	193(96)
J1022+1001	222.3	23.44	0.064	0.12	2699	79	280(140)
J1041-1942	131.6	45.31	0.038	0.05	1440	9	8(4)
J1041-1942	169.1	28.12	0.024	0.05	2055	9	7(3)
J1041-1942	196.5	28.12	0.052	0.1	3176	17	21(10)
J1057-5226	70.7	32.81	0.487	0.66	1334	42	1407(703)

Table B2 *continued*

Table B2 (*continued*)

Name	ν (MHZ)	BW (MHz)	W_{50} (phase)	W_{10} (phase)	T (s)	S/N	S_ν (mJy)
J1057-5226	131.6	45.31	0.536	0.69	1482	47	398(199)
J1057-5226	166.8	25.0	0.475	0.63	1333	43	389(194)
J1057-5226	198.8	28.12	0.454	0.61	1376	58	567(283)
J1057-5226	225.4	28.12	0.501	0.66	1599	22	274(137)
J1059-5742	166.8	25.0	0.029	0.05	2135	47	92(46)
J1059-5742	196.5	28.12	0.094	0.14	2757	23	73(36)
J1059-5742	225.4	28.12	0.02	0.04	3255	28	42(21)
J1112-6926	131.6	45.31	0.074	0.13	2925	19	48(24)
J1112-6926	169.1	28.12	0.068	0.1	2925	19	56(28)
J1112-6926	197.3	28.12	0.064	0.11	2385	26	99(49)
J1112-6926	225.4	28.12	0.025	0.04	2385	35	100(50)
J1116-4122	70.7	32.81	0.025	0.05	1559	54	185(92)
J1116-4122	131.6	45.31	0.018	0.03	1089	126	102(51)
J1116-4122	169.1	28.12	0.014	0.03	1319	133	102(51)
J1116-4122	196.5	28.12	0.018	0.03	1406	105	114(57)
J1116-4122	225.0	28.91	0.014	0.03	1616	60	71(35)
J1136+1551	70.7	32.81	0.038	0.08	426	55	604(302)
J1136+1551	131.6	45.31	0.22	0.34	1017	147	1260(630)
J1136+1551	169.1	28.12	0.094	0.15	1747	151	788(394)
J1136+1551	196.5	28.12	0.084	0.14	1616	98	557(278)
J1136+1551	225.4	28.12	0.091	0.16	1439	148	1107(553)
J1202-5820	169.1	28.12	0.059	0.11	2220	46	114(57)
J1202-5820	197.3	28.12	0.035	0.06	2324	51	102(51)
J1202-5820	225.4	28.12	0.035	0.06	2925	46	99(49)
J1224-6407	156.7	52.34	0.035	0.07	2443	33	67(33)
J1224-6407	196.5	28.12	0.025	0.04	2036	58	145(72)
J1224-6407	227.0	28.12	0.02	0.04	3118	29	60(30)
J1225-5556	169.1	28.12	0.023	0.04	1980	15	21(10)
J1239+2453	131.6	45.31	0.102	0.18	899	13	158(79)
J1239+2453	169.1	28.12	0.07	0.11	3266	17	101(50)
J1239+2453	196.5	28.12	0.195	0.28	1675	32	503(251)
J1239+2453	225.4	28.12	0.118	0.22	3401	18	175(87)
J1239-6832	131.6	45.31	0.023	0.04	2381	12	24(12)
J1239-6832	166.8	25.0	0.02	0.04	1797	35	87(43)
J1239-6832	196.5	28.12	0.012	0.02	2156	22	41(20)
J1239-6832	225.4	28.12	0.004	0.01	2531	11	13(6)
J1240-4124	169.1	28.12	0.059	0.11	5336	43	37(18)
J1240-4124	197.3	28.12	0.027	0.05	6445	32	22(11)
J1311-1228	131.6	45.31	0.018	0.03	1302	51	45(22)

Table B2 *continued*

Table B2 (*continued*)

Name	ν (MHZ)	BW (MHz)	W_{50} (phase)	W_{10} (phase)	T (s)	S/N	S_ν (mJy)
J1311-1228	169.1	28.12	0.045	0.07	3267	21	25(12)
J1311-1228	197.3	28.12	0.012	0.02	2099	38	35(17)
J1311-1228	225.4	28.12	0.012	0.03	3075	29	27(13)
J1320-5359	131.6	45.31	0.07	0.13	3075	38	72(36)
J1320-5359	169.1	28.12	0.043	0.07	1978	66	132(66)
J1320-5359	197.3	28.12	0.027	0.06	1604	51	102(51)
J1320-5359	225.4	28.12	0.137	0.26	2323	18	88(44)
J1355-5153	131.6	45.31	0.243	0.4	1439	48	311(155)
J1355-5153	166.8	25.0	0.069	0.14	1275	32	116(58)
J1355-5153	196.5	28.12	0.027	0.05	1437	94	205(102)
J1355-5153	225.4	28.12	0.02	0.04	1777	53	105(52)
J1418-3921	131.6	45.31	0.043	0.07	3029	71	80(40)
J1418-3921	169.1	28.12	0.029	0.05	1797	72	95(47)
J1418-3921	196.5	28.12	0.021	0.04	1919	52	66(33)
J1418-3921	225.0	28.91	0.018	0.03	2909	29	35(17)
J1430-6623	71.1	33.59	0.063	0.09	3464	23	284(142)
J1430-6623	131.6	45.31	0.063	0.12	1590	40	208(104)
J1430-6623	169.1	28.12	0.06	0.11	1777	38	191(95)
J1430-6623	197.3	28.12	0.052	0.11	1539	34	180(90)
J1430-6623	225.4	28.12	0.062	0.1	1509	41	274(137)
J1440-6344	169.1	28.12	0.039	0.07	3573	25	71(35)
J1440-6344	197.3	28.12	0.023	0.04	3573	20	44(22)
J1453-6413	131.6	45.31	0.32	0.47	1604	180	2368(1184)
J1453-6413	166.8	25.0	0.1	0.17	1466	252	1965(982)
J1453-6413	196.5	28.12	0.088	0.14	1436	247	1761(880)
J1453-6413	225.4	28.12	0.074	0.12	1640	198	1316(658)
J1455-3330	146.1	74.22	0.252	0.39	3574	60	115(57)
J1455-3330	210.9	57.03	0.22	0.37	3578	59	155(77)
J1456-6843	71.1	33.59	0.19	0.32	3578	46	847(423)
J1456-6843	131.6	45.31	0.152	0.28	1574	82	638(319)
J1456-6843	166.8	25.0	0.155	0.29	1350	86	943(471)
J1456-6843	196.5	28.12	0.169	0.3	1409	79	905(452)
J1456-6843	225.4	28.12	0.207	0.3	1400	63	953(476)
J1507-4352	131.6	45.31	0.102	0.18	2399	29	83(41)
J1507-4352	169.1	28.12	0.133	0.22	3578	63	173(86)
J1507-4352	196.5	28.12	0.027	0.05	2276	31	51(25)
J1507-4352	225.4	28.12	0.027	0.05	2561	41	74(37)
J1510-4422	131.6	45.31	0.11	0.19	3356	28	74(37)
J1510-4422	169.1	28.12	0.074	0.13	2684	32	76(38)

Table B2 *continued*

Table B2 (*continued*)

Name	ν (MHZ)	BW (MHz)	W_{50} (phase)	W_{10} (phase)	T (s)	S/N	S_ν (mJy)
J1510-4422	197.3	28.12	0.07	0.12	3573	42	92(46)
J1510-4422	225.4	28.12	0.074	0.11	2625	21	64(32)
J1527-3931	131.6	45.31	0.021	0.05	2471	17	20(10)
J1527-3931	168.4	28.12	0.021	0.05	1621	19	27(13)
J1527-3931	196.5	28.12	0.021	0.05	2696	18	23(11)
J1527-3931	225.4	28.12	0.032	0.07	2558	14	27(13)
J1534-5334	71.1	33.59	0.051	0.09	2834	50	814(407)
J1534-5334	134.4	39.84	0.191	0.31	2249	62	559(279)
J1534-5334	168.4	28.12	0.136	0.22	2549	65	407(203)
J1534-5334	196.5	28.12	0.112	0.22	2759	54	276(138)
J1534-5334	225.0	28.91	0.075	0.15	2369	33	154(77)
J1543-0620	70.7	32.81	0.027	0.06	1559	33	155(77)
J1543-0620	131.6	45.31	0.068	0.11	1650	88	187(93)
J1543-0620	166.8	25.0	0.04	0.08	1664	66	137(68)
J1543-0620	197.3	28.12	0.039	0.08	1599	40	102(51)
J1543-0620	225.4	28.12	0.031	0.06	1569	23	65(32)
J1543+0929	71.1	33.59	0.059	0.11	1569	51	486(243)
J1543+0929	131.6	45.31	0.053	0.1	1380	147	529(264)
J1543+0929	168.4	28.12	0.053	0.1	1560	138	636(318)
J1543+0929	196.5	28.12	0.049	0.09	1424	109	577(288)
J1543+0929	225.4	28.12	0.053	0.1	2370	86	405(202)
J1544-5308	211.3	56.25	0.035	0.06	6625	36	52(26)
J1603-2712	131.6	45.31	0.02	0.04	1559	88	99(49)
J1603-2712	166.8	25.0	0.045	0.07	1589	33	65(32)
J1603-2712	196.5	28.12	0.02	0.04	1436	47	69(34)
J1603-2712	225.4	28.12	0.02	0.04	3179	37	47(23)
J1607-0032	70.7	32.81	0.045	0.08	1094	33	267(133)
J1607-0032	131.6	45.31	0.046	0.08	1122	68	170(85)
J1607-0032	166.8	25.0	0.051	0.09	1332	58	187(93)
J1607-0032	196.5	28.12	0.054	0.1	1737	45	155(77)
J1607-0032	224.6	28.12	0.052	0.09	1196	23	110(55)
J1614+0737	70.7	32.81	0.012	0.02	4000	11	30(15)
J1614+0737	134.8	39.06	0.004	0.01	2878	16	10(5)
J1614+0737	169.1	28.12	0.004	0.01	3209	13	10(5)
J1614+0737	196.5	28.12	0.012	0.01	3359	15	23(11)
J1614+0737	225.4	28.12	0.012	0.01	3119	13	23(11)
J1645-0317	71.1	33.59	0.018	0.03	3104	101	328(164)
J1645-0317	131.6	45.31	0.03	0.06	1736	274	432(216)
J1645-0317	169.1	28.12	0.03	0.06	1579	382	750(375)

Table B2 *continued*

Table B2 (*continued*)

Name	ν (MHZ)	BW (MHz)	W_{50} (phase)	W_{10} (phase)	T (s)	S/N	S_ν (mJy)
J1645-0317	196.5	28.12	0.03	0.06	1736	447	1000(500)
J1645-0317	225.4	28.12	0.03	0.06	1600	447	1255(627)
J1703-3241	169.1	28.12	0.059	0.11	3030	68	164(82)
J1703-3241	196.5	28.12	0.043	0.08	3476	75	141(70)
J1703-3241	225.4	28.12	0.043	0.07	3015	46	106(53)
J1709-1640	70.7	32.81	0.02	0.04	1529	38	239(119)
J1709-1640	131.6	45.31	0.018	0.03	1329	122	166(83)
J1709-1640	168.4	28.12	0.027	0.04	1514	128	209(104)
J1709-1640	196.5	28.12	0.02	0.04	1604	126	194(97)
J1709-1640	225.0	28.91	0.02	0.04	1454	103	202(101)
J1711-5350	169.1	28.12	0.023	0.04	3282	13	22(11)
J1720-1633	71.1	33.59	0.043	0.07	3158	35	253(126)
J1720-1633	131.6	45.31	0.012	0.03	2215	31	29(14)
J1720-1633	169.1	28.12	0.012	0.02	3551	17	12(6)
J1720-1633	197.3	28.12	0.012	0.02	2894	21	19(9)
J1720-1633	225.4	28.12	0.012	0.01	2995	16	17(8)
J1720-2933	131.6	45.31	0.051	0.1	2760	87	290(145)
J1720-2933	169.1	28.12	0.051	0.1	3135	65	171(85)
J1720-2933	197.3	28.12	0.051	0.1	3135	65	161(80)
J1720-2933	225.4	28.12	0.051	0.09	2670	40	116(58)
J1731-4744	131.6	45.31	0.159	0.26	1424	119	824(412)
J1731-4744	166.8	25.0	0.083	0.14	1545	134	633(316)
J1731-4744	196.5	28.12	0.062	0.11	1545	132	513(256)
J1731-4744	225.4	28.12	0.053	0.09	1429	97	401(200)
J1733-2228	131.6	45.31	0.02	0.03	3105	38	59(29)
J1733-2228	166.8	25.0	0.012	0.03	1440	34	54(27)
J1733-2228	197.3	28.12	0.014	0.03	2399	71	89(44)
J1733-2228	225.4	28.12	0.02	0.04	2909	38	59(29)
J1735-0724	210.9	57.03	0.027	0.06	3299	28	32(16)
J1751-4657	71.1	33.59	0.197	0.32	1777	29	745(372)
J1751-4657	131.6	45.31	0.033	0.06	630	179	649(324)
J1751-4657	166.8	25.0	0.049	0.08	1710	90	262(131)
J1751-4657	196.5	28.12	0.046	0.08	1316	85	277(138)
J1751-4657	225.4	28.12	0.049	0.08	1529	37	135(67)
J1752-2806	72.7	28.91	0.043	0.07	1424	47	1738(869)
J1752-2806	131.6	45.31	0.074	0.12	1365	280	3371(1685)
J1752-2806	166.8	25.0	0.049	0.09	1631	278	2135(1067)
J1752-2806	196.5	28.12	0.038	0.07	1439	361	1959(979)
J1752-2806	225.4	28.12	0.038	0.06	940	297	1841(920)

Table B2 *continued*

Table B2 (*continued*)

Name	ν (MHZ)	BW (MHz)	W_{50} (phase)	W_{10} (phase)	T (s)	S/N	S_ν (mJy)
J1820-0427	131.6	45.31	0.619	0.79	1769	71	1621(810)
J1820-0427	169.1	28.12	0.586	0.77	2077	130	2324(1162)
J1820-0427	196.5	28.12	0.246	0.38	1736	41	379(189)
J1820-0427	225.4	28.12	0.242	0.38	945	49	651(325)
J1823+0550	131.6	45.31	0.012	0.03	1228	20	43(21)
J1823+0550	169.1	28.12	0.012	0.02	1590	29	57(28)
J1823+0550	197.3	28.12	0.012	0.02	2684	19	30(15)
J1823+0550	225.4	28.12	0.012	0.02	2459	17	33(16)
J1823-3106	169.1	28.12	0.029	0.06	3480	61	81(40)
J1823-3106	197.3	28.12	0.029	0.06	3555	65	89(44)
J1823-3106	225.4	28.12	0.035	0.07	3578	33	58(29)
J1825-0935	70.7	32.81	0.027	0.06	1485	33	711(355)
J1825-0935	131.6	45.31	0.02	0.03	1590	78	308(154)
J1825-0935	166.8	25.0	0.014	0.02	1395	72	225(112)
J1825-0935	196.5	28.12	0.012	0.03	1499	57	132(66)
J1825-0935	225.4	28.12	0.012	0.03	1509	40	92(46)
J1834-0426	131.6	45.31	0.376	0.56	2925	78	1190(595)
J1834-0426	169.1	28.12	0.266	0.42	3345	71	669(334)
J1834-0426	197.3	28.12	0.149	0.24	3570	39	222(111)
J1834-0426	225.4	28.12	0.051	0.09	3300	52	173(86)
J1841+0912	169.1	28.12	0.041	0.07	3578	13	39(19)
J1841+0912	197.3	28.12	0.092	0.16	3578	14	68(34)
J1841+0912	225.4	28.12	0.078	0.13	3195	9	48(24)
J1844+1454	131.6	45.31	0.02	0.04	1619	30	95(47)
J1844+1454	166.8	25.0	0.02	0.04	1619	25	94(47)
J1844+1454	197.3	28.12	0.02	0.04	1935	32	110(55)
J1844+1454	225.4	28.12	0.02	0.04	2355	22	76(38)
J1900-2600	71.1	33.59	0.554	0.78	3578	88	2632(1316)
J1900-2600	131.6	45.31	0.159	0.25	1659	129	482(241)
J1900-2600	166.8	25.0	0.085	0.15	1699	92	262(131)
J1900-2600	196.5	28.12	0.08	0.11	1559	74	229(114)
J1900-2600	224.6	28.12	0.086	0.12	1199	33	153(76)
J1901+0156	168.4	28.12	0.043	0.08	3420	44	152(76)
J1901+0156	196.5	28.12	0.02	0.04	3360	33	73(36)
J1901+0156	225.4	28.12	0.02	0.04	3578	22	49(24)
J1913-0440	131.6	45.31	0.081	0.13	1575	84	362(181)
J1913-0440	166.8	25.0	0.056	0.1	1499	81	308(154)
J1913-0440	196.5	28.12	0.045	0.08	1499	106	358(179)
J1913-0440	225.4	28.12	0.044	0.08	1559	71	256(128)

Table B2 *continued*

Table B2 (*continued*)

Name	ν (MHZ)	BW (MHz)	W_{50} (phase)	W_{10} (phase)	T (s)	S/N	S_ν (mJy)
J1916+0951	210.9	57.03	0.02	0.04	3574	27	49(24)
J1917+1353	196.5	28.12	0.14	0.23	1377	11	149(74)
J1917+1353	222.3	23.44	0.088	0.14	2577	10	84(42)
J1921+2153	70.7	32.81	0.059	0.11	945	41	1092(546)
J1921+2153	131.6	45.31	0.045	0.08	285	70	1057(528)
J1921+2153	166.8	25.0	0.045	0.08	735	72	858(429)
J1921+2153	196.5	28.12	0.045	0.08	1616	146	1174(587)
J1921+2153	225.4	28.12	0.045	0.07	1360	60	608(304)
J1929+00	196.5	28.12	0.02	0.04	2038	23	48(24)
J1932+1059	131.6	45.31	0.271	0.43	2820	40	389(194)
J1932+1059	166.8	25.0	0.191	0.3	1959	25	262(131)
J1932+1059	196.5	28.12	0.158	0.25	2638	53	431(215)
J1932+1059	225.4	28.12	0.153	0.26	3578	53	397(198)
J1935+1616	169.1	28.12	0.029	0.05	3578	65	219(109)
J1935+1616	197.3	28.12	0.108	0.18	3000	51	396(198)
J1935+1616	225.4	28.12	0.025	0.04	2489	110	465(232)
J1943-1237	131.6	45.31	0.012	0.03	1589	61	55(27)
J1943-1237	169.1	28.12	0.012	0.02	1539	48	49(24)
J1943-1237	197.3	28.12	0.012	0.02	1019	52	77(38)
J1943-1237	225.4	28.12	0.012	0.03	1335	34	58(29)
J2018+2839	71.1	33.59	0.012	0.02	3578	20	125(62)
J2018+2839	131.6	45.31	0.072	0.12	2108	52	543(271)
J2018+2839	169.1	28.12	0.045	0.1	1238	48	655(327)
J2018+2839	196.9	27.34	0.055	0.1	1796	89	1157(578)
J2018+2839	225.4	28.12	0.052	0.09	1529	69	1036(518)
J2046-0421	131.6	45.31	0.012	0.03	2370	37	26(13)
J2046-0421	166.0	21.88	0.012	0.03	2145	46	50(25)
J2046-0421	196.5	28.12	0.012	0.03	2040	56	67(33)
J2046-0421	225.4	28.12	0.012	0.03	2217	31	42(21)
J2048-1616	131.6	45.31	0.068	0.13	1635	79	128(64)
J2048-1616	168.4	28.12	0.069	0.12	1330	103	238(119)
J2048-1616	196.5	28.12	0.069	0.12	1619	80	222(111)
J2048-1616	225.4	28.12	0.081	0.13	1489	48	195(97)
J2053-7200	169.1	28.12	0.035	0.07	3574	31	100(50)
J2053-7200	197.3	28.12	0.121	0.19	3374	23	170(85)
J2113+2754	169.1	28.12	0.014	0.03	2627	33	153(76)
J2113+2754	197.3	28.12	0.01	0.02	2627	26	101(50)
J2145-0750	131.6	45.31	0.216	0.35	1529	132	468(234)
J2145-0750	169.1	28.12	0.327	0.49	1484	111	694(347)

Table B2 *continued*

Table B2 (*continued*)

Name	ν (MHz)	BW (MHz)	W_{50} (phase)	W_{10} (phase)	T (s)	S/N	S_ν (mJy)
J2145-0750	196.5	28.12	0.312	0.48	2220	56	344(172)
J2145-0750	225.4	28.12	0.176	0.28	2037	42	229(114)
J2155-3118	70.7	32.81	0.052	0.08	1771	31	138(69)
J2155-3118	131.6	45.31	0.043	0.07	1380	40	47(23)
J2155-3118	166.8	25.0	0.045	0.08	1455	34	55(27)
J2155-3118	196.5	28.12	0.061	0.1	1076	38	105(52)
J2155-3118	225.4	28.12	0.057	0.12	1680	21	61(30)
J2219+4754	131.6	45.31	0.012	0.03	1537	36	1136(568)
J2219+4754	169.1	28.12	0.014	0.02	1279	68	2354(1177)
J2219+4754	197.3	28.12	0.014	0.02	1530	71	2000(1000)
J2219+4754	225.4	28.12	0.014	0.03	2190	46	1242(621)
J2256-1024	131.6	45.31	0.141	0.23	2519	41	75(37)
J2256-1024	169.1	28.12	0.078	0.17	1875	25	46(23)
J2256-1024	196.5	28.12	0.109	0.2	1605	31	96(48)
J2317+2149	131.6	45.31	0.02	0.04	1484	28	75(37)
J2317+2149	166.8	25.0	0.012	0.03	1605	29	72(36)
J2317+2149	196.5	28.12	0.012	0.03	1438	28	78(39)
J2317+2149	225.4	28.12	0.012	0.03	3236	25	62(31)
J2330-2005	71.1	33.59	0.016	0.03	3578	36	60(30)
J2330-2005	131.6	45.31	0.015	0.04	1539	33	20(10)
J2330-2005	166.8	25.0	0.021	0.05	1619	32	28(14)
J2330-2005	197.3	28.12	0.018	0.02	1670	58	57(28)
J2330-2005	225.4	28.12	0.015	0.04	1480	31	39(19)
J2346-0609	169.1	28.12	0.026	0.04	7174	14	9(4)
J2346-0609	197.3	28.12	0.039	0.08	2879	9	11(5)

ν , BW, T, and S/N are the center frequency, bandwidth, integration time and signal-to-noise ratio of the average pulse profile

W_{50} and W_{10} are the fraction pulse width at FWHM and 10%

S_ν is the flux density calculated with W_{50} and equation 2

C. SPECTRAL INDEX AND OTHER PARAMETERS OF PULSARS DETECTED BY EDA2

Table C3. Best fitting model parameter for spectral fitting of pulsars detected with EDA2. The table is published in its entirety in a machine readable online format.

Name	ν_{range}^a (MHz)	ν_0^a (MHz)	a_1^c	a_2^d (MHz)	$a_3 3^e$	a_4^f	P_{best}^b	Type ^b	References
J0034-0534	49-1660	287	-4.69(28)	84(0)	16.59(1484)	1.29(9)	0.99	DT	5, 10, 11, 21, 39, 45, 46, 47, 58, 60, 65, 71, 72, 73, 77, 82
J0034-0721	20-1435	169	-3.52(17)	72(2)	14.34(931)	0.7(4)	0.89	DT	4, 5, 10, 21, 25, 29, 31, 35, 45, 49, 51, 55, 60, 65, 69, 75, 82, 83, 86
J0038-2501	131-350	214	-2.21(77)	—	—	—	0.92	PL	2, 5, 60
J0051+0423*	25-1360	184	-1.13(12)	—	—	—	0.85	PL	5, 10, 35, 45, 60, 67, 68, 83
J0151-0635	25-1408	187	0.52(32)	733(157)	-2.75(111)	—	0.69	BPL	5, 21, 31, 35, 51, 55, 56, 60, 69, 83
J0152-1637	35-4750	408	-2.92(24)	20(8)	—	0.27(2)	0.71	PLL	5, 10, 21, 29, 31, 35, 45, 51, 56, 60, 66, 69, 75, 86
J0206-4028	107-1440	392	-1.25(45)	1829(597)	—	—	0.47	PLH	5, 31, 35, 56, 65, 66, 76, 86
J0304+1932	24-4850	346	-7.89(9)	179(11)	—	0.11(0)	0.65	PLL	5, 8, 9, 21, 25, 28, 29, 35, 38, 44, 45, 51, 55, 56, 69, 75, 80
J0401-7608	154-3100	691	-1.38(18)	—	—	—	0.82	PL	5, 30, 31, 35, 56, 66, 76, 86
J0418-4154	131-843	333	-1.81(18)	—	—	—	0.95	PL	5, 7, 31, 82
J0437-4715	76-17000	1136	-2.27(0)	108(0)	—	0.38(0)	0.99	PLL	4, 5, 15, 16, 21, 23, 30, 31, 33, 37, 42, 43, 49, 57, 58, 59, 65, 71, 77, 82, 84
J0450-1248	64-1420	302	-1.43(11)	2316(432)	—	—	0.88	PLH	5, 21, 31, 35, 45, 51, 55, 56, 60, 69
J0452-1759	64-4850	559	-7.18(6)	171(6)	—	0.13(0)	0.78	PLL	5, 21, 25, 29, 31, 35, 38, 45, 49, 51, 54, 56, 60, 65, 69, 86
J0459-0210	49-1360	260	-2.66(19)	686(2746)	-0.17(678)	—	0.65	BPL	5, 21, 35, 45, 55, 58, 60, 67
J0520-2553	131-1360	423	-1.18(29)	—	—	—	0.94	PL	5, 24, 35, 53, 60
J0525+1115	61-1420	294	-0.77(17)	426(44)	-1.95(9)	—	0.68	BPL	5, 8, 21, 29, 31, 35, 36, 51, 55, 56, 67, 69, 80
J0528+2200	35-22700	892	-0.56(19)	758(180)	-2.8(35)	—	0.99	BPL	3, 5, 8, 10, 25, 28, 29, 35, 45, 51, 55, 62, 67, 69, 75, 79, 80, 85
J0534+2200	102-1435	383	-2.98(17)	—	—	—	0.67	PL	5, 8, 21, 25, 51, 55, 69, 78
J0630-2834	35-10550	608	-1.86(3)	83(0)	105.49(6586)	2.09(12)	0.99	DT	4, 5, 10, 16, 21, 25, 29, 30, 31, 34, 35, 38, 45, 49, 51, 56, 60, 62, 65, 69, 75, 82, 86
J0636-4549	131-1360	423	-2.21(18)	—	—	—	0.99	PL	5, 35
J0729-1836	154-3100	691	-5.08(20)	191(21)	—	0.28(1)	0.46	PLL	5, 27, 30, 31, 35, 51, 56, 60, 66, 69
J0737-3039A*	99-5000	703	-1.45(8)	842(1)	-2.15(16)	—	0.8	BPL	5, 12, 16, 21, 31, 39, 60, 65, 71
J0742-2822	102-10550	1039	-0.48(20)	408(0)	-1.79(15)	—	0.99	BPL	5, 21, 25, 27, 28, 29, 30, 31, 34, 35, 51, 54, 56, 60, 69, 82, 84, 85, 86
J0758-1528	102-4850	705	-0.6(34)	5833(846)	—	—	0.74	PLH	5, 30, 31, 35, 38, 51, 55, 56, 60, 69
J0820-1350	49-4850	491	-4.0(31)	70(15)	—	0.26(1)	0.6	PLL	5, 10, 21, 25, 29, 30, 31, 35, 38, 45, 49, 51, 54, 56, 60, 65, 66, 69, 75, 82, 85, 86
J0820-4114*	76-3100	485	-0.71(22)	512(157)	-2.32(42)	—	0.64	BPL	5, 21, 27, 30, 31, 35, 56, 65, 66, 76
J0823+0159*	49-4750	486	-7.99(769)	99(5)	—	0.11(0)	0.62	PLL	5, 21, 30, 35, 45, 51, 55, 56, 60, 67, 69, 82
J0826+2637*	20-22700	673	0.18(20)	207(27)	-1.6(5)	—	0.99	BPL	3, 5, 8, 9, 10, 21, 25, 28, 29, 45, 49, 51, 52, 55, 60, 62, 65, 67, 69, 70, 75, 79, 80, 83, 85
J0835-4510	76-343500	5109	-0.51(3)	787(51)	-2.02(8)	—	0.99	BPL	4, 5, 21, 30, 34, 35, 37, 49, 56, 63, 65, 76, 85, 86
J0837+0610	20-4850	311	-6.61(81)	67(8)	—	0.21(1)	0.98	PLL	5, 10, 21, 25, 29, 30, 35, 38, 45, 49, 51, 55, 56, 60, 62, 65, 69, 70, 75, 80, 82, 83, 86
J0837-4135	131-8600	1064	-2.44(21)	270(11)	—	1.02(21)	0.84	PLL	5, 21, 27, 30, 31, 34, 35, 56, 65, 76, 82, 84, 85, 86
J0855-3331	131-3100	638	-2.45(27)	127(1)	—	1.39(49)	0.97	PLL	5, 21, 30, 31, 51, 56, 60, 65, 82, 86
J0856-6137	151-3100	685	-2.19(7)	—	—	—	0.75	PL	5, 30, 35, 56, 65, 76
J0902-6325	154-1360	458	-1.14(18)	—	—	—	0.99	PL	5, 35, 56, 76
J0908-1739*	49-4850	491	-1.48(6)	120(1)	—	2.09(20)	0.53	PLL	5, 10, 21, 29, 30, 35, 38, 45, 51, 54, 55, 56, 60, 69, 75

Table C3 continued

Table C3 (continued)

Name	ν_{range}^a (MHz)	ν_0^a (MHz)	a_1^c	a_2^d (MHz)	a_{33}^e	a_4^f	P_{best}^b	Type ^b	References
J0922+0638	20-10550	459	-1.86(19)	46(1)	—	0.88(30)	0.99	PLL	5, 10, 21, 25, 28, 29, 30, 31, 34, 35, 45, 51, 52, 55, 56, 60, 61, 65, 69, 70, 80, 82, 83, 86
J0924-5302*	131-3100	638	-2.21(11)	114(21)	—	2.09(131)	0.67	PLL	5, 6, 27, 30, 32, 35, 56, 65, 76
J0924-5814	154-3100	691	-0.93(9)	—	—	—	0.45	PL	5, 27, 30, 31, 35, 56, 76
J0942-5552	131-3100	638	-4.15(3)	306(7)	—	0.57(0)	0.87	PLL	5, 26, 27, 30, 32, 35, 56, 65, 76, 86
J0942-5657	131-3100	638	-2.21(8)	—	—	—	0.71	PL	5, 27, 30, 31, 32, 35, 56, 65, 66, 76
J0946+0951	20-1418	168	-7.99(621)	54(3)	14.17(763)	0.4(1)	0.71	DT	5, 8, 9, 10, 21, 29, 51, 55, 67, 69, 70, 80, 83
J0953+0755	20-22700	673	-2.96(18)	116(5)	—	0.35(5)	0.99	PLL	3, 4, 5, 10, 21, 25, 28, 29, 30, 31, 34, 35, 45, 49, 51, 55, 56, 64, 65, 67, 69, 70, 80, 82, 83, 84, 85, 86
J0955-5304	131-1440	435	-0.52(26)	1535(39)	—	—	0.87	PLH	5, 27, 31, 56, 66, 76, 86
J0959-4809	147-3100	676	-1.58(8)	—	—	—	0.8	PL	5, 21, 30, 35, 56, 65, 76
J1001-5507	151-3100	685	-2.8(20)	220(22)	—	1.34(113)	0.92	PLL	27, 30, 31, 32, 35, 56, 65, 76, 86
J1012-2337	151-1369	455	-2.57(9)	—	—	—	0.96	PL	5, 51, 56, 60, 65, 81
J1018-1642	102-1420	381	-1.26(26)	1924(363)	—	—	0.72	PLH	5, 18, 30, 35, 51, 55, 60, 69
J1022+1001	35-4850	412	-1.43(54)	86(19)	9.02(424)	0.73(50)	0.99	DT	5, 11, 15, 21, 22, 23, 25, 38, 39, 42, 43, 45, 47, 55, 59, 67, 68, 71, 72, 73, 82
J1041-1942	131-4850	799	-0.93(10)	—	—	—	0.66	PL	5, 30, 35, 38, 51, 56, 60, 69
J1057-5226	70-3100	468	-1.72(6)	—	—	—	0.52	PL	4, 5, 30, 31, 35, 56, 65, 76, 86
J1059-5742*	154-3100	691	-3.03(216)	157(111)	—	0.8(126)	0.73	PLL	5, 13, 27, 30, 31, 32, 35, 56, 76, 86
J1112-6926	131-3100	638	-1.75(16)	—	—	—	0.79	PL	5, 30, 35, 56, 76, 82
J1116-4122	70-3100	468	-1.17(14)	3361(157)	—	—	0.71	PLH	5, 21, 30, 31, 35, 49, 56, 65, 66, 76, 82, 86
J1136+1551	20-22700	673	-1.79(5)	67(3)	226.99(11649)	1.1(13)	0.99	DT	3, 5, 8, 9, 10, 21, 25, 28, 29, 30, 31, 34, 35, 45, 51, 55, 56, 62, 65, 67, 69, 70, 75, 80, 82, 83, 84, 85, 86
J1202-5820*	154-3100	691	-1.64(10)	—	—	—	0.67	PL	5, 27, 30, 31, 32, 35, 56, 76
J1224-6407*	154-3100	691	-0.92(8)	842(13)	-1.53(15)	—	0.62	BPL	5, 27, 30, 31, 32, 35, 56, 76, 86
J1225-5556	154-1360	458	-1.88(23)	—	—	—	1	PL	5, 35, 58
J1239+2453	20-22700	673	-1.73(20)	73(11)	—	1.04(34)	0.8	PLL	3, 8, 9, 10, 21, 25, 28, 29, 35, 45, 51, 55, 60, 61, 62, 67, 69, 70, 75, 79, 80, 83, 84, 85
J1239-6832	131-3100	638	-1.29(15)	4143(971)	—	—	0.68	PLH	5, 27, 30, 31, 56, 76
J1240-4124	154-1360	458	-1.87(19)	—	—	—	0.97	PL	5, 6, 35, 56, 76
J1311-1228	102-1420	381	-1.94(24)	—	—	—	0.83	PL	5, 18, 51, 55, 60, 69
J1320-5359	131-3100	638	-0.94(40)	608(209)	-1.96(17)	—	0.85	BPL	5, 6, 13, 30, 31, 35, 56, 76
J1355-5153	131-1369	424	-3.85(175)	150(39)	—	0.91(139)	0.6	PLL	5, 6, 21, 31, 56, 76, 81
J1418-3921	131-1369	424	-1.96(5)	—	—	—	0.91	PL	5, 21, 35, 36, 58, 60
J1430-6623	71-8356	770	-1.88(18)	207(20)	—	2.09(153)	0.88	PLL	5, 27, 31, 34, 35, 36, 56, 65, 76, 82, 86
J1440-6344*	154-1400	464	-0.89(20)	1520(48)	—	—	0.97	PLH	5, 27, 31, 56, 76, 82
J1453-6413	102-8356	923	-2.65(17)	193(9)	—	2.09(14)	0.83	PLL	4, 5, 27, 30, 31, 34, 35, 49, 56, 65, 76, 82, 86
J1455-3330	146-1625	487	-6.02(11)	20(3)	—	0.12(0)	0.92	PLL	1, 5, 17, 23, 50, 58, 60, 71, 77
J1456-6843	71-8356	770	-1.94(8)	219(2)	—	2.09(7)	0.95	PLL	4, 5, 31, 34, 35, 49, 56, 65, 82, 86
J1507-4352	131-1360	423	-2.37(13)	—	—	—	0.79	PL	5, 21, 31, 35, 56, 76, 82
J1510-4422	131-408	231	-1.38(52)	—	—	—	0.95	PL	5, 56, 76
J1527-3931	131-843	333	-1.37(21)	—	—	—	0.5	PL	5, 31, 56, 60, 76

Table C3 continued

Table C3 (continued)

Name	ν_{range}^a (MHz)	ν_0^a (MHz)	a_1^c	a_2^d (MHz)	a_{33}^c	a_4^f	P_{best}^b	Type ^b	References
J1534-5334	71-1520	328	-1.57(19)	—	—	—	0.53	PL	4, 5, 27, 31, 32, 35, 56, 76, 82, 86
J1543-0620	25-4750	344	-2.1(17)	79(3)	47.49(2574)	1.47(26)	0.99	DT	5, 10, 21, 25, 45, 51, 54, 55, 56, 60, 65, 69, 75, 83
J1543+0929	49-4850	491	-1.92(17)	82(2)	5.52(31)	1.46(32)	0.99	DT	5, 8, 9, 10, 21, 25, 29, 38, 45, 51, 56, 65, 67, 69, 70, 75, 80
J1544-5308	185-1520	530	-1.36(9)	—	—	—	0.92	PL	27, 31, 32, 35, 36, 56, 76, 82
J1603-2712	49-1420	265	-1.12(19)	1806(228)	—	—	0.53	PLH	21, 45, 51, 56, 60, 69
J1607-0032	25-10550	513	-1.92(13)	79(3)	105.49(5516)	1.63(24)	0.99	DT	10, 21, 25, 29, 35, 38, 45, 51, 55, 56, 60, 65, 67, 69, 75, 80, 82, 83, 86
J1614+0737	25-4850	348	-0.48(29)	314(105)	-2.22(17)	—	0.7	BPL	10, 21, 38, 45, 51, 54, 55, 56, 67, 69, 75, 80, 83
J1645-0317	35-22700	892	-2.36(8)	144(1)	—	0.79(5)	0.99	PLL	3, 10, 21, 25, 28, 29, 31, 35, 36, 45, 49, 51, 55, 56, 60, 62, 65, 67, 69, 70, 75, 82, 84, 85, 86
J1703-3241	147-5124	869	-1.34(7)	11424(5754)	—	—	0.47	PLH	21, 25, 27, 30, 31, 35, 51, 56, 60, 85, 86
J1709-1640	35-22700	892	-0.92(3)	24912(2831)	—	—	0.58	PLH	3, 10, 21, 29, 31, 35, 45, 49, 51, 56, 69, 75, 82, 84, 86
J1711-5350	169-3100	724	-1.75(17)	—	—	—	0.96	PL	30, 31, 56, 76, 81
J1720-1633*	49-4850	491	-1.26(12)	5581(330)	—	—	0.87	PLH	21, 30, 31, 38, 45, 51, 74
J1720-2933	49-1420	265	-2.65(7)	152(16)	—	2.09(16)	0.89	PLL	21, 27, 31, 35, 36, 45, 51, 54, 56, 60, 69
J1731-4744	131-3100	638	-2.09(8)	214(2)	—	2.09(30)	0.99	PLL	21, 30, 35, 49, 56, 65, 82, 86
J1733-2228	131-1435	434	-0.42(85)	1787(683)	—	—	0.91	PLH	25, 27, 35, 36, 51, 56, 60
J1735-0724	102-1408	379	-0.1(29)	1574(74)	—	—	0.99	PLH	35, 36, 51, 55, 56, 60, 69
J1751-4657	35-3100	329	-0.38(32)	245(47)	-2.41(28)	—	0.59	BPL	21, 30, 31, 35, 45, 49, 56, 76, 82, 86
J1752-2806	61-22700	1176	-3.81(13)	144(4)	226.99(20255)	0.66(1)	0.91	DT	3, 4, 21, 25, 27, 29, 30, 31, 32, 34, 35, 45, 51, 56, 60, 62, 65, 69, 75, 82, 84, 85, 86
J1820-0427	102-4920	710	-2.34(3)	127(0)	—	2.09(6)	0.99	PLL	4, 21, 25, 27, 29, 31, 35, 36, 38, 49, 51, 54, 56, 60, 65, 67, 69, 82, 85, 86
J1823+0550	49-4850	491	-1.27(6)	—	—	—	0.74	PL	21, 25, 29, 38, 45, 51, 54, 56, 67, 69, 80
J1823-3106	147-3100	676	-1.57(5)	—	—	—	0.87	PL	21, 25, 30, 31, 35, 51, 56, 60, 82
J1825-0935	25-10550	513	-1.01(8)	55(5)	12.57(131)	2.09(27)	0.99	DT	10, 21, 25, 27, 28, 29, 31, 35, 36, 45, 51, 56, 60, 69, 75, 82, 83, 85, 86
J1834-0426	79-4850	619	-1.38(2)	11538(3224)	—	—	0.51	PLH	21, 25, 27, 29, 31, 36, 38, 45, 51, 54, 56, 60, 67, 69
J1841+0912*	59-4850	538	-0.8(94)	332(257)	-1.94(9)	—	0.73	BPL	8, 9, 25, 31, 38, 51, 54, 56, 67, 69, 80
J1844+1454	35-4750	408	-1.81(6)	—	—	—	0.84	PL	8, 9, 10, 21, 29, 35, 45, 51, 56, 67, 69, 75, 80
J1900-2600	64-4820	557	-5.65(7)	46(3)	—	0.13(0)	0.77	PLL	4, 21, 25, 30, 31, 35, 45, 49, 51, 56, 60, 65, 69, 82, 85, 86
J1901+0156	135-1418	437	-2.83(11)	—	—	—	0.84	PL	27, 48, 51, 60, 67, 74, 80
J1913-0440	64-4850	559	-2.77(83)	45(6)	—	0.43(24)	0.71	PLL	21, 25, 29, 30, 31, 35, 38, 45, 49, 51, 54, 56, 60, 62, 65, 67, 82, 86
J1916+0951	102-4850	705	-1.86(5)	—	—	—	0.84	PL	21, 27, 31, 35, 38, 48, 51, 55, 56, 67, 80
J1917+1353	102-4850	705	-2.9(110)	103(69)	—	0.65(71)	0.6	PLL	21, 27, 28, 35, 38, 48, 51, 55, 56, 67, 69, 80, 82
J1921+2153	20-4750	308	-2.62(6)	79(2)	16.06(3536)	2.09(30)	1	DT	8, 9, 10, 21, 29, 35, 45, 51, 55, 60, 62, 69, 70, 75, 79, 80, 82, 83
J1929+00	49-350	132	-2.06(23)	—	—	—	0.98	PL	45, 60, 67
J1932+1059	20-43000	927	-1.06(3)	65(6)	51.16(602)	1.5(30)	0.99	DT	3, 8, 9, 10, 21, 25, 27, 28, 29, 31, 35, 41, 45, 49, 51, 52, 55, 56, 62, 65, 69, 80, 82, 83, 84, 85, 86
J1935+1616	102-22700	1525	-4.04(197)	299(14)	—	0.42(34)	0.77	PLL	3, 21, 25, 35, 51, 52, 54, 56, 62, 67, 69, 80, 82, 84, 85
J1943-1237	49-1408	264	-5.48(12)	34(4)	—	0.15(0)	0.7	PLL	21, 31, 35, 45, 51, 54, 56, 60, 69, 82, 86
J2018+2839	25-22700	753	-7.99(505)	149(4)	—	0.13(0)	0.61	PLL	3, 8, 9, 10, 21, 25, 28, 29, 38, 45, 49, 51, 55, 60, 62, 67, 69, 70, 75, 79, 80, 82, 83, 85
J2046-0421	64-3100	447	-6.85(16)	144(11)	—	0.19(0)	0.66	PLL	21, 29, 30, 31, 45, 51, 54, 55, 56, 60, 67, 82, 86

Table C3 continued

Table C3 (continued)

Name	ν_{range}^a (MHz)	ν_0^a (MHz)	a_1^c	a_2^d (MHz)	a_{33}^c	a_4^f	P_{best}^b	Type ^b	References
J2048-1616	49-22700	1063	-5.26(7)	77(6)	—	0.11(0)	0.99	PLL	3, 4, 5, 16, 21, 25, 28, 29, 30, 31, 35, 38, 45, 49, 51, 56, 60, 62, 65, 69, 82, 84, 86
J2053-7200	151-3100	685	-1.17(17)	3421(364)	—	—	0.86	PLH	30, 31, 56, 65, 66, 76, 86
J2113+2754	25-4850	348	-1.85(17)	43(6)	—	1.9(190)	0.67	PLL	8, 10, 38, 45, 51, 55, 60, 67, 69, 70, 75, 79, 80, 83
J2145-0750*	35-5124	424	-1.72(6)	45(0)	—	1.0(10)	0.99	PLL	1, 5, 10, 11, 15, 16, 17, 19, 21, 23, 25, 30, 31, 38, 39, 42, 43, 45, 46, 47, 55, 58, 59, 60, 71, 72, 73, 77, 82, 85
J2155-3118*	49-1408	264	-6.45(7)	36(3)	—	0.14(0)	0.66	PLL	5, 21, 31, 35, 36, 45, 51, 56, 60, 65, 86
J2219+4754	35-1435	224	-0.47(16)	238(12)	-2.71(11)	—	0.52	BPL	8, 9, 10, 20, 21, 25, 29, 40, 45, 51, 55, 60, 62, 67, 69, 70, 75
J2256-1024	131-1500	444	-1.99(22)	—	—	—	0.92	PL	14, 60
J2317+2149*	25-4850	348	0.39(23)	196(6)	-2.05(7)	—	0.92	BPL	5, 8, 9, 10, 29, 38, 45, 51, 52, 55, 60, 67, 69, 79, 80, 83
J2330-2005	35-4920	415	-1.07(14)	28(12)	5.56(41)	2.09(119)	0.75	DT	5, 10, 21, 25, 29, 31, 35, 45, 51, 56, 60, 69, 75, 85, 86
J2346-0609	102-1360	373	-0.06(43)	1712(265)	—	—	0.49	PLH	31, 35, 55, 58, 60

^a ν_{range} and ν_0 are the frequency range used in fitting and reference frequency.

^b P_{best} is probability that the best-fit model is the true model, and Type is the type of best fitting model.

^c Spectral index for PL, PLH, PLL and DT, and spectral index below break frequency for BPL model.

^d Break frequency (BPL), Cut-off frequency (PLH), and Turn-over frequency (PLL and DT).

^e Spectral index above break frequency (BPL), and Cut-off frequency (DT) in GHz

^f Curvature parameter for PLL and DT

Pulsars whose spectral modeling has improved with the addition of EDA2 measurements are marked by *

References: (1)M. F. Alam et al. (2021), (2)R. J. Aloisi et al. (2019), (3)N. Bartel et al. (1978), (4)M. E. Bell et al. (2016), (5)N. D. R. Bhat et al. (2023), (6)B. Bhattacharyya et al. (2016), (7)B. Bhattacharyya et al. (2016), (8)A. V. Bilous et al. (2016), (9)A. V. Bilous et al. (2020), (10)L. Bondonneau et al. (2020), (11)L. Bondonneau et al. (2021), (12)S. Chatterjee et al. (2005), (13)M. E. Costa et al. (1991), (14)K. Crowter et al. (2020), (15)S. Dai et al. (2015), (16)A. T. Deller et al. (2009), (17)P. B. Demorest et al. (2013), (18)R. J. Dewey et al. (1985), (19)J. Dowell et al. (2013), (20)E. B. Fomalont et al. (1992), (21)D. A. Frail et al. (2016), (22)P. A. Gentile et al. (2018), (23)P. Gitika et al. (2023), (24)D. M. Gould & A. G. Lyne (1998), (25)J. L. Han & W. W. Tian (1999), (26)J. Han et al. (2016), (27)G. Hobbs et al. (2004), (28)A. von Hoensbroech & K. M. Xilouris (1997), (29)V. A. Izvekova et al. (1981), (30)F. Jankowski et al. (2018), (31)F. Jankowski et al. (2018), (32)S. Johnston et al. (1992), (33)S. Johnston et al. (1993), (34)S. Johnston et al. (2006), (35)S. Johnston & M. Kerr (2018), (36)S. Johnston et al. (2021), (37)M. J. Keith et al. (2011), (38)J. Kijak et al. (1998), (39)V. I. Kondratiev et al. (2016), (40)M. L. A. Kouwenhoven (2000), (41)M. Kramer et al. (1997), (42)M. Kramer et al. (1998), (43)M. Kramer et al. (1999), (44)I. P. Kravtsov et al. (2022), (45)P. Kumar et al. (2025), (46)M. Kuniyoshi et al. (2015), (47)A. D. Kuzmin & B. Y. Losovsky (2001), (48)P. Lazarus et al. (2015), (49)C. P. Lee et al. (2022), (50)D. R. Lorimer et al. (1995b), (51)D. R. Lorimer et al. (1995a), (52)D. R. Lorimer et al. (2005), (53)A. G. Lyne et al. (1998), (54)V. M. Malofeev (1993), (55)V. M. Malofeev et al. (2000), (56)R. N. Manchester et al. (1978), (57)R. N. Manchester & S. Johnston (1995), (58)R. N. Manchester et al. (1996), (59)R. N. Manchester et al. (2013), (60)A. E. McEwen et al. (2020), (61)R. S. McGary et al. (2001), (62)A. I. O. McLean (1973), (63)R. P. Mignani et al. (2017), (64)K. Mikhailov & J. van Leeuwen (2016), (65)T. Murphy et al. (2017), (66)G. Qiao et al. (1995), (67)S. Sanidas et al. (2019), (68)R. W. Sayer et al. (1997), (69)J. H. Seiradakis et al. (1995), (70)J. A. Shrauner et al. (1998), (71)R. Spiewak et al. (2022), (72)I. H. Stairs et al. (1999), (73)B. W. Stappers et al. (2008), (74)G. H. Stokes et al. (1985), (75)K. Stovall et al. (2015), (76)J. H. Taylor et al. (1993), (77)M. Toscano et al. (1998), (78)M. Toscano et al. (1998), (79)S. A. Tyul'bashev et al. (2016), (80)J. M. Weisberg et al. (1999), (81)Y.-W. Xie et al. (2019), (82)M. Xue et al. (2017), (83)V. V. Zakharenko et al. (2013), (84)R.-S. Zhao et al. (2017), (85)R.-S. Zhao et al. (2019), (86)T. D. van Ommen et al. (1997)

D. RM VALUES FOR PULSARS DETECTED BY EDA2

Table D4. EDA2 RM measurements for 40 pulsars. For comparison we give the RM reported in ATNF pulsar catalog (R. N. Manchester et al. 2005) and with MeerKAT (B. Posselt et al. 2023), along with Δ RM between our measurements and these two catalog. Pulsar whose RM could be affected instrumental polarization near RM=0, are marked by asterisk. The table is published in its entirety in a machine readable online format.

Name	RM _{obs} (rad m ⁻²)	RM _{ion} rad m ⁻²	RM _{ISM} (rad m ⁻²)	RM _{ISM} ^{ATNF} (rad m ⁻²)	Δ RM _{Obs} ^{ATNF} (rad m ⁻²)	RM _{ISM} ^{MeerKat} (rad m ⁻²)	δ RM _{Obs} ^{MeerKat} (rad m ⁻²)	B (μ G)
J0034-0721	8.31(5)	-1.65(10)	9.96(11)	9.89(7)	0.07(13)	9.9(29)	0.06(290)	1.12
J0437-4715*	-0.59(14)	-5.45(10)	4.86(17)	0.15(1)	4.7(17)	—	—	0.07
J0534+2200	-44.53(8)	-1.16(8)	-43.36(11)	-45.44(8)	2.07(14)	—	—	-0.99
J0630-2834	43.34(1)	-3.24(14)	46.59(14)	46.53(12)	0.06(19)	46.5(290)	0.09(290)	1.67
J0742-2822	147.3(7)	-3.58(10)	150.89(13)	149.94(5)	0.94(14)	149.9(290)	0.99(290)	2.50
J0820-1350*	0.46(19)	-3.65(2)	4.11(20)	-1.2(40)	5.31(44)	-1.2(290)	5.31(290)	-0.04
J0826+2637*	-0.04(21)	-2.28(5)	2.24(22)	5.38(6)	-3.13(22)	—	—	0.34
J0835-4510	42.43(13)	-3.66(4)	46.1(14)	31.38(1)	14.72(14)	39.4(290)	6.7(290)	0.57
J0837+0610	20.75(1)	-2.61(3)	23.37(3)	25.32(7)	-1.94(7)	25.3(290)	-1.92(290)	2.42
J0837-4135	143.59(32)	-4.35(25)	147.95(40)	144.5(70)	3.45(81)	145.0(290)	2.95(292)	1.21
J0922+0638	30.37(30)	-1.73(4)	32.11(31)	29.2(30)	2.91(43)	29.2(290)	2.91(291)	1.32
J0942-5657	139.09(24)	-4.49(18)	143.58(30)	135.0(400)	8.58(401)	141.5(290)	2.08(291)	1.04
J0946+0951	9.36(5)	-2.76(12)	12.13(13)	14.1(8)	-1.96(15)	—	—	1.13
J0953+0755*	-1.02(11)	-1.77(15)	0.75(19)	-0.66(4)	1.41(19)	-0.7(300)	1.45(300)	-0.28
J1022+1001*	0.4(27)	-1.12(5)	1.52(28)	1.39(5)	0.13(28)	—	—	0.17
J1057-5226	45.15(17)	-2.64(33)	47.79(37)	47.2(80)	0.59(88)	47.2(290)	0.59(292)	1.96
J1136+1551*	-1.6(6)	-2.9(6)	1.3(8)	3.97(7)	-2.66(11)	4.0(290)	-2.69(290)	1.02
J1224-6407*	-3.24(30)	-1.62(8)	-1.62(31)	-5.6(60)	3.97(67)	-3.6(290)	1.97(291)	-0.07
J1239+2453*	-0.96(15)	-0.55(2)	-0.41(15)	-0.12(6)	-0.29(17)	-0.1(290)	-0.31(290)	-0.02
J1453-6413	-21.72(9)	-1.99(13)	-19.72(16)	-18.6(20)	-1.12(25)	-18.6(290)	-1.12(290)	-0.32
J1456-6843*	-0.56(14)	-1.55(14)	0.99(20)	-0.1(60)	1.09(63)	-4.0(290)	4.99(290)	-0.01
J1507-4352	-33.33(56)	-2.68(14)	-30.64(58)	-34.0(700)	3.35(702)	-34.0(290)	3.35(295)	-0.85
J1527-3931	-10.57(36)	-1.42(6)	-9.15(36)	4.0(100)	-13.15(106)	-10.19(310)	1.04(312)	0.10
J1543-0620	-6.33(26)	-0.88(10)	-5.44(28)	-1.8(80)	-3.64(84)	-1.8(290)	-3.64(291)	-0.12
J1607-0032	5.07(1)	-1.19(14)	6.26(14)	6.5(100)	-0.23(101)	6.5(330)	-0.23(330)	0.75
J1645-0317	14.52(10)	-1.0(12)	15.53(16)	15.8(30)	-0.27(34)	15.8(290)	-0.27(290)	0.54
J1709-1640	-2.77(2)	-1.34(8)	-1.43(9)	1.5(90)	-2.93(90)	-1.3(290)	-0.13(290)	0.07
J1751-4657	18.33(24)	-1.19(5)	19.53(24)	19.0(100)	0.53(103)	19.0(290)	0.53(291)	1.14
J1752-2806	94.53(11)	-1.26(3)	95.79(11)	96.0(20)	-0.2(23)	96.0(300)	-0.2(300)	2.35
J1825-0935	67.05(23)	-1.0(13)	68.06(26)	67.0(60)	1.06(65)	65.2(290)	2.86(291)	4.27
J1913-0440*	3.67(25)	-0.73(5)	4.4(25)	3.98(5)	0.42(26)	4.0(290)	0.4(291)	0.05
J1921+2153	-17.93(30)	-0.5(3)	-17.42(30)	-16.98(5)	-0.43(30)	-17.0(290)	-0.42(291)	-1.69

Table D4 continued

Table D4 (*continued*)

Name	RM_{obs} (rad m^{-2})	RM_{ion} rad m^{-2}	RM_{ISM} (rad m^{-2})	RM_{ISM}^{ATNF} (rad m^{-2})	ΔRM_{Obs}^{ATNF} (rad m^{-2})	$RM_{ISM}^{MeerKat}$ (rad m^{-2})	$\delta RM_{Obs}^{MeerKat}$ (rad m^{-2})	B_{\parallel} (μ G)
J1932+1059	-7.75(10)	-0.62(4)	-7.12(11)	-6.87(2)	-0.25(11)	-6.9(290)	-0.22(290)	-2.68
J1935+1616*	-1.52(41)	-0.6(4)	-0.91(42)	-10.19(30)	9.28(51)	-3.0(290)	2.08(293)	-0.08
J2018+2839	-35.84(58)	-0.48(3)	-35.36(58)	-34.9(10)	-0.46(59)	—	—	-3.06
J2046-0421*	-3.61(35)	-1.14(6)	-2.46(35)	-1.0(300)	-1.46(302)	-1.0(290)	-1.46(292)	-0.03
J2048-1616	-10.51(11)	-0.89(6)	-9.61(12)	-10.0(30)	0.38(32)	-10.0(290)	0.38(290)	-1.07
J2155-3118	13.8(3)	-0.95(13)	14.75(13)	21.0(300)	-6.24(300)	21.0(310)	-6.24(310)	1.75
J2219+4754	-37.32(27)	-0.19(4)	-37.12(28)	-35.93(6)	-1.19(28)	—	—	-1.02
J2330-2005	8.6(1)	-1.08(4)	9.69(4)	9.19(80)	0.49(80)	9.19(290)	0.49(290)	1.37

^a ΔRM_{Obs}^{ATNF} and $\delta RM_{Obs}^{MeerKat}$ are difference in ionospheric corrected RM between ATNF and EDA2, and MeerKAT and EDA2 respectively.

^b B_{\parallel} is calculated using equation 1 with RM_{ISM} and DM_{EDA2} from Table A1

E. MULTI-FREQUENCY PULSE PROFILES OF EDA2 DETECTED PULSARS

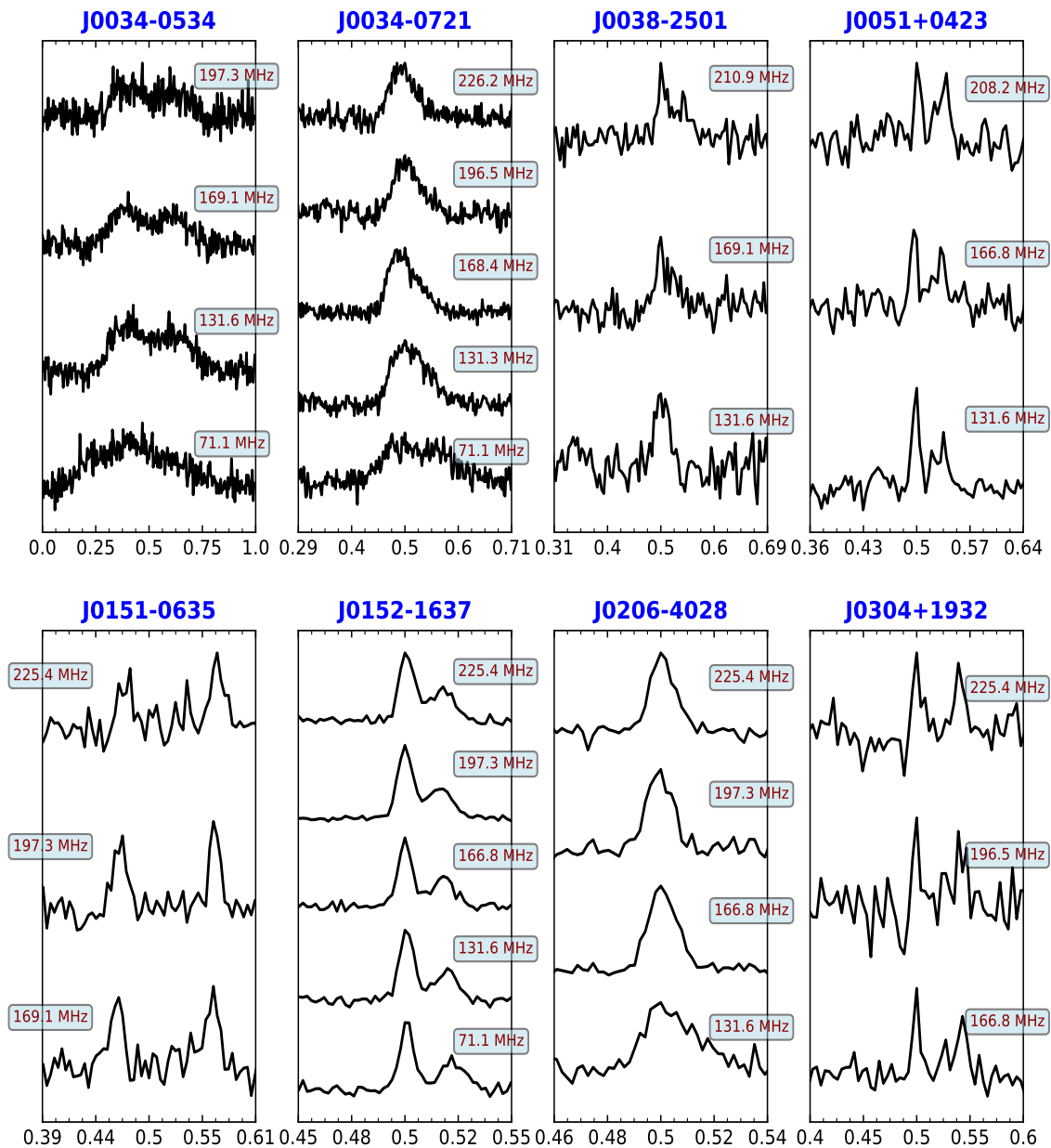


Figure E1. Average integrated pulse profiles, with x-axis zoomed on the phase region with emission. The center frequency of each profile is shown alongside, and the corresponding bandwidth is shown in Table B2. Profiles are aligned using their peaks.

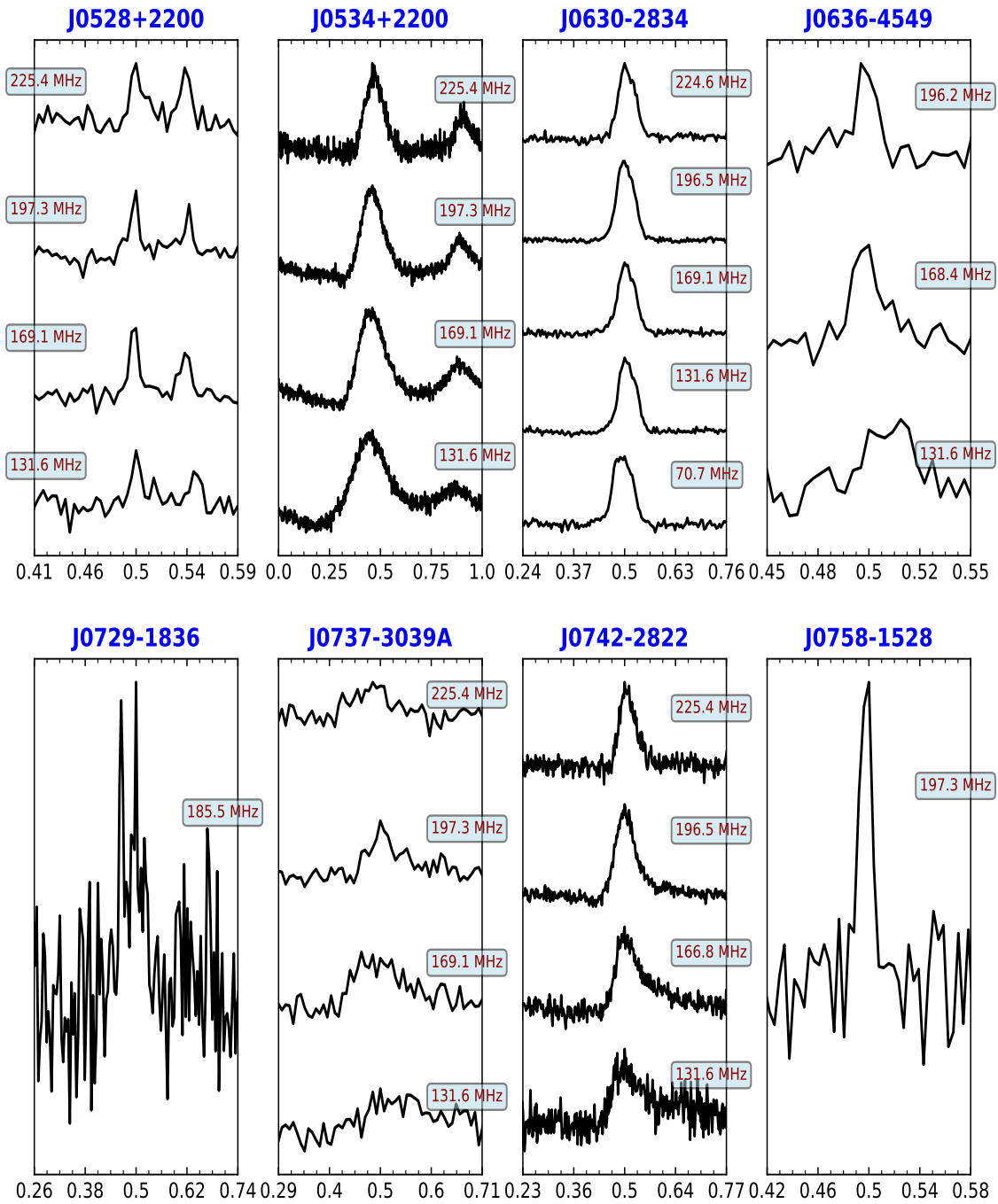


Figure E2. Fig E1 Continued

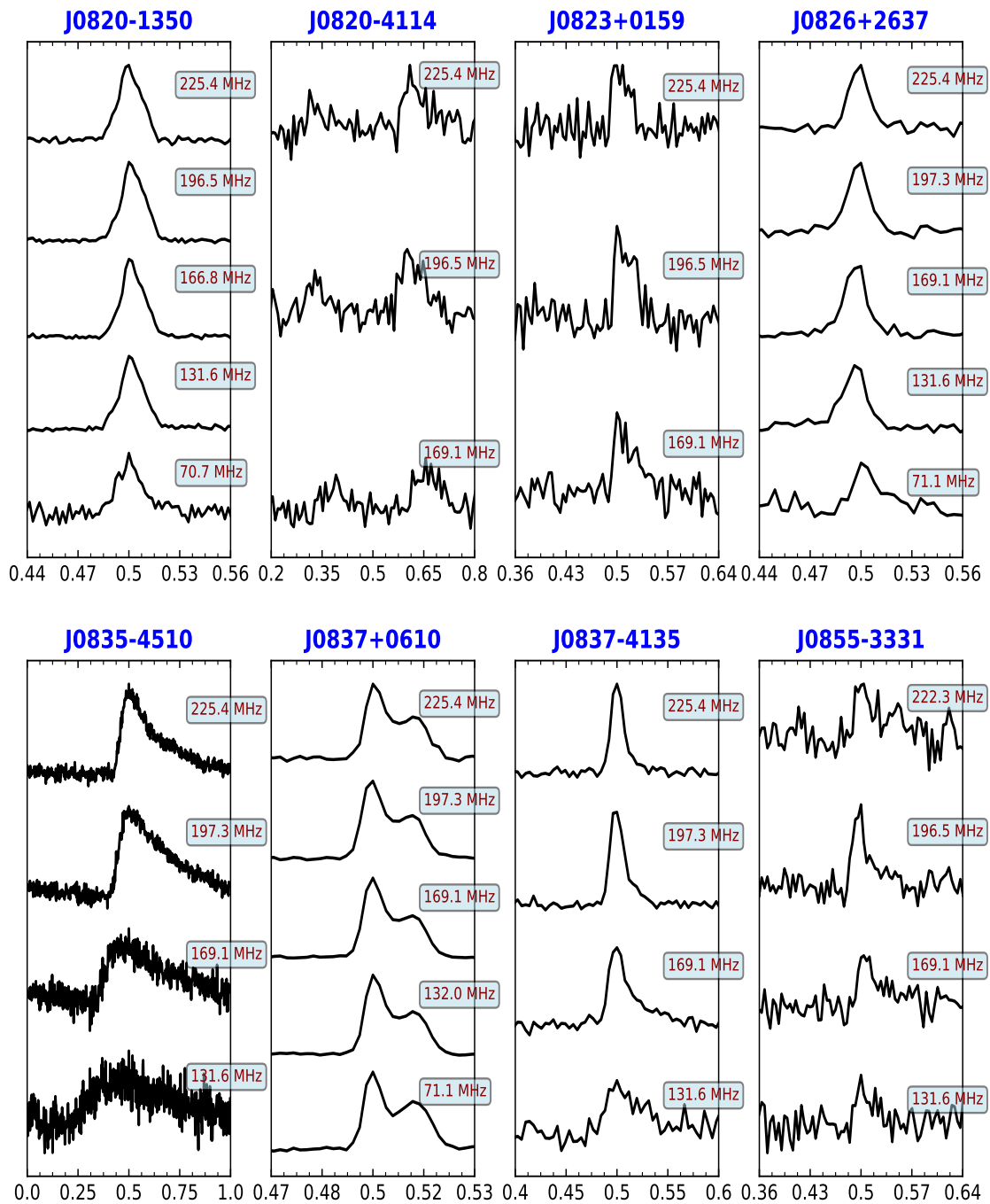


Figure E3. Fig E1 Continued

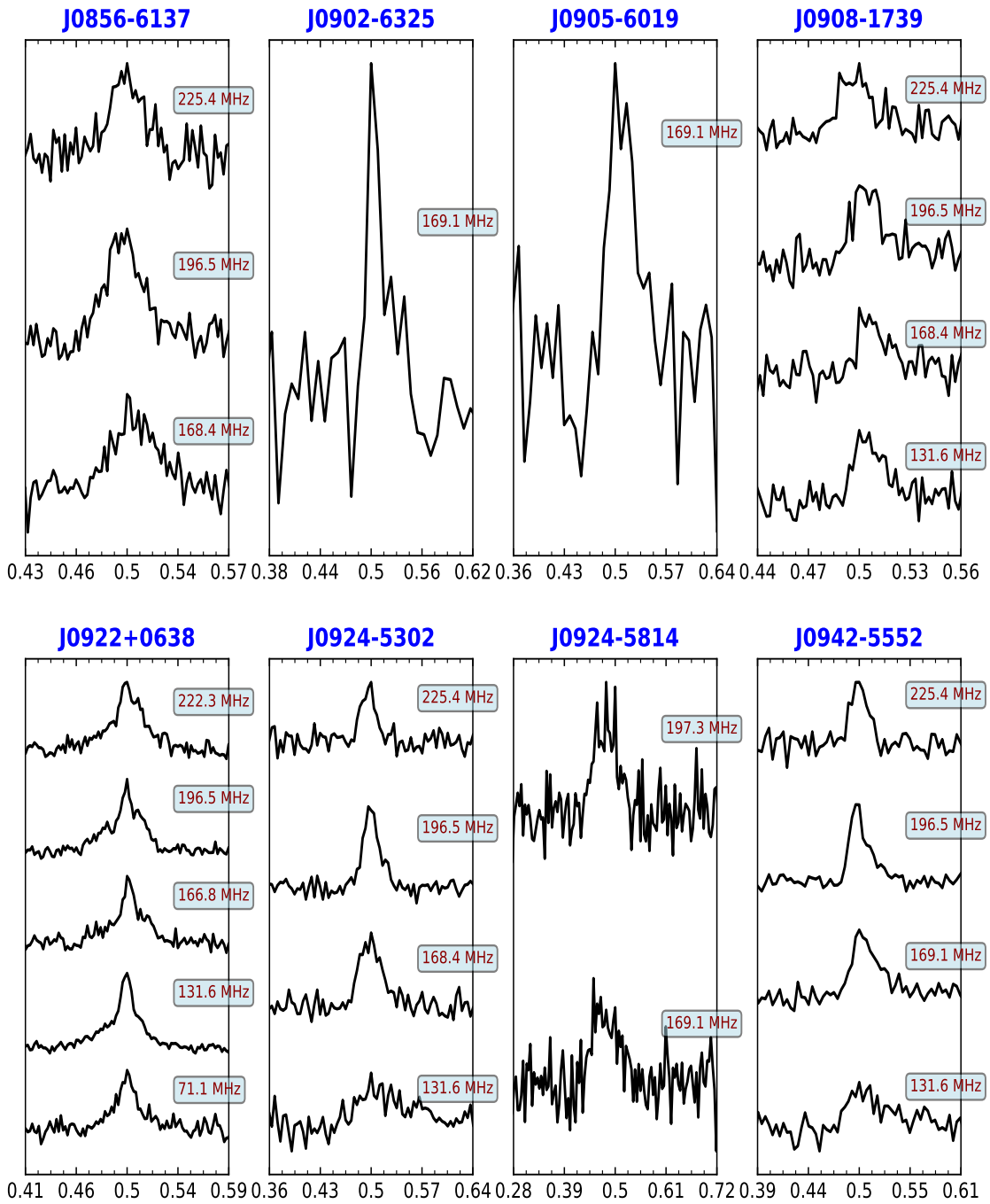


Figure E4. Fig E1 Continued

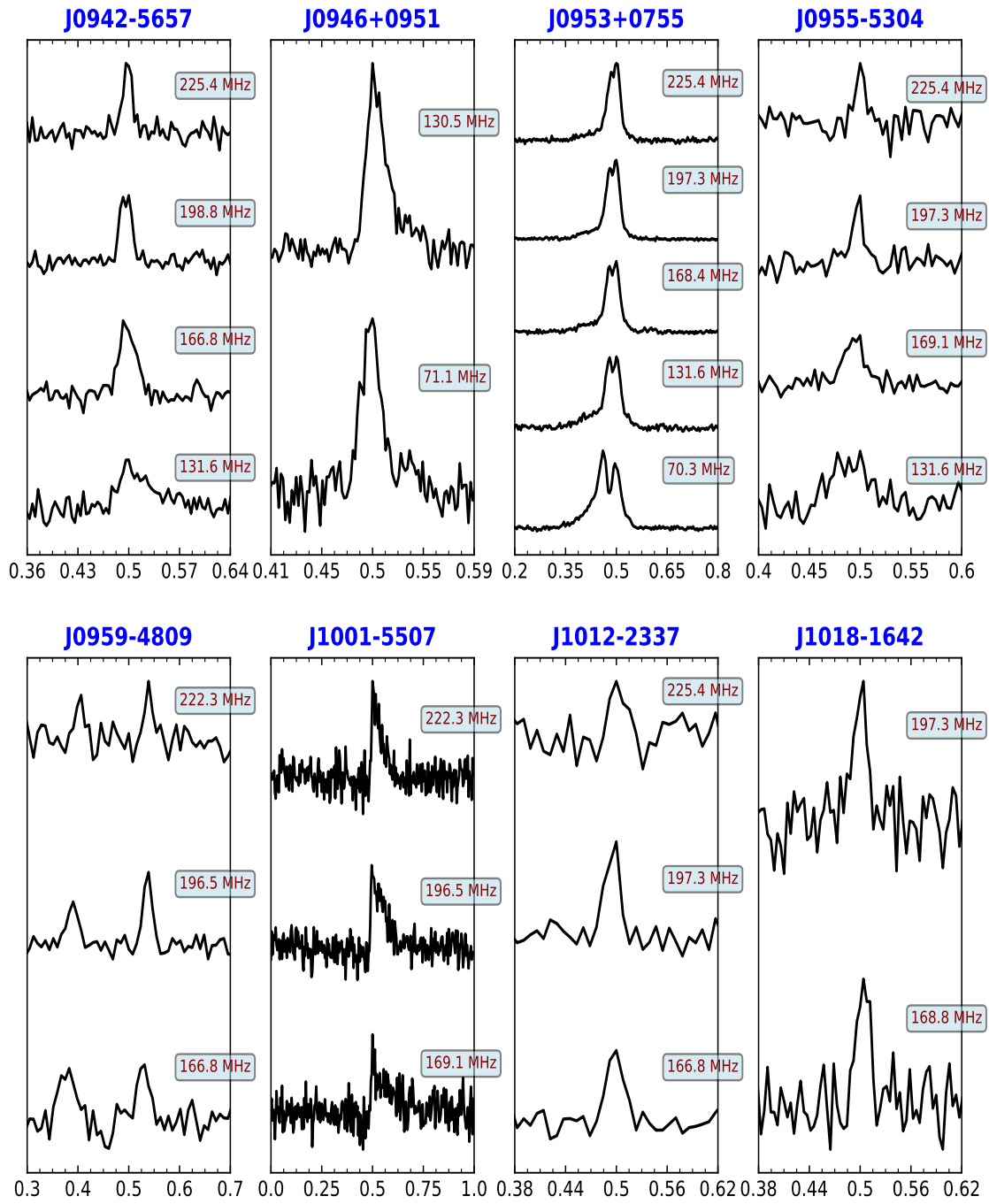


Figure E5. Fig E1 Continued

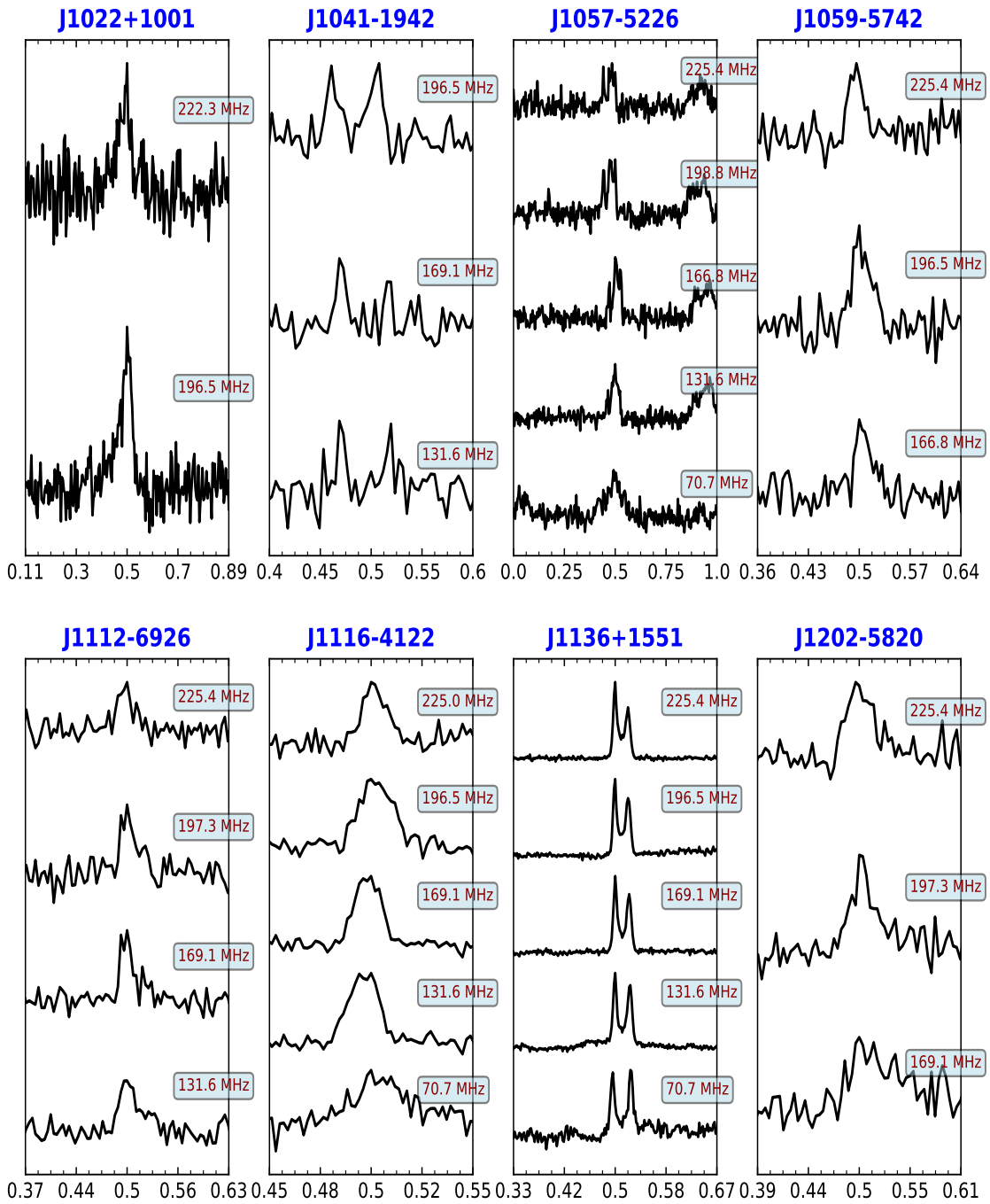


Figure E6. Fig E1 Continued

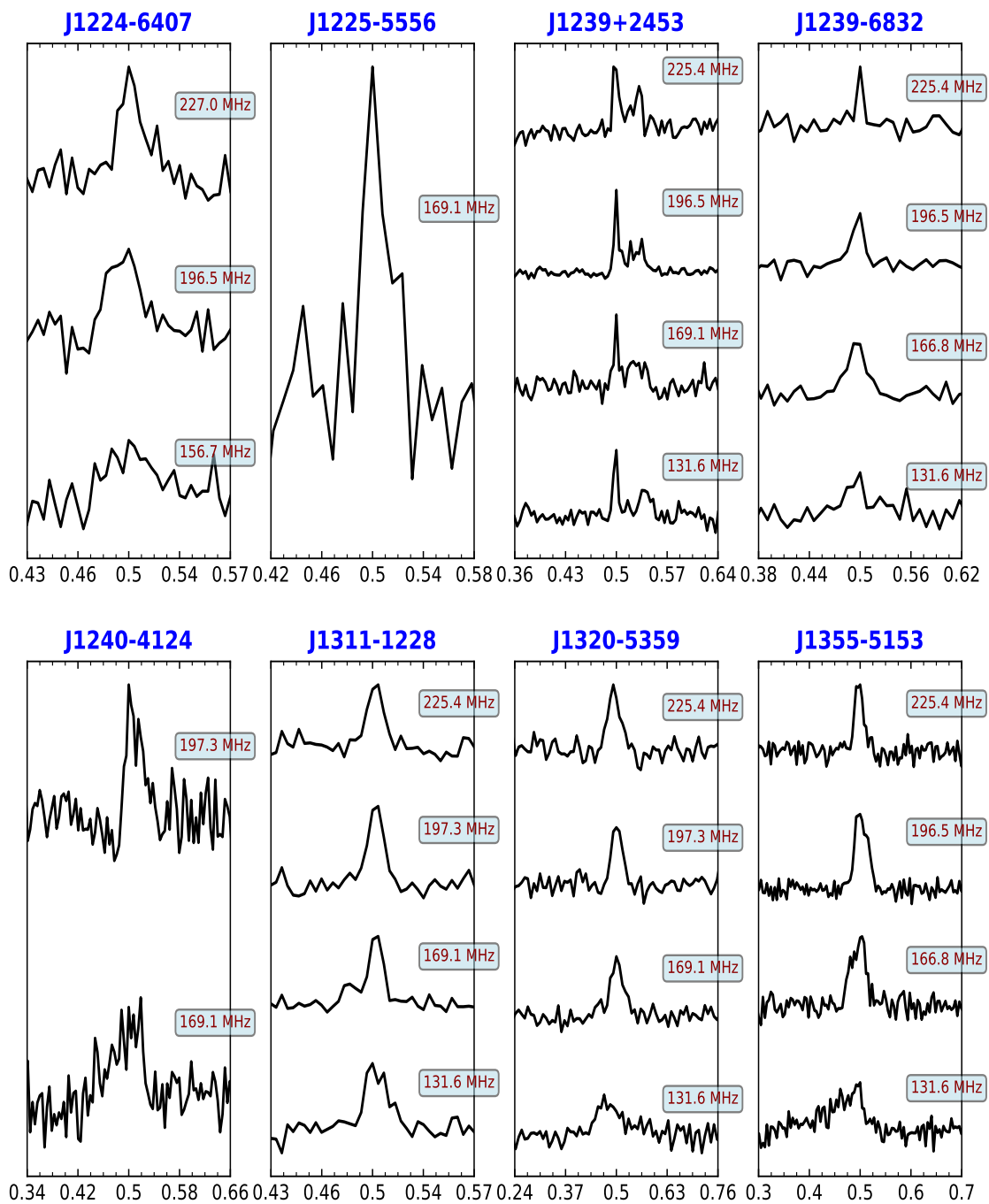


Figure E7. Fig E1 Continued

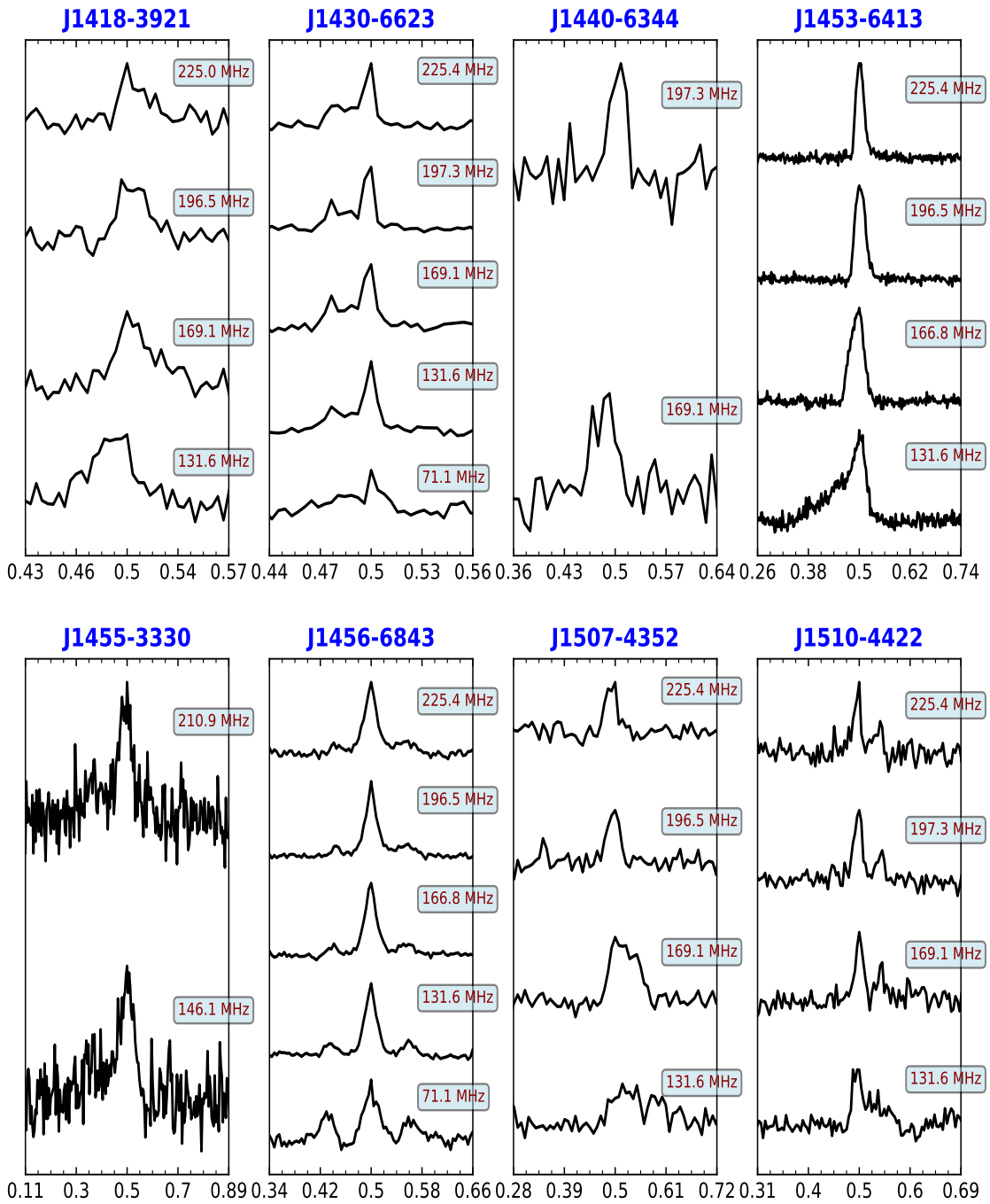


Figure E8. Fig E1 Continued

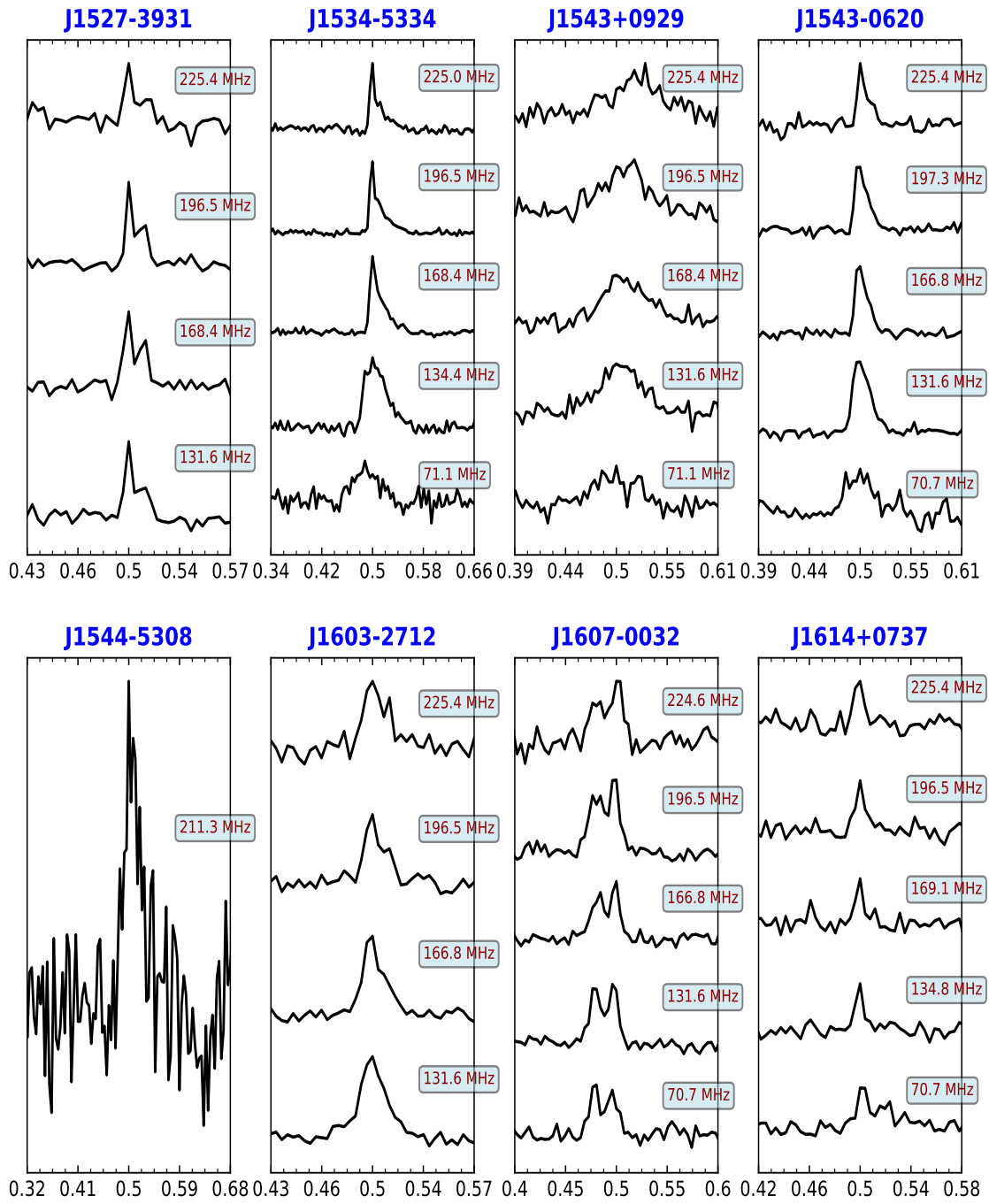


Figure E9. Fig E1 Continued

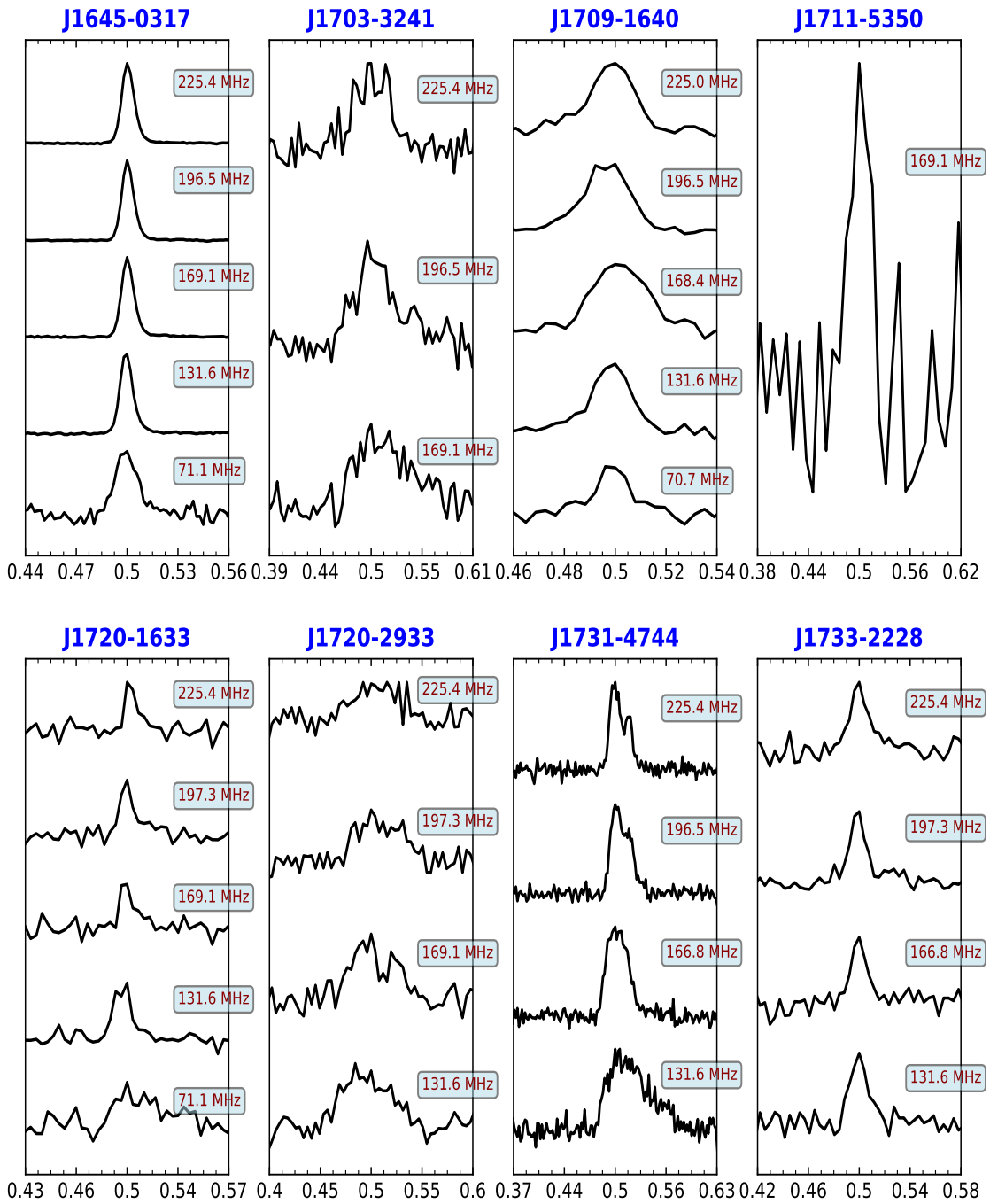


Figure E10. Fig E1 Continued

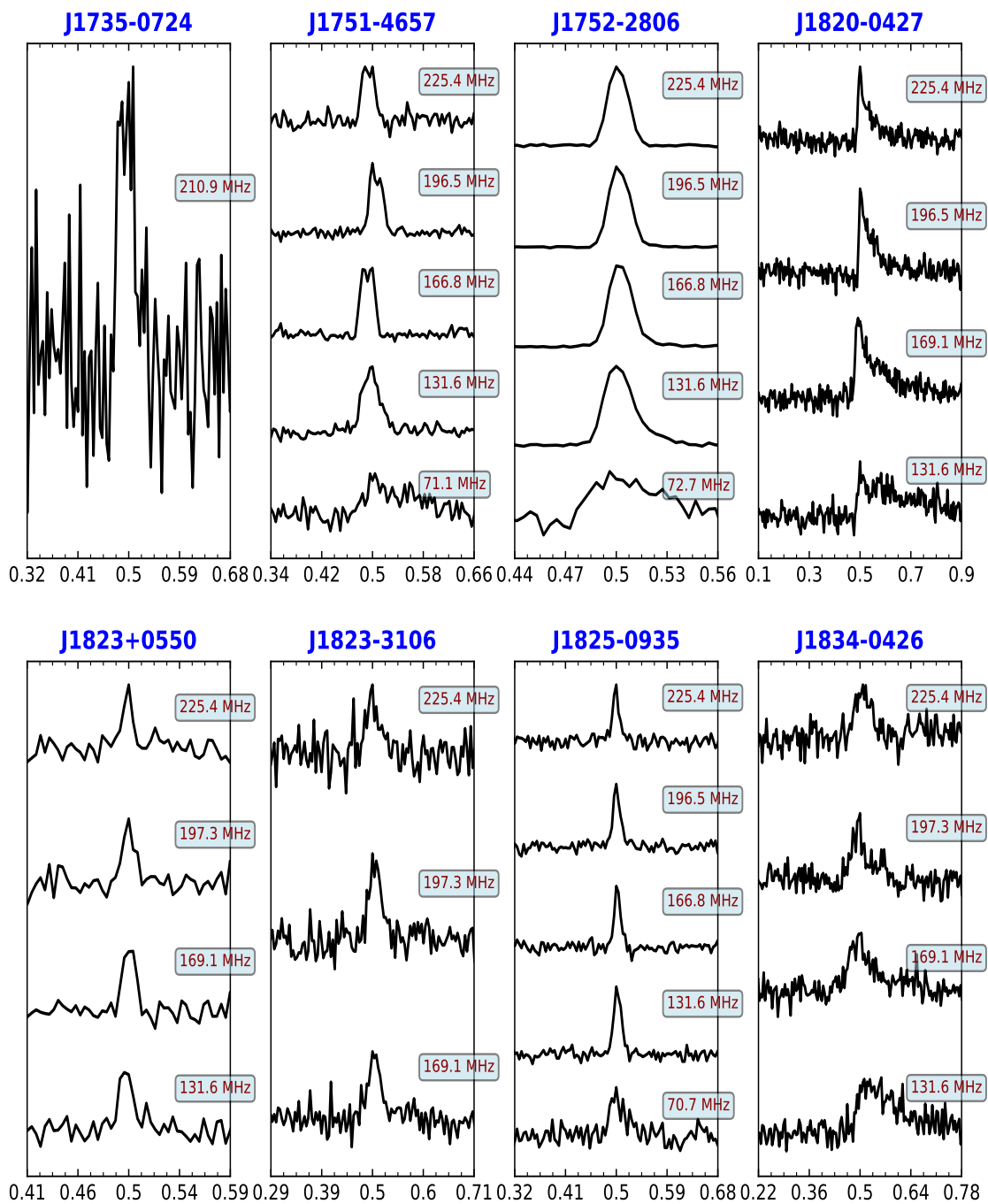


Figure E11. Fig E1 Continued

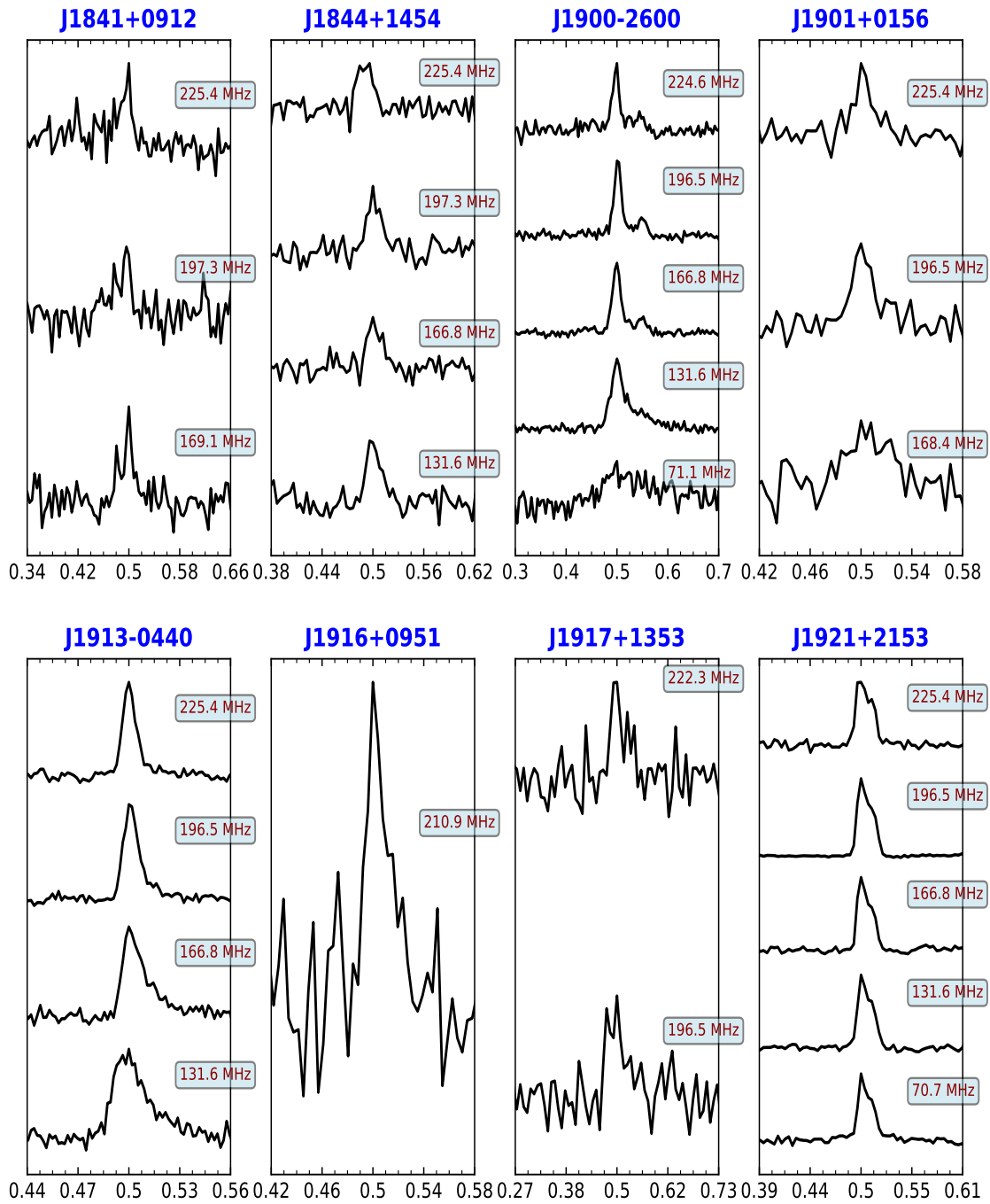


Figure E12. Fig E1 Continued

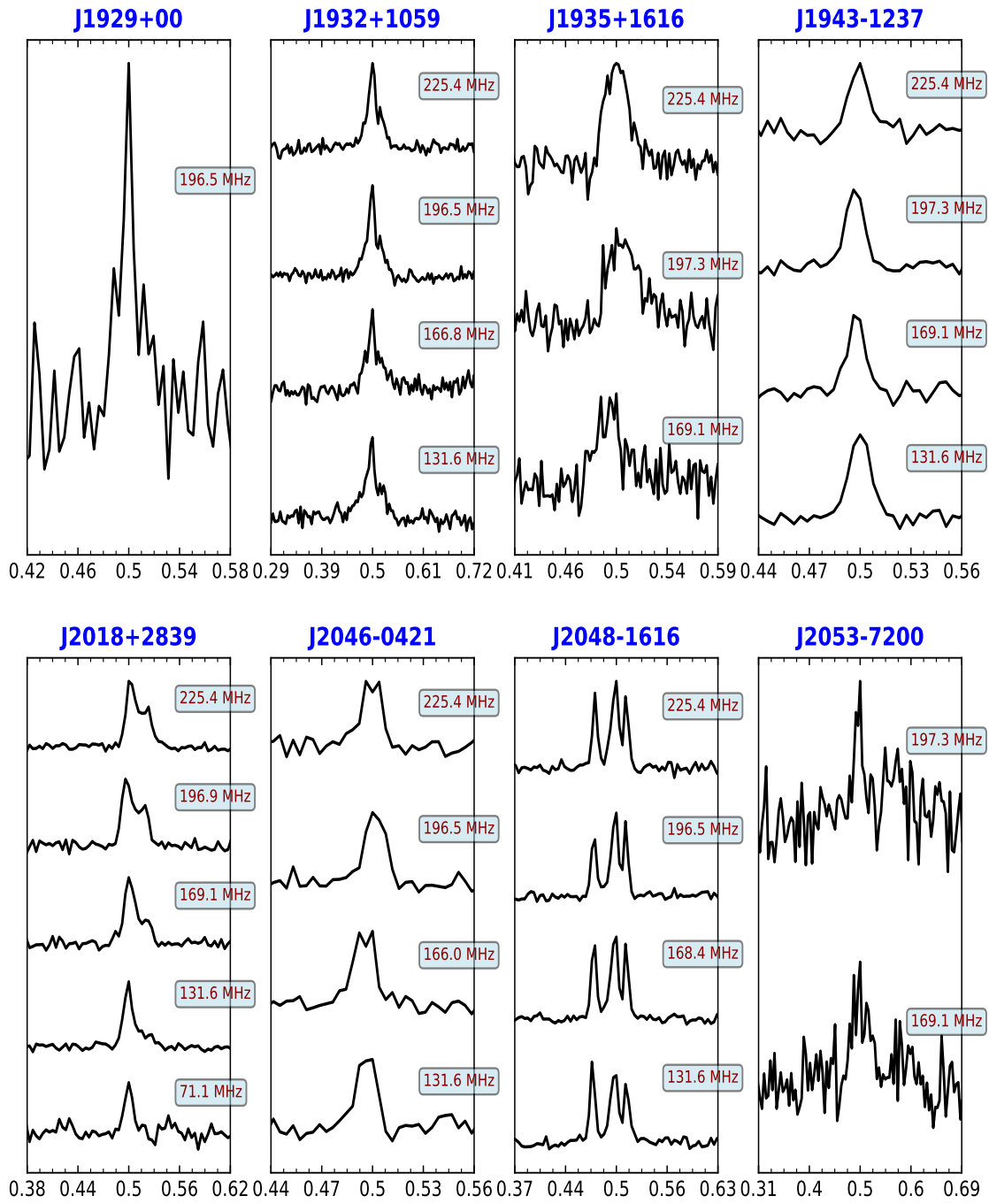


Figure E13. Fig E1 Continued

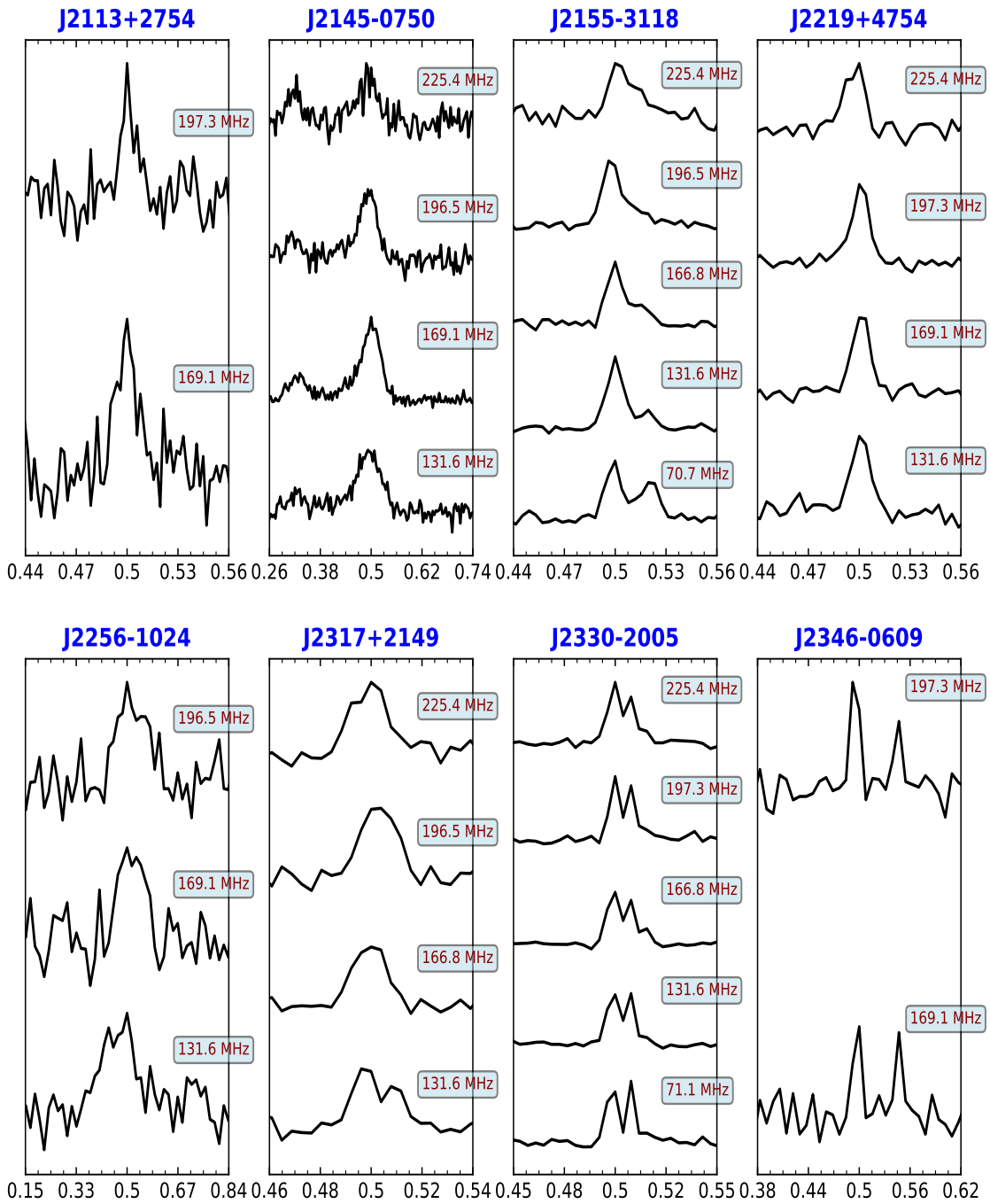


Figure E14. Fig E1 Continued

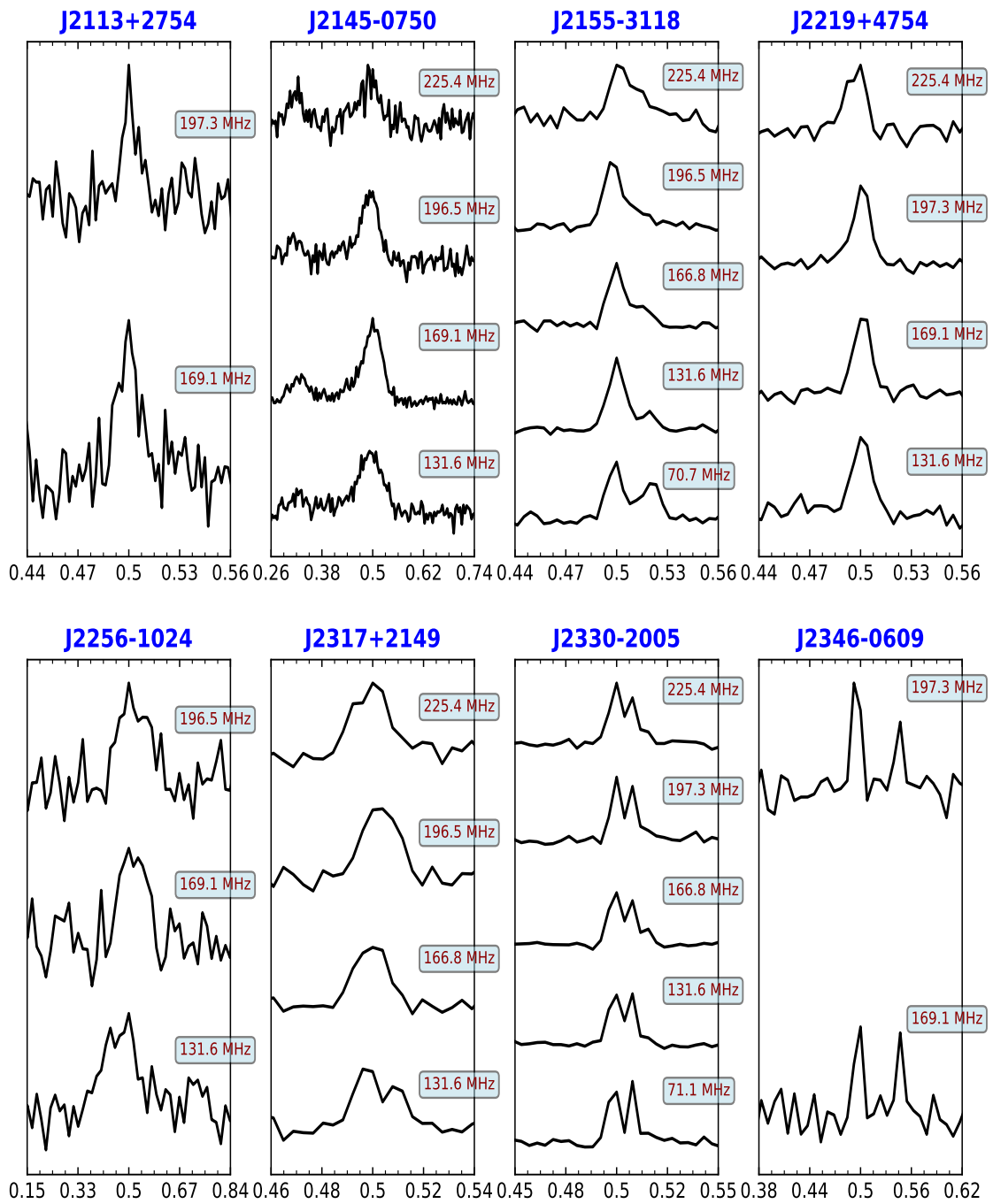


Figure E15. Fig E1 Continued

F. SPECTRA OF EDA2 DETECTED PULSARS

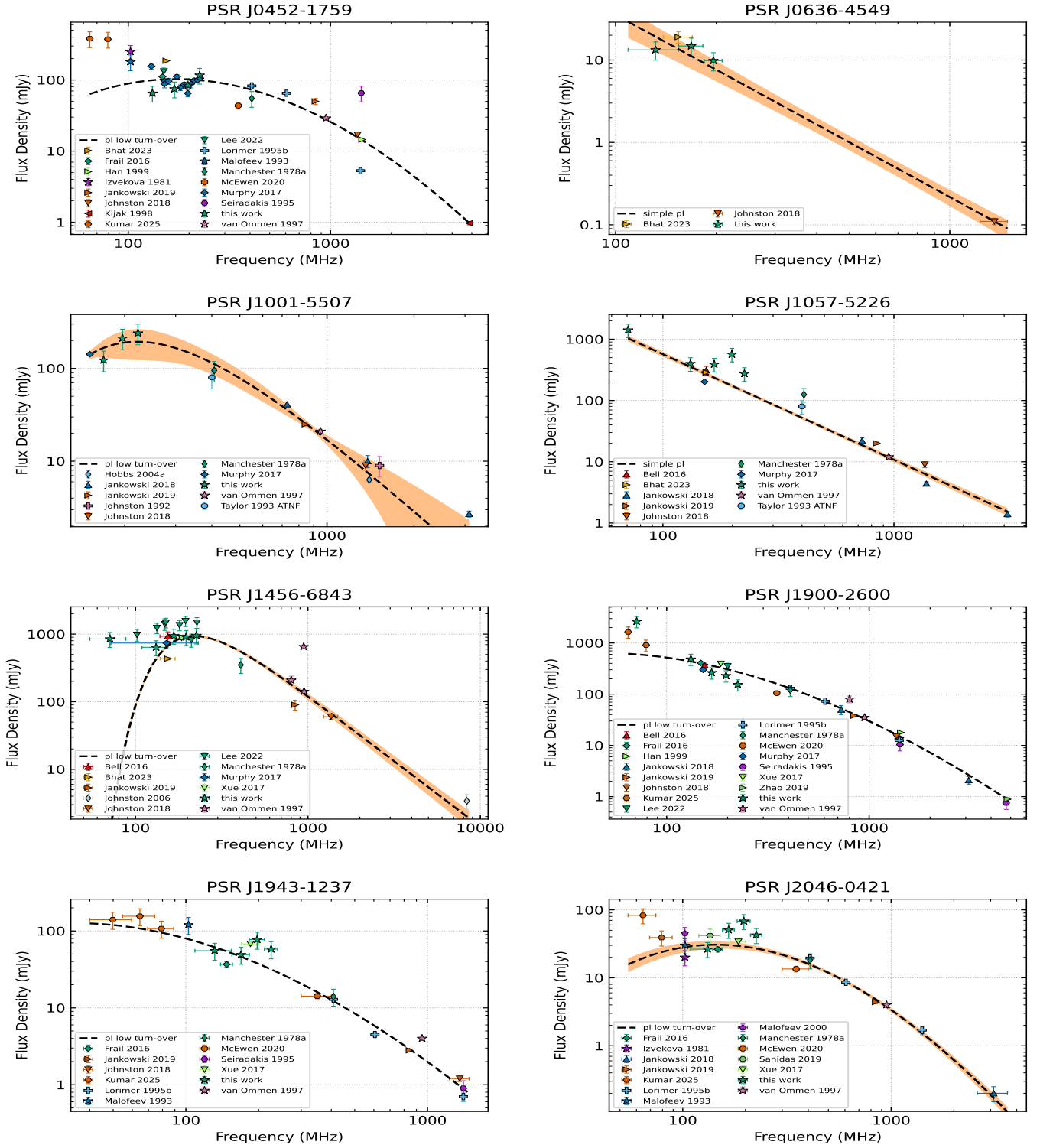


Figure F16. Flux density spectra for detected census pulsars, where measurements from this work are shown in green stars. Black dashed lines show the best fit model along with the 1σ uncertainty in the orange envelope.

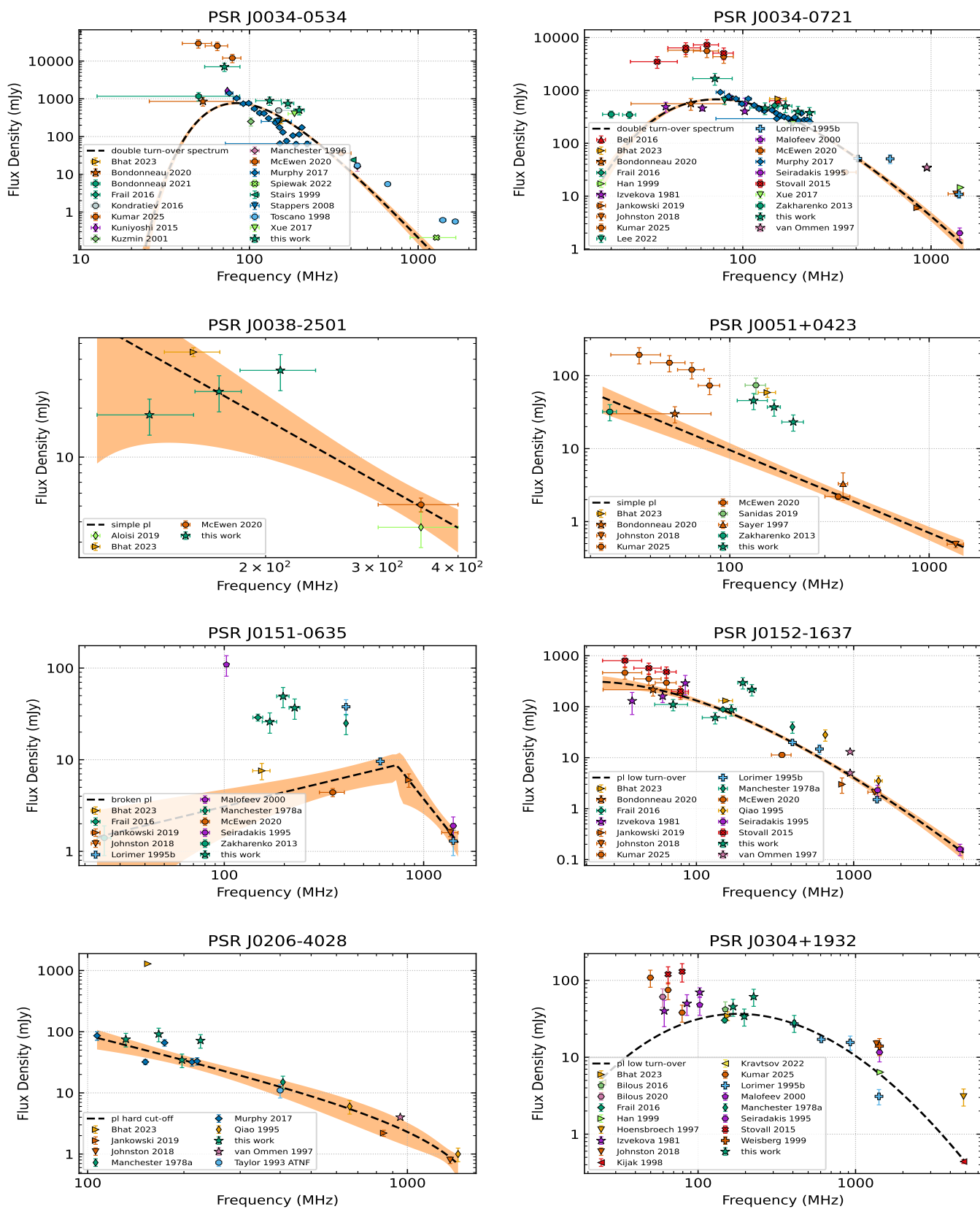


Figure F17. Fig F16 Continued

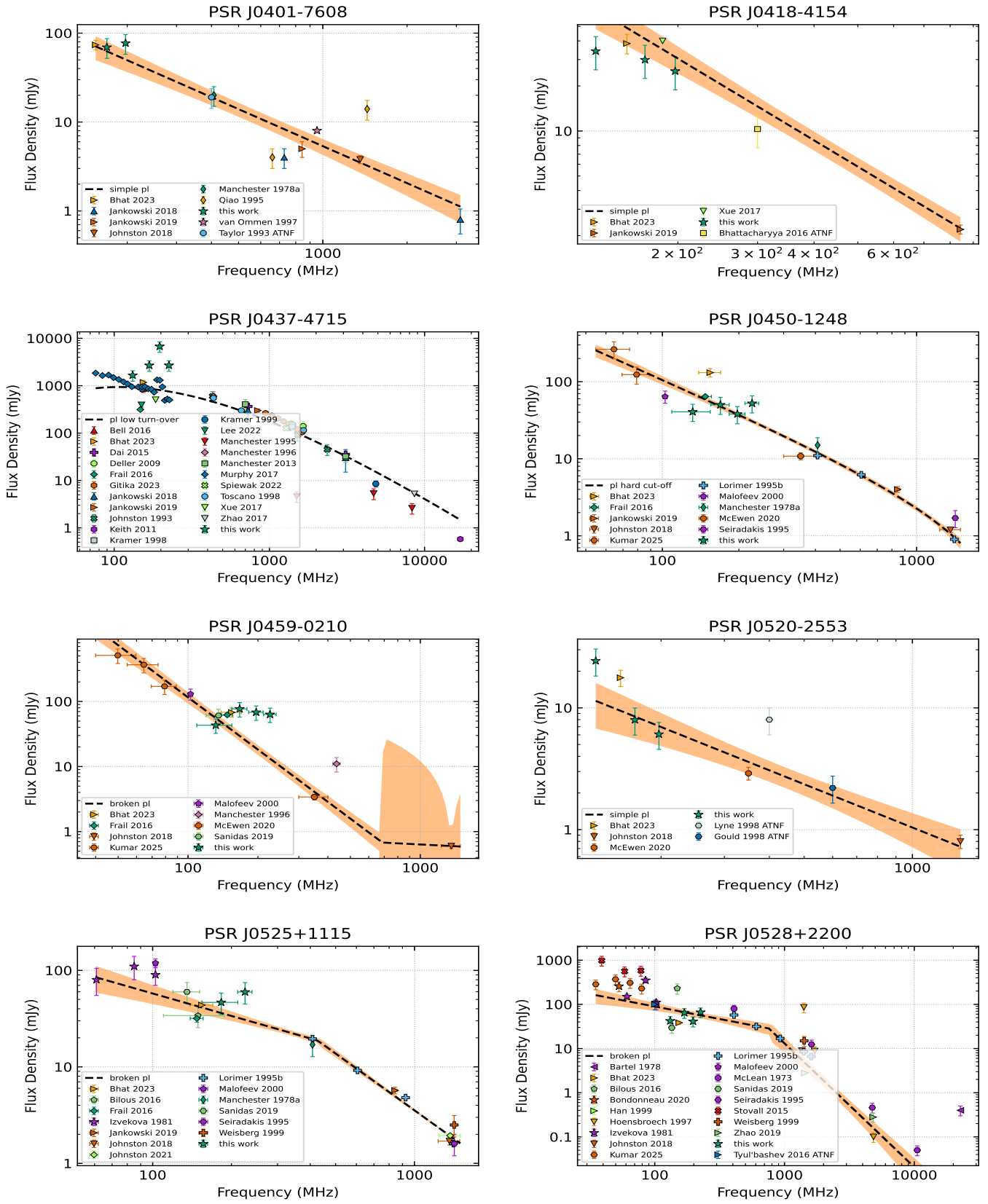


Figure F18. Fig F16 Continued

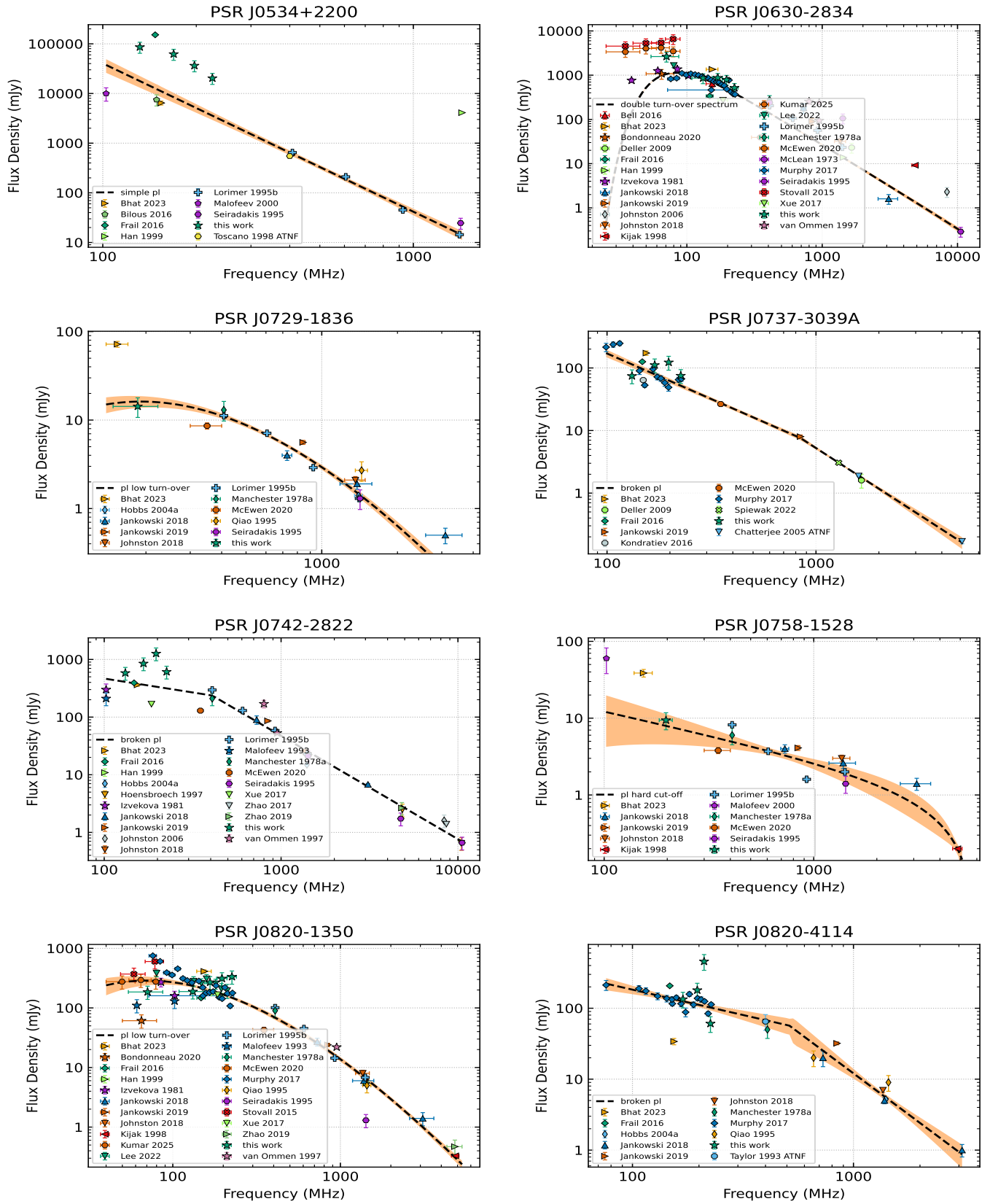


Figure F19. Fig F16 Continued

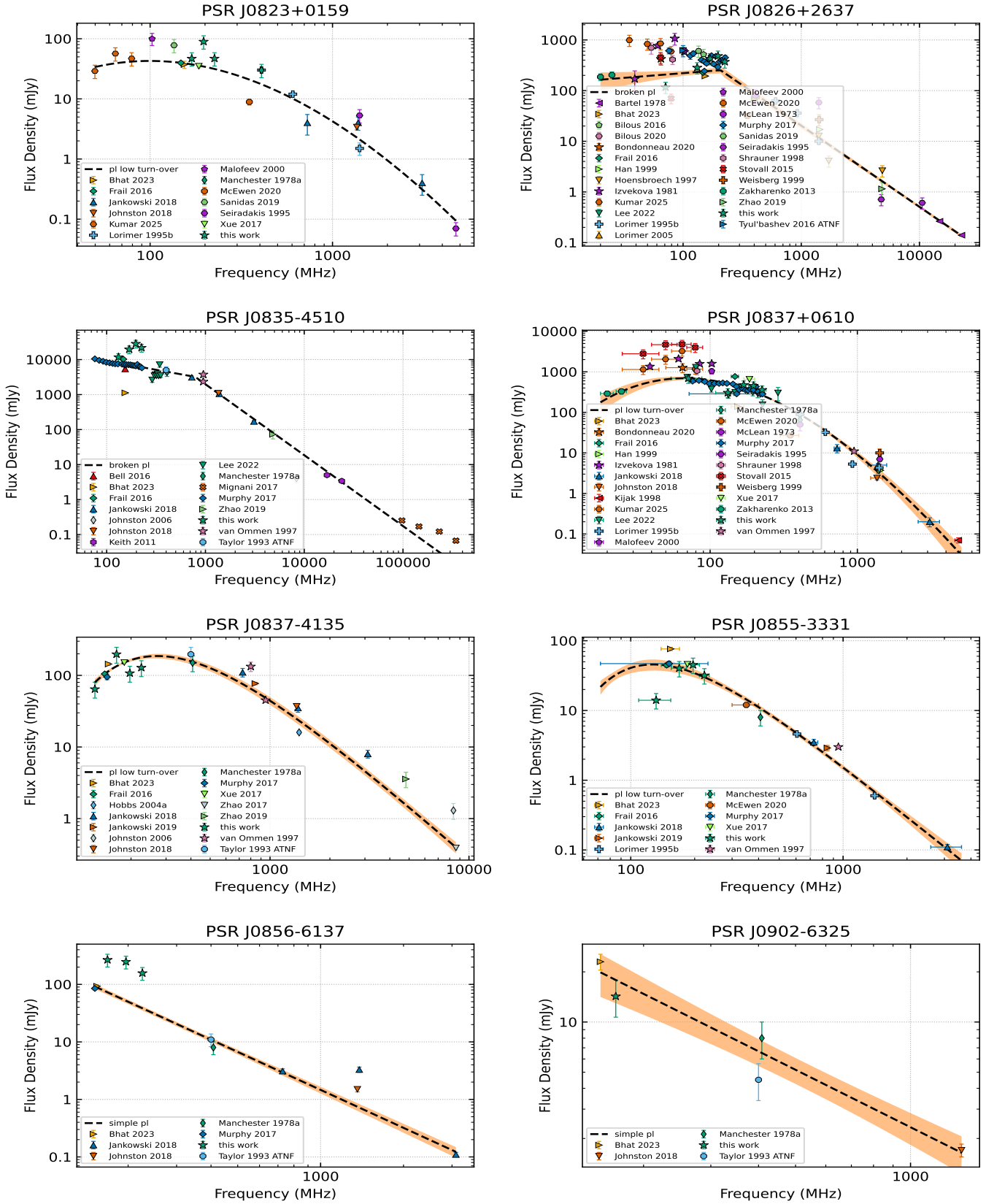


Figure F20. Fig F16 Continued

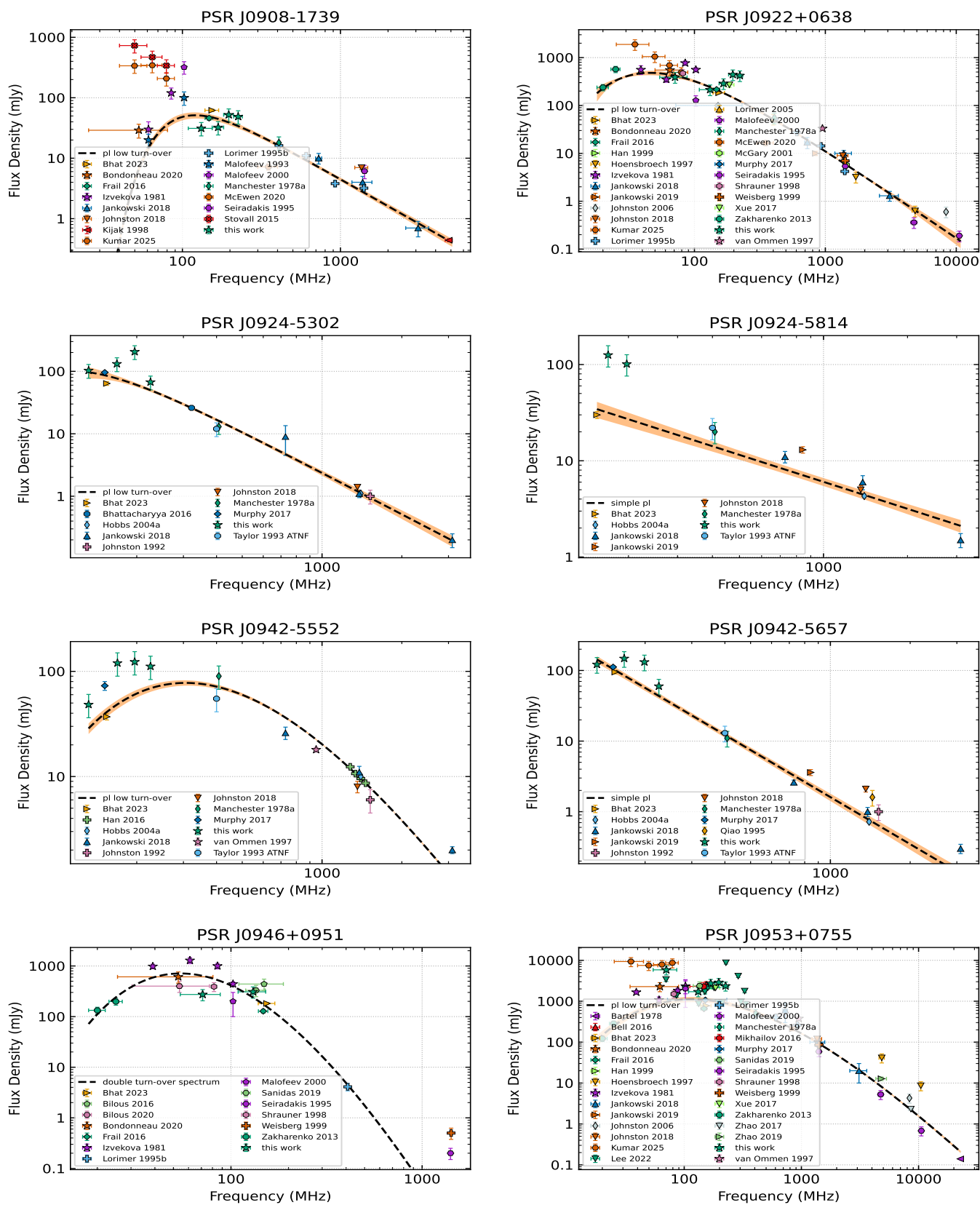


Figure F21. Fig F16 Continued

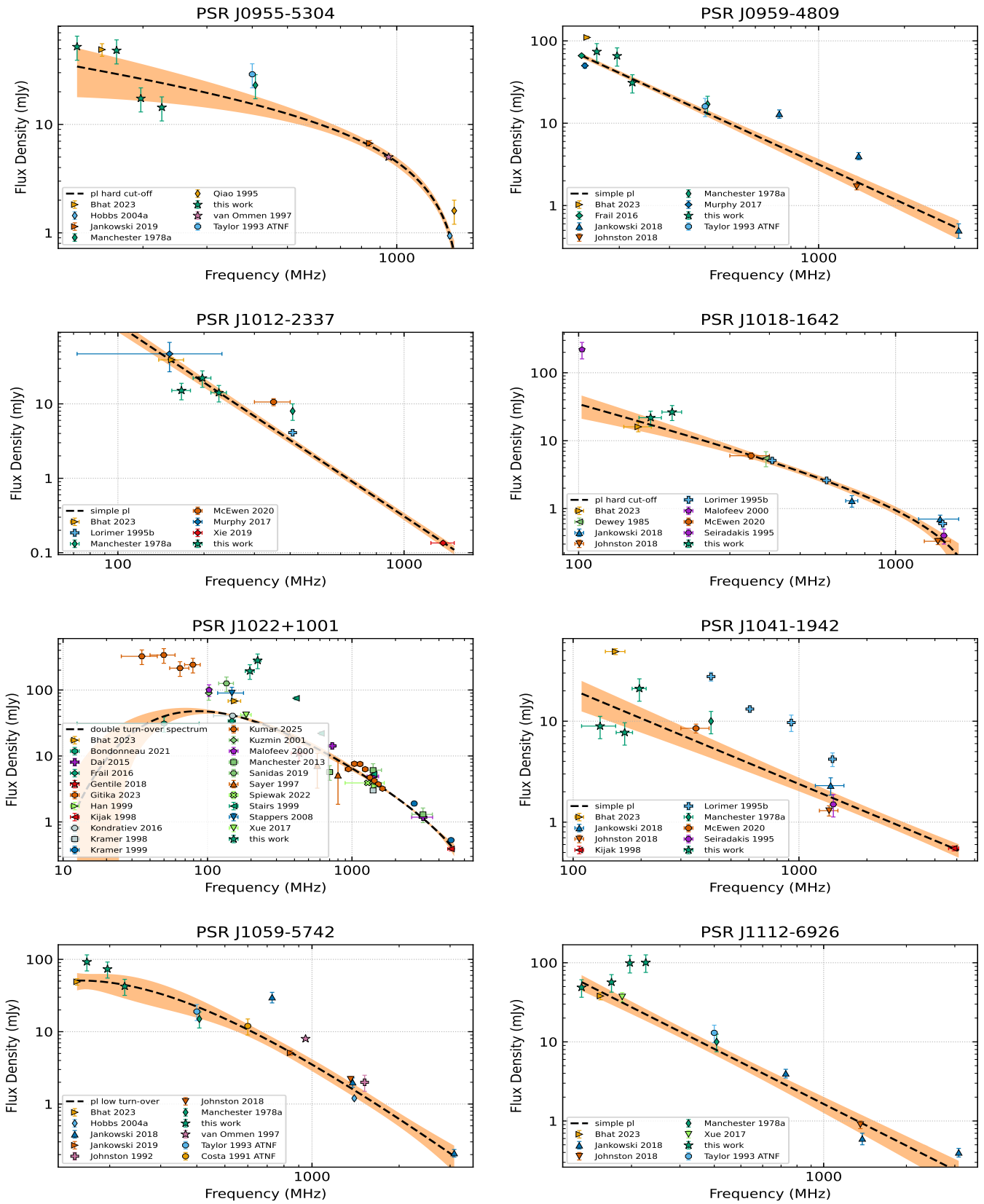


Figure F22. Fig F16 Continued

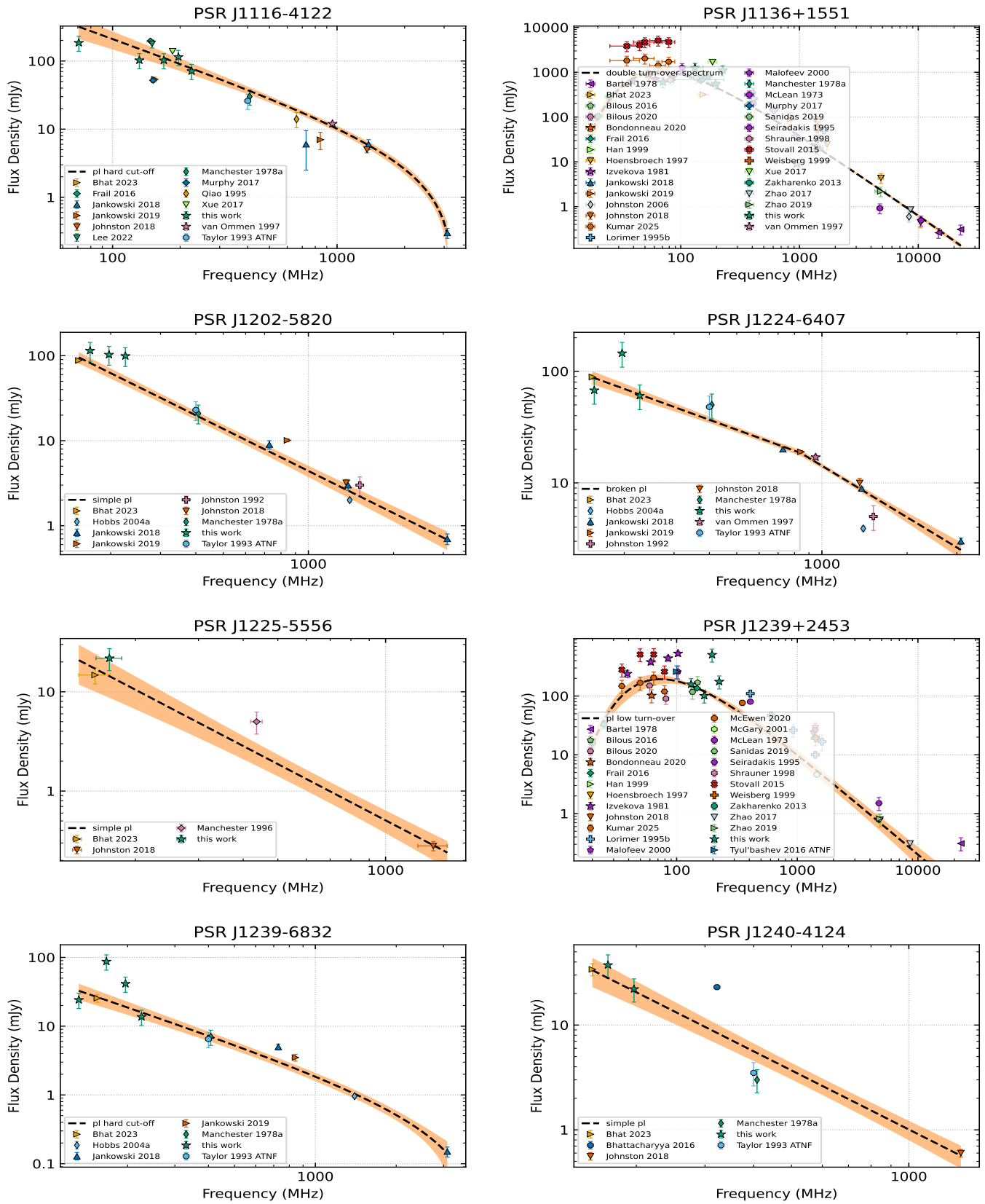


Figure F23. Fig F16 Continued

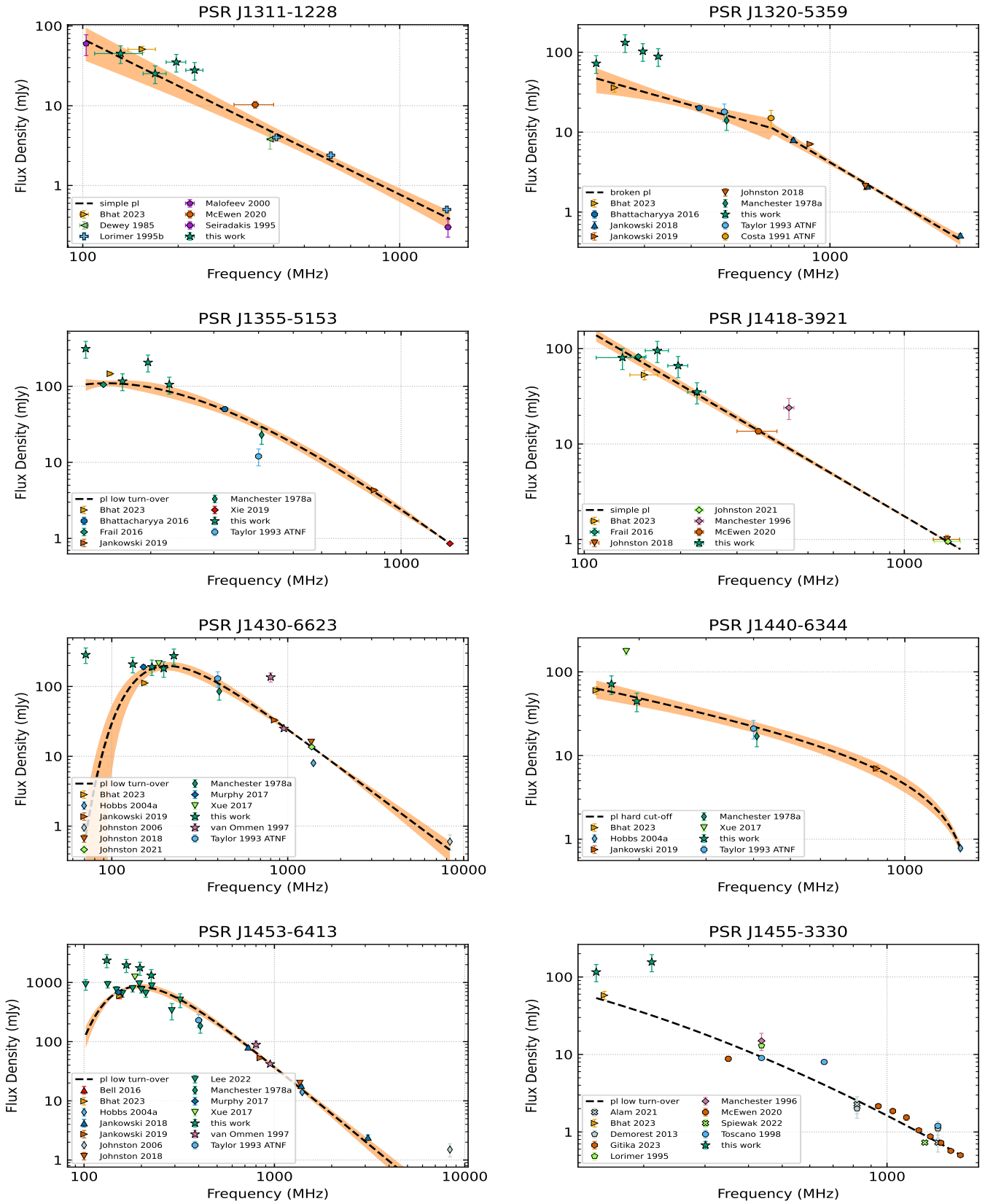


Figure F24. Fig F16 Continued

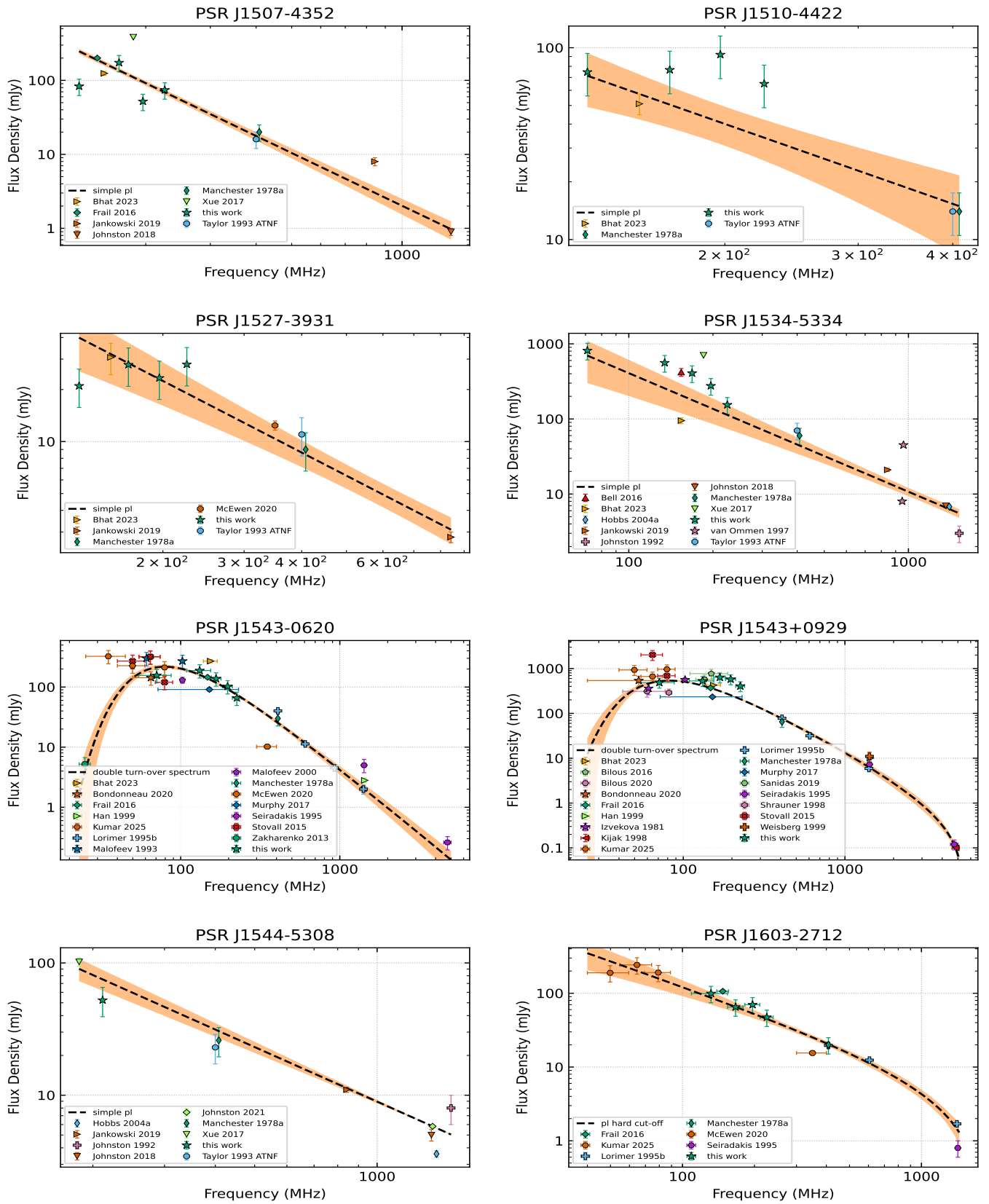


Figure F25. Fig F16 Continued

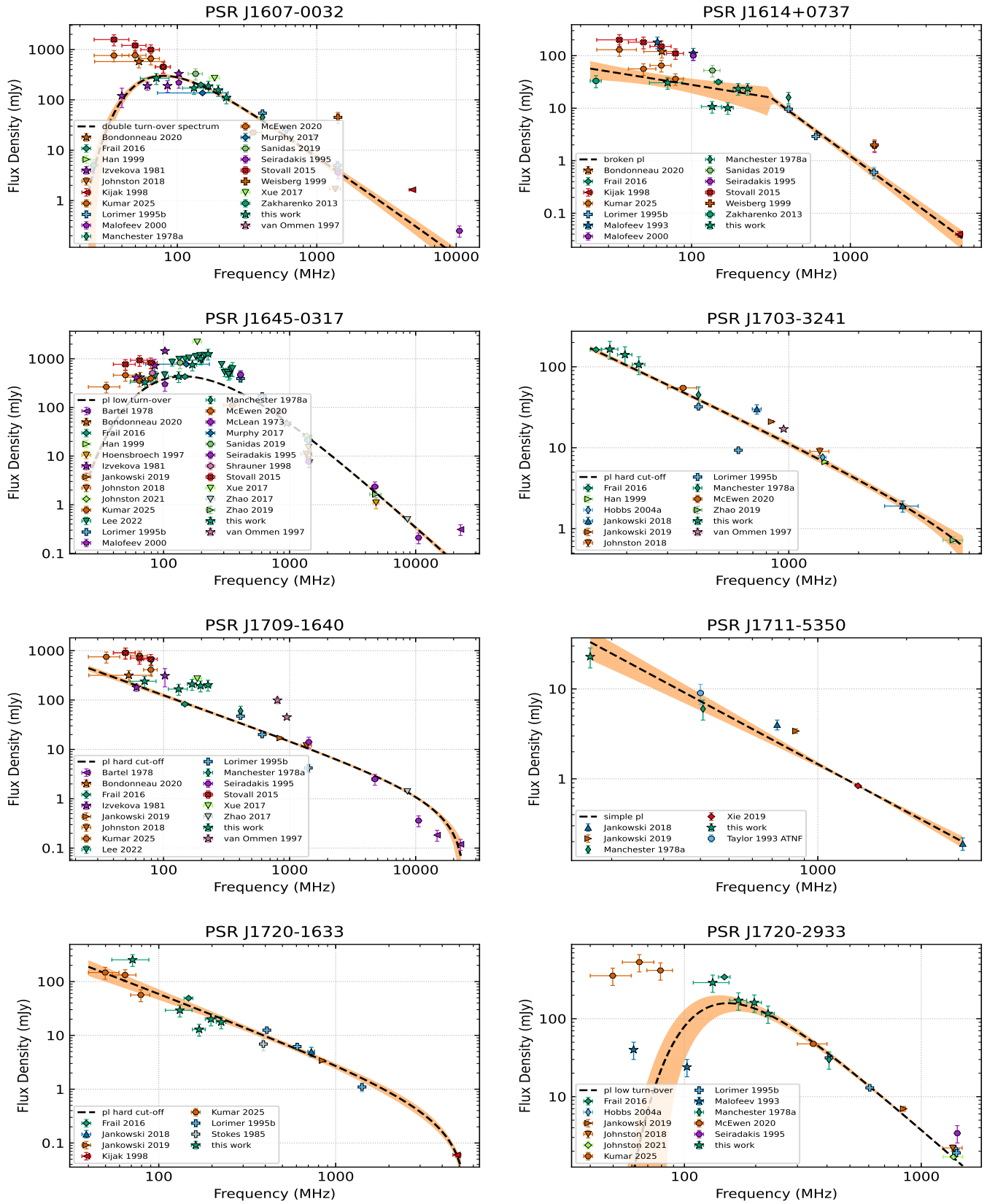


Figure F26. Fig F16 Continued

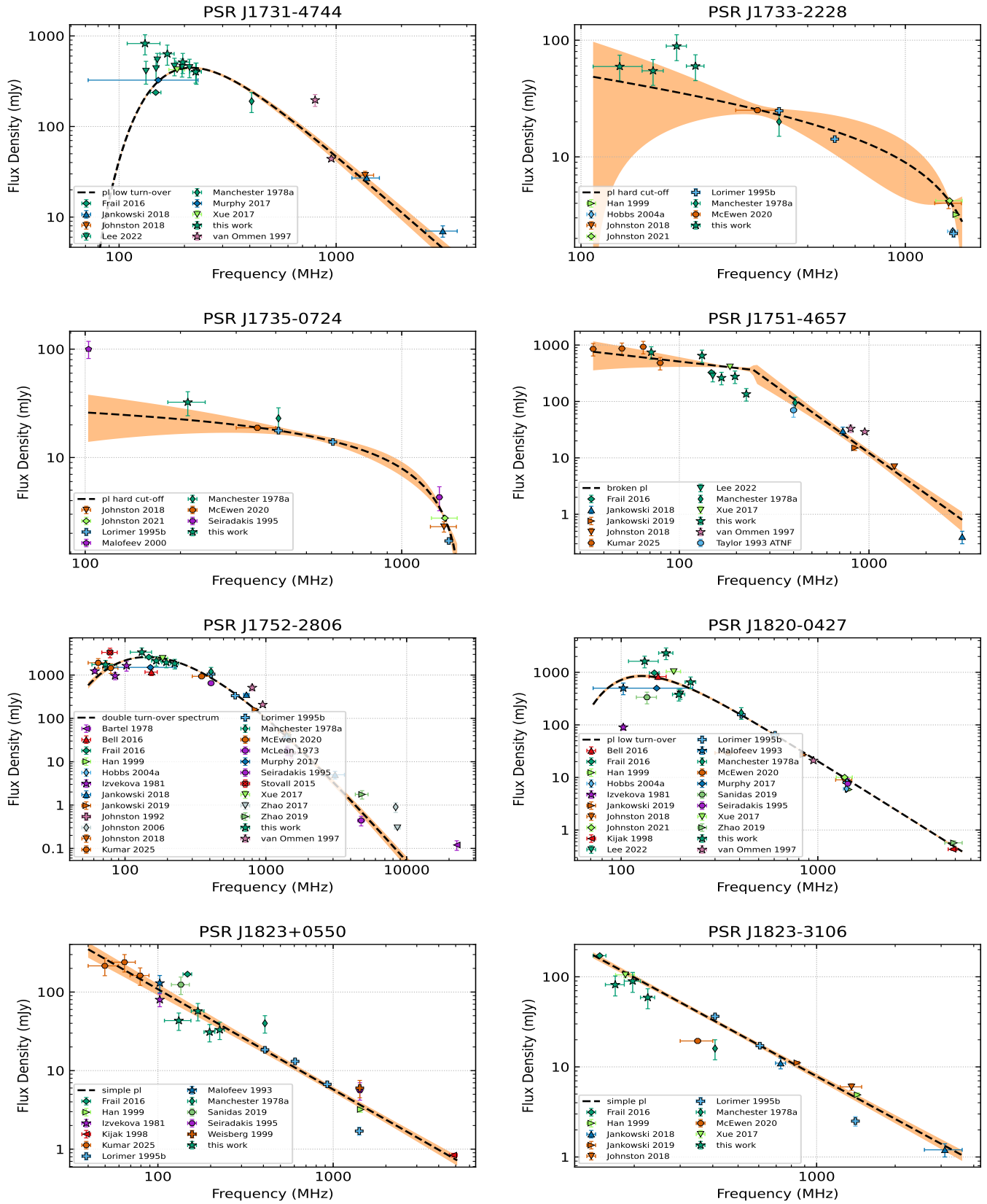


Figure F27. Fig F16 Continued

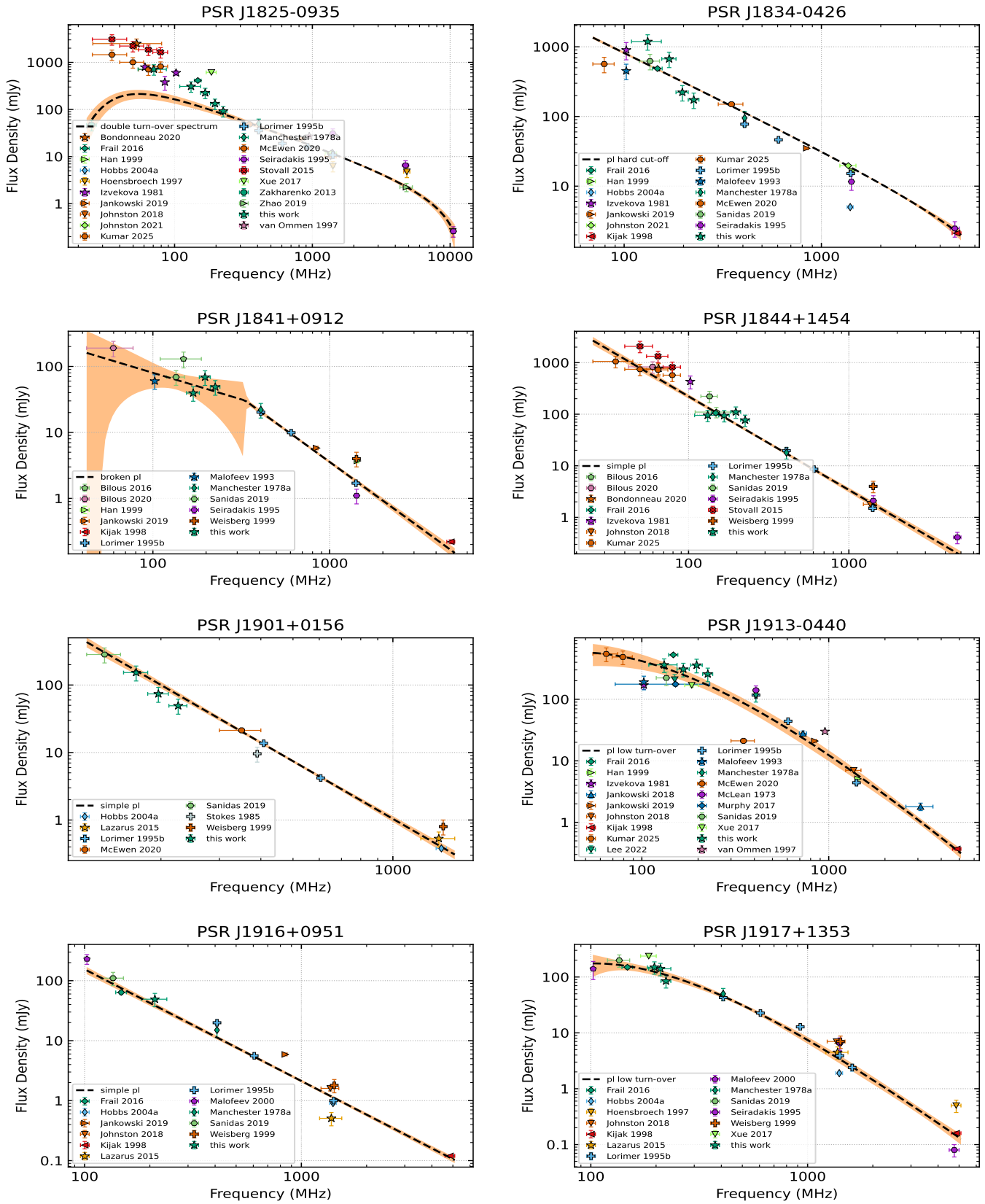


Figure F28. Fig F16 Continued

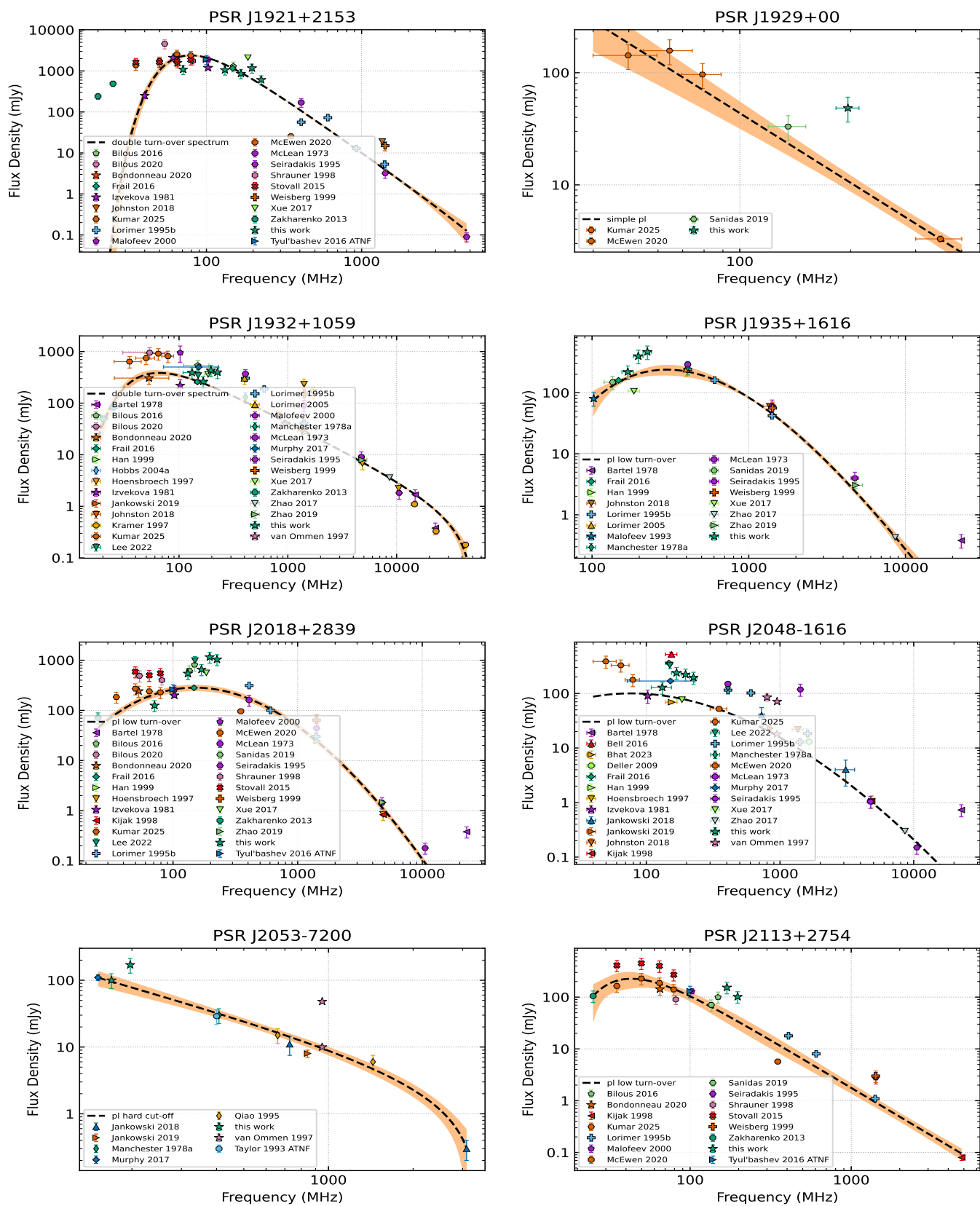


Figure F29. Fig F16 Continued

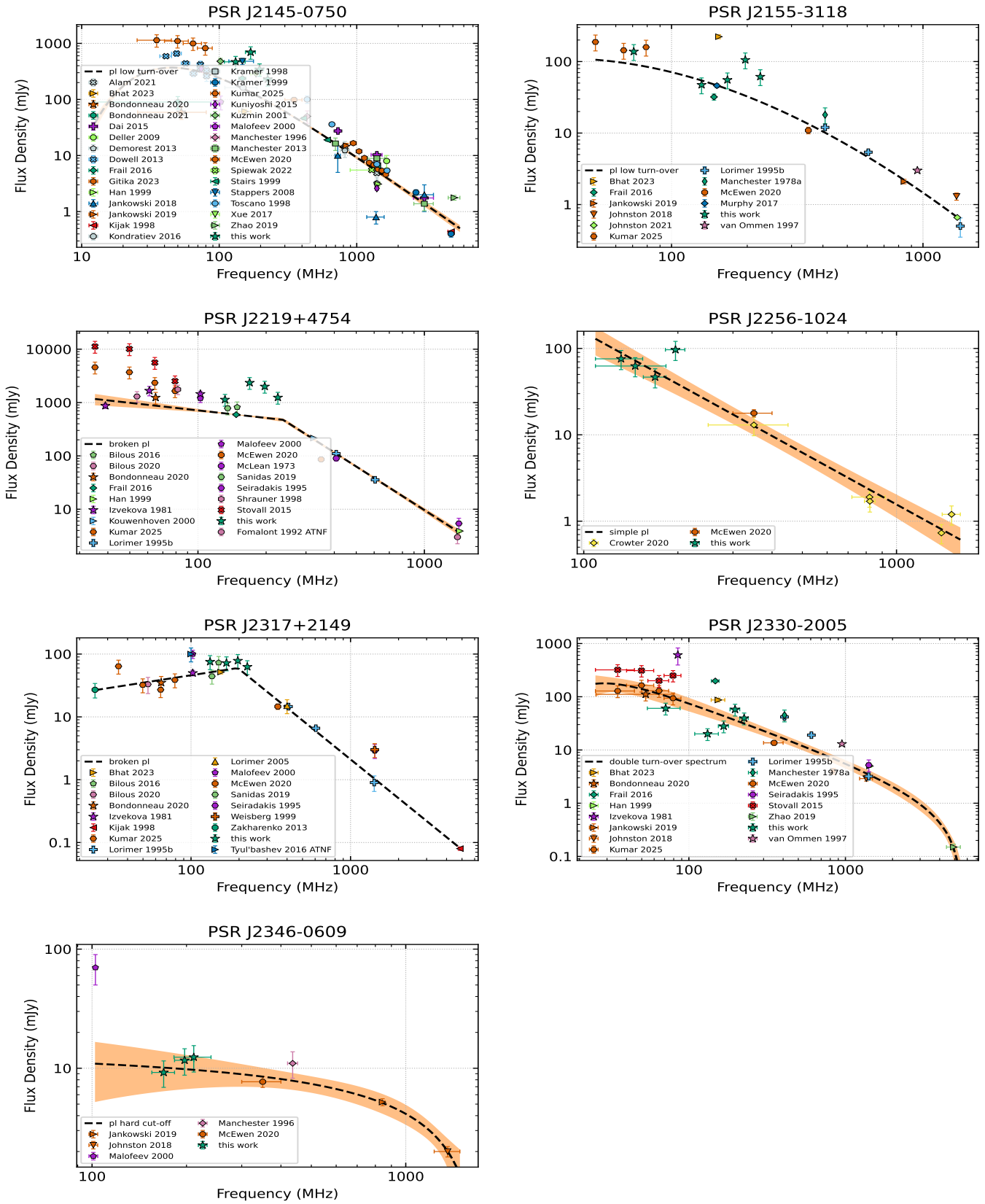


Figure F30. Fig F16 Continued

G. BEST POLARIMETRIC PROFILE OF 36 PULSARS

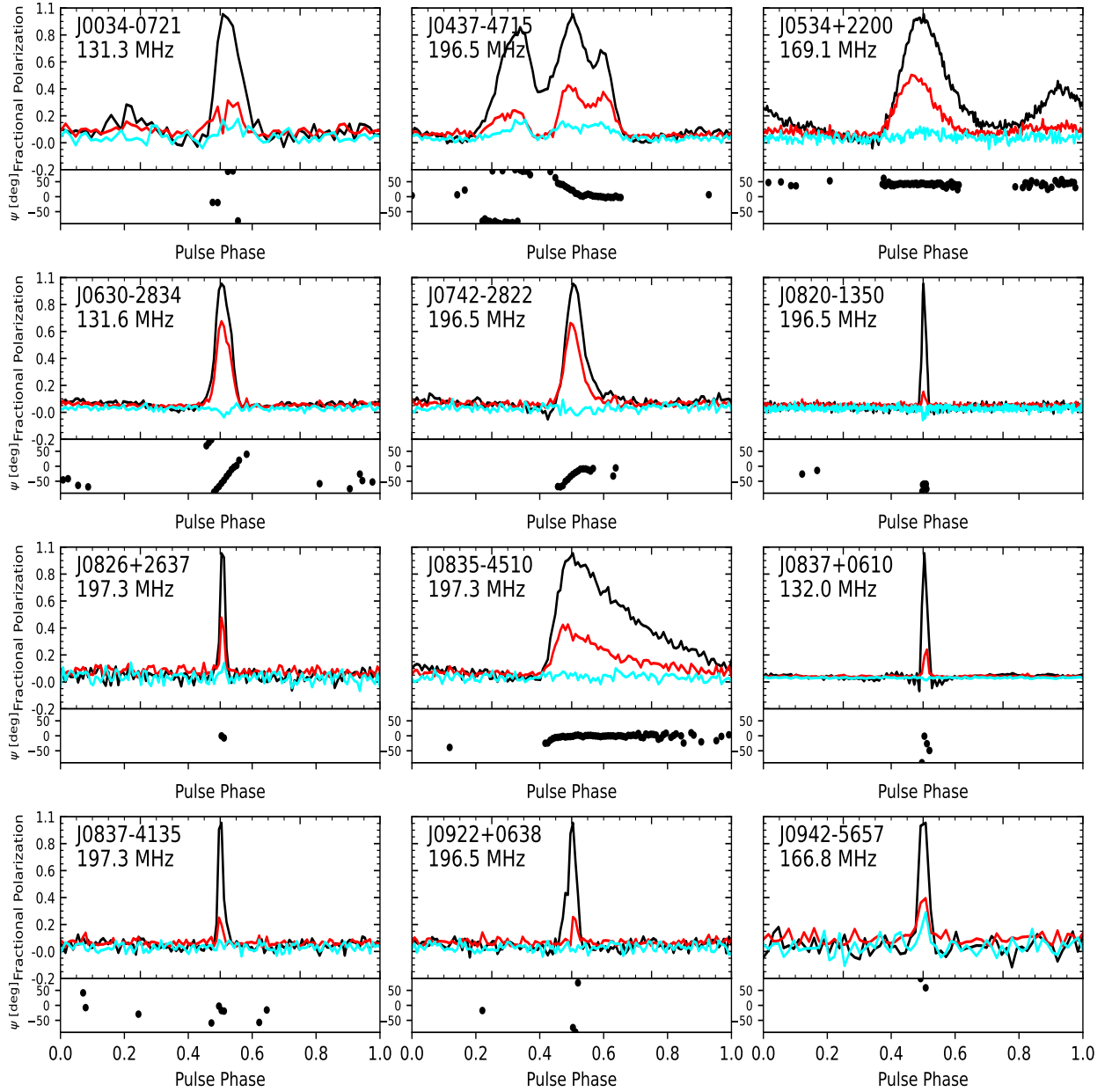


Figure G31. Full Stokes best polarimetric pulse profiles for pulsars with RM detection in Table D4. For each subplot, the top panel shows the fractional linear and circular polarization in red and cyan, respectively, and the total intensity in black. The bottom panel shows the position angle.

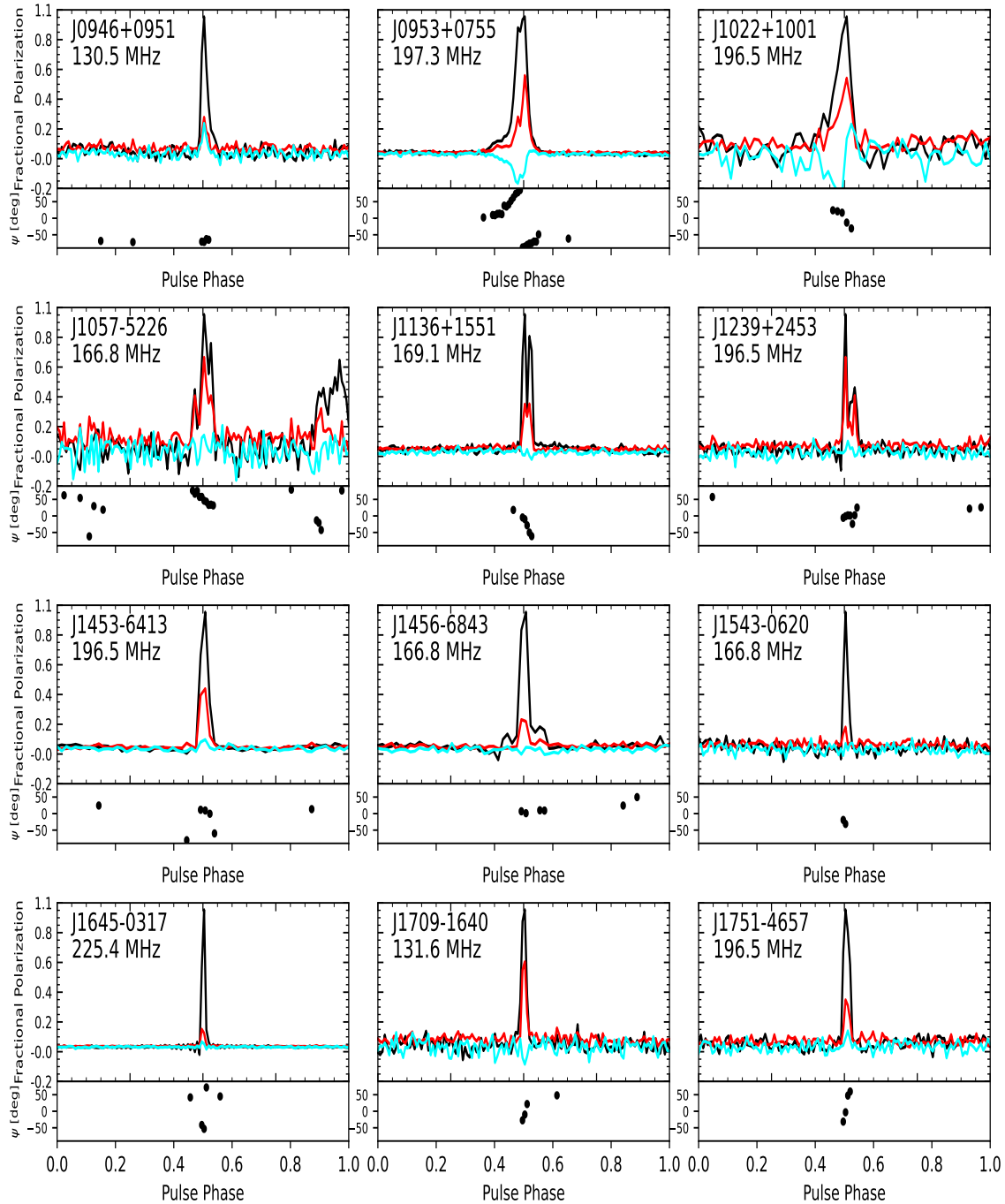


Figure G32. Fig G31 Continued

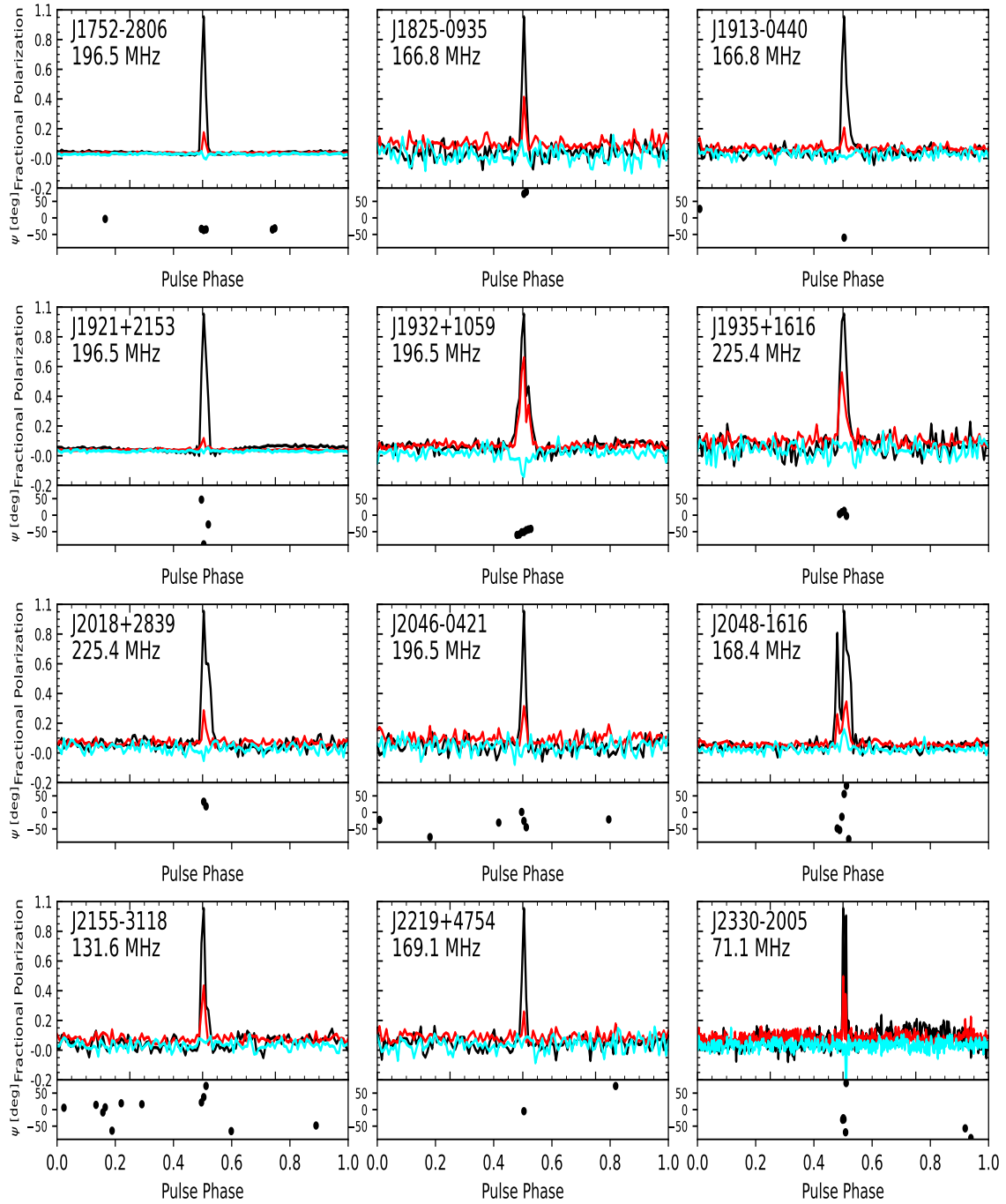


Figure G33. Fig G31 Continued

H. MULTI-FREQUENCY POLARIMETRIC PROFILES FOR 20 PULSARS

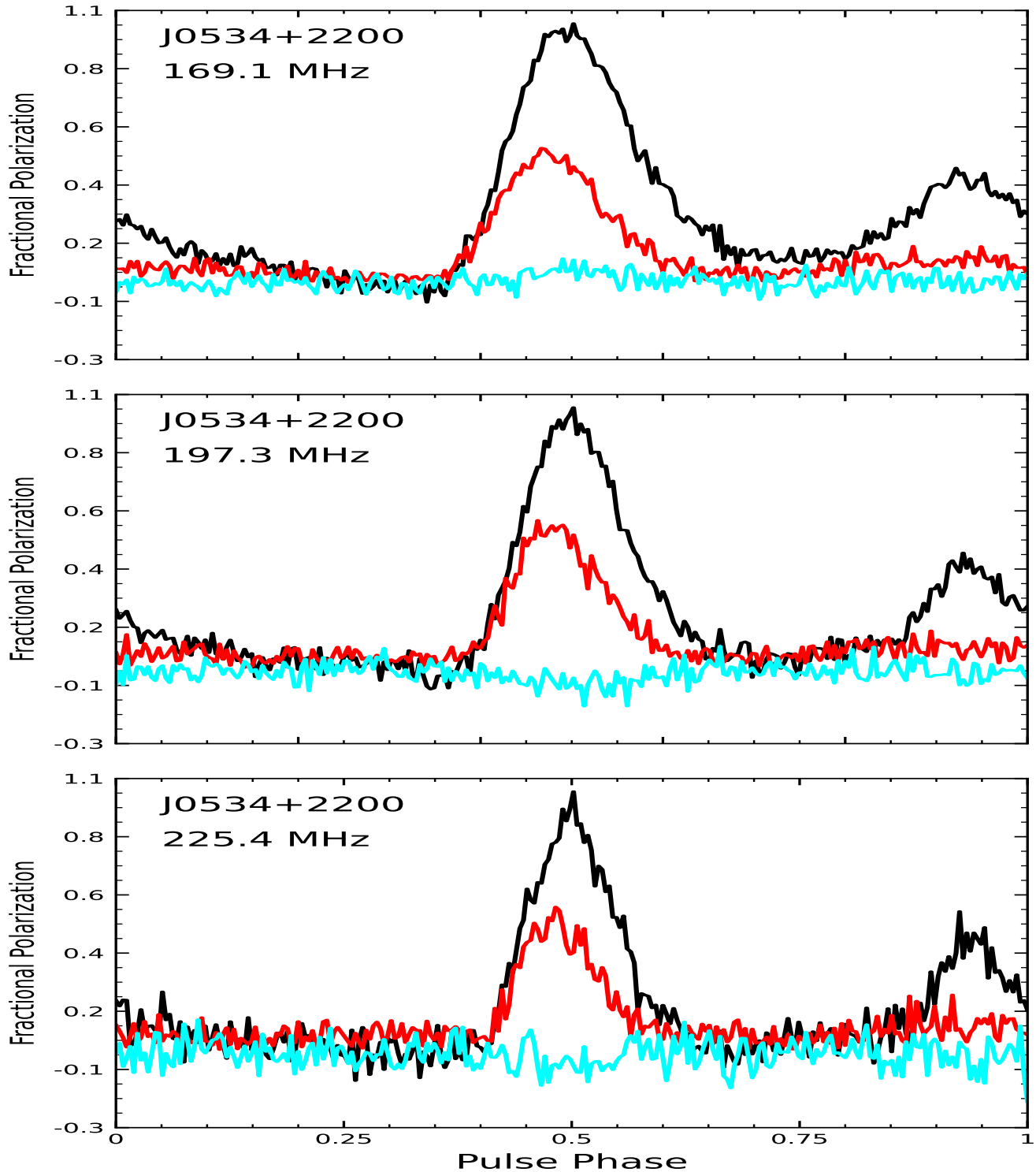


Figure H34. Multi-frequency polarization profiles for EDA2 pulsar, where black is the total intensity, and red and cyan show the fraction of linear and circular polarization.

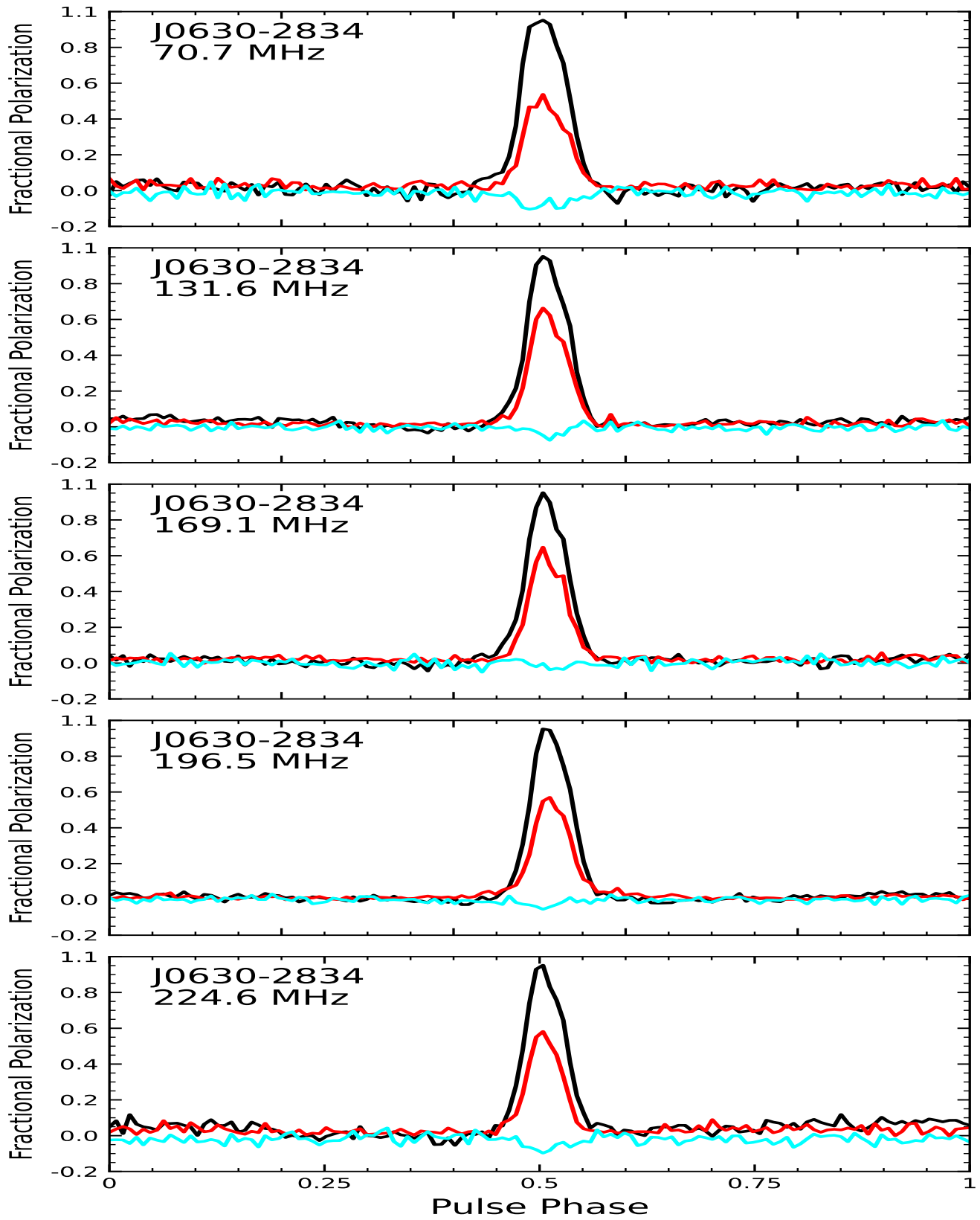


Figure H35. Fig H34 Continued

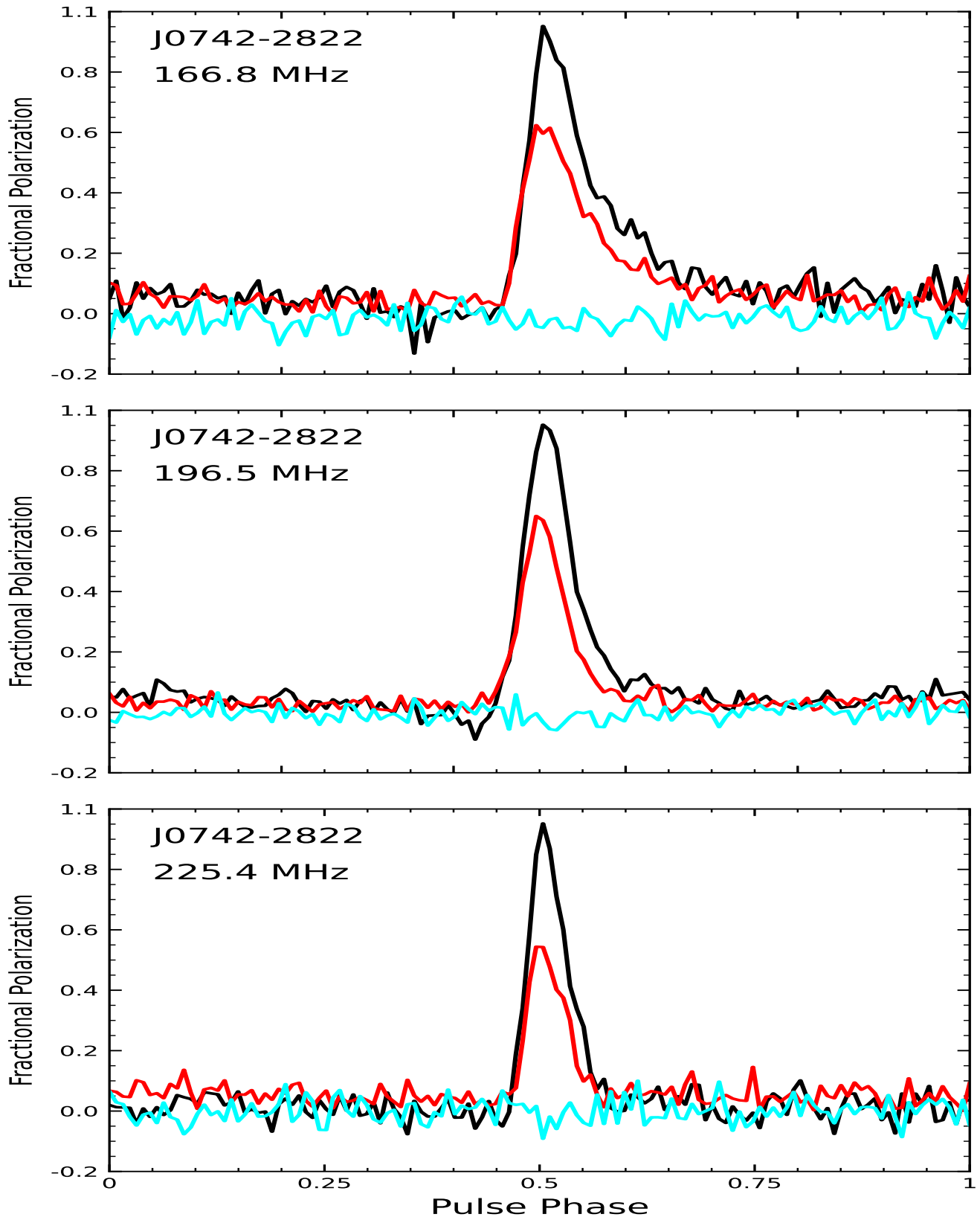


Figure H36. Fig H34 Continued

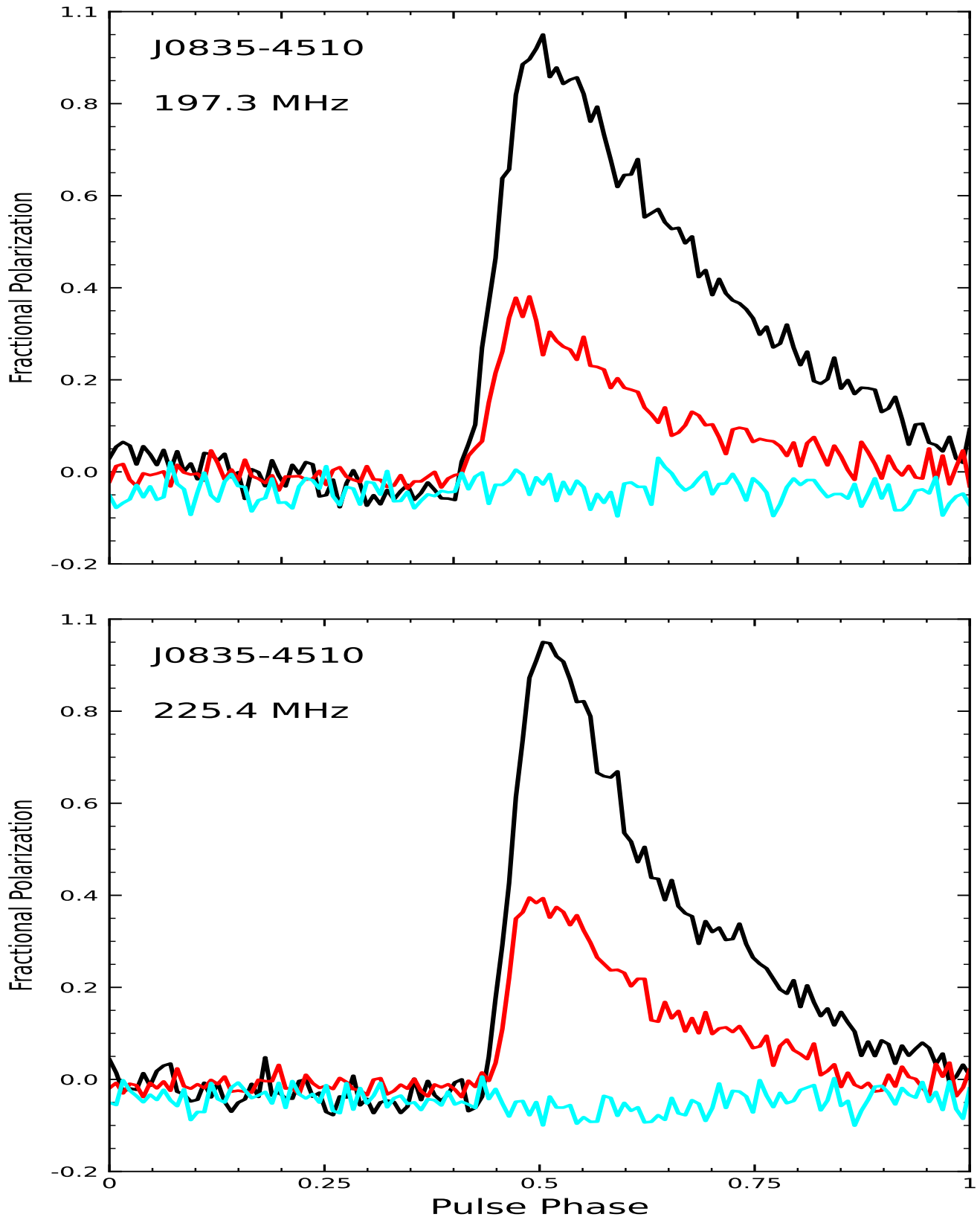


Figure H37. Fig H34 Continued

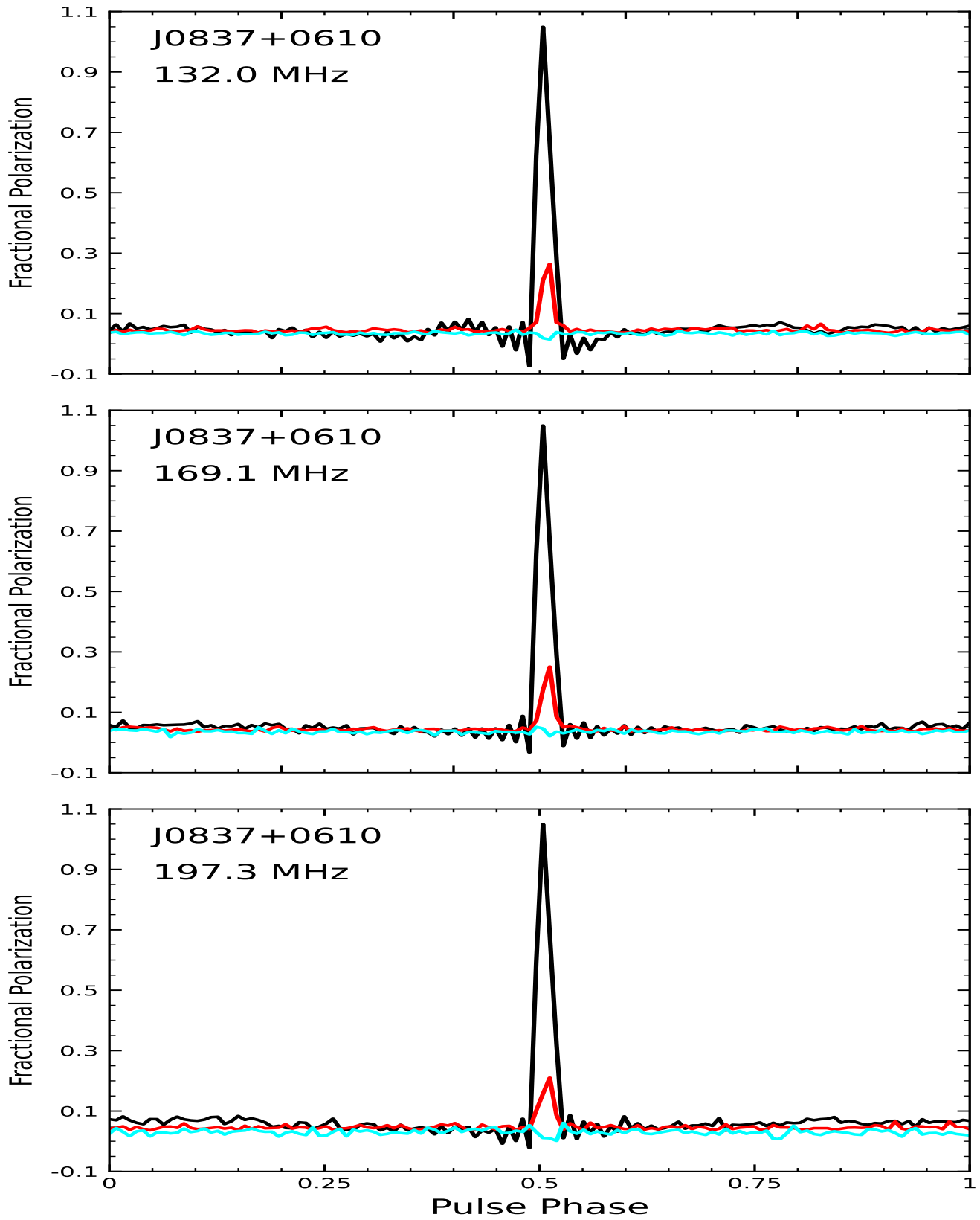


Figure H38. Fig H34 Continued

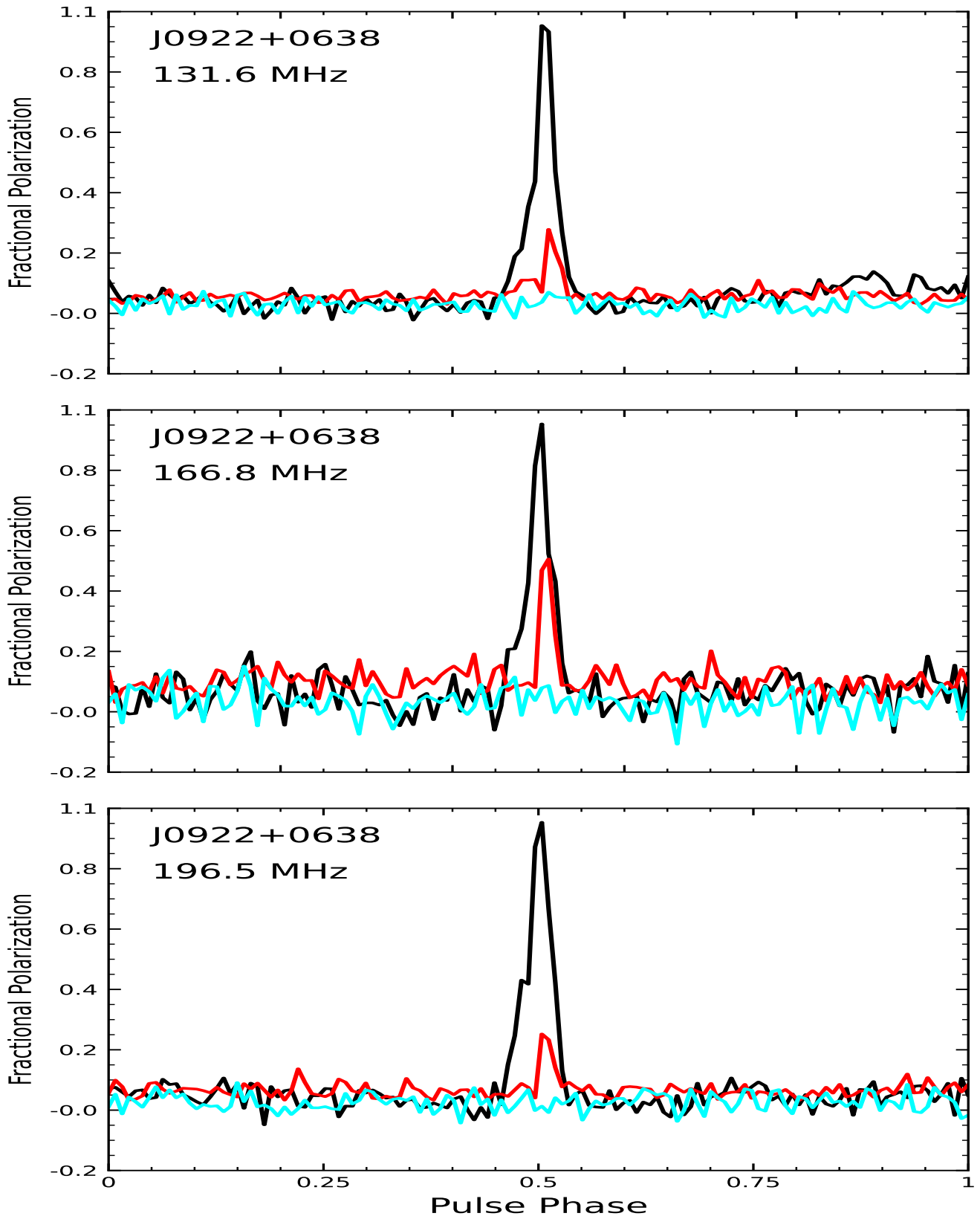


Figure H39. Fig H34 Continued

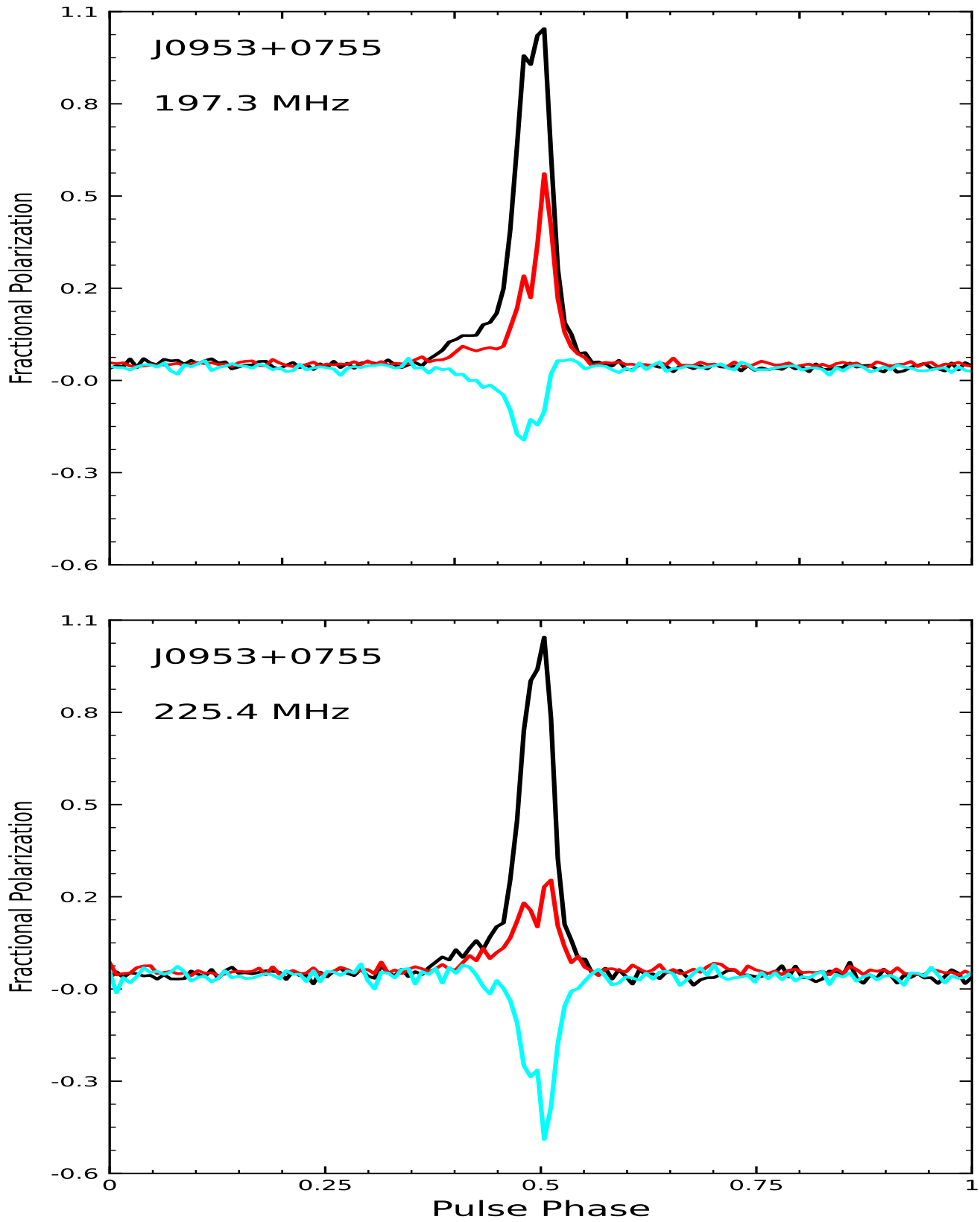


Figure H40. Fig H34 Continued

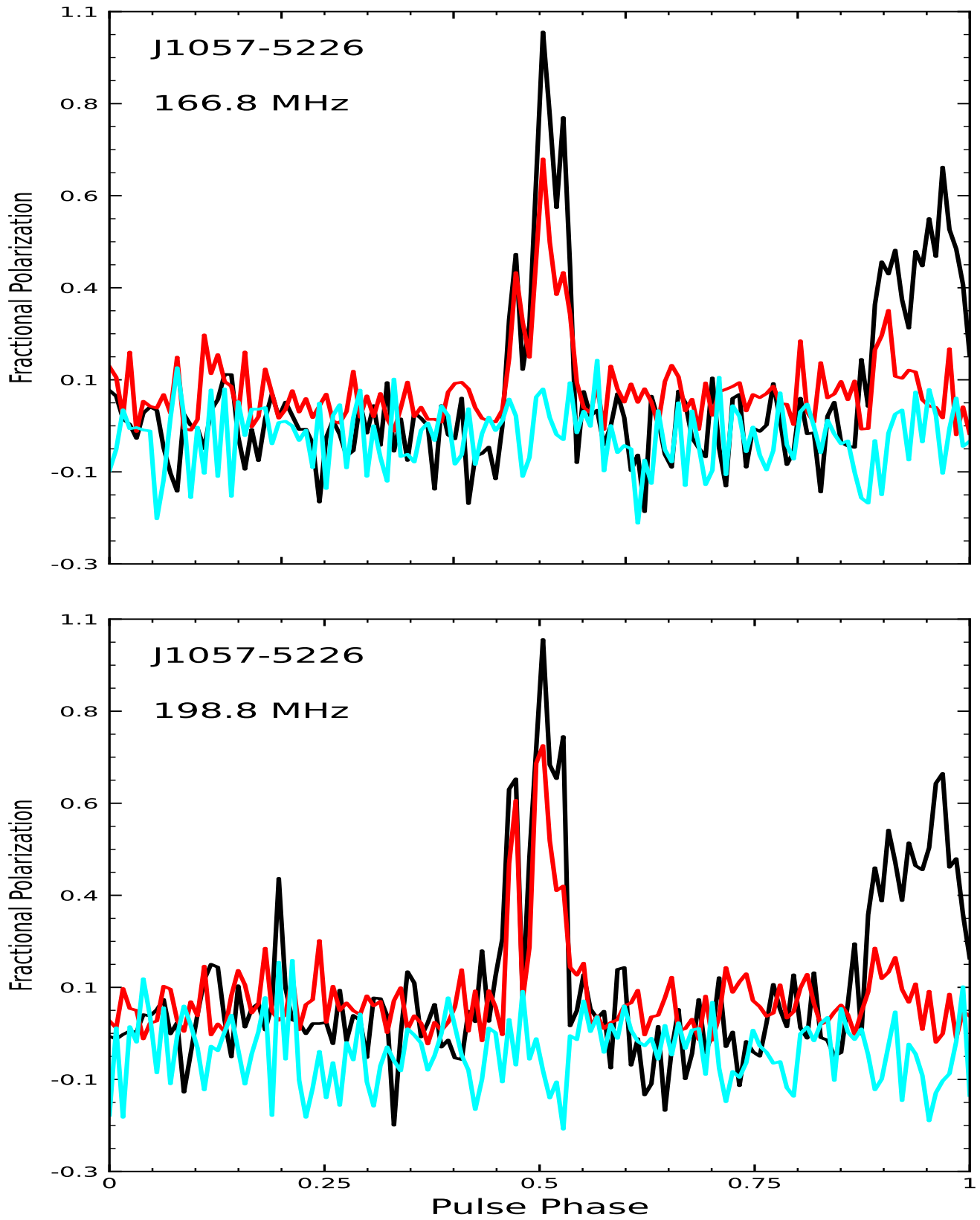


Figure H41. Fig H34 Continued

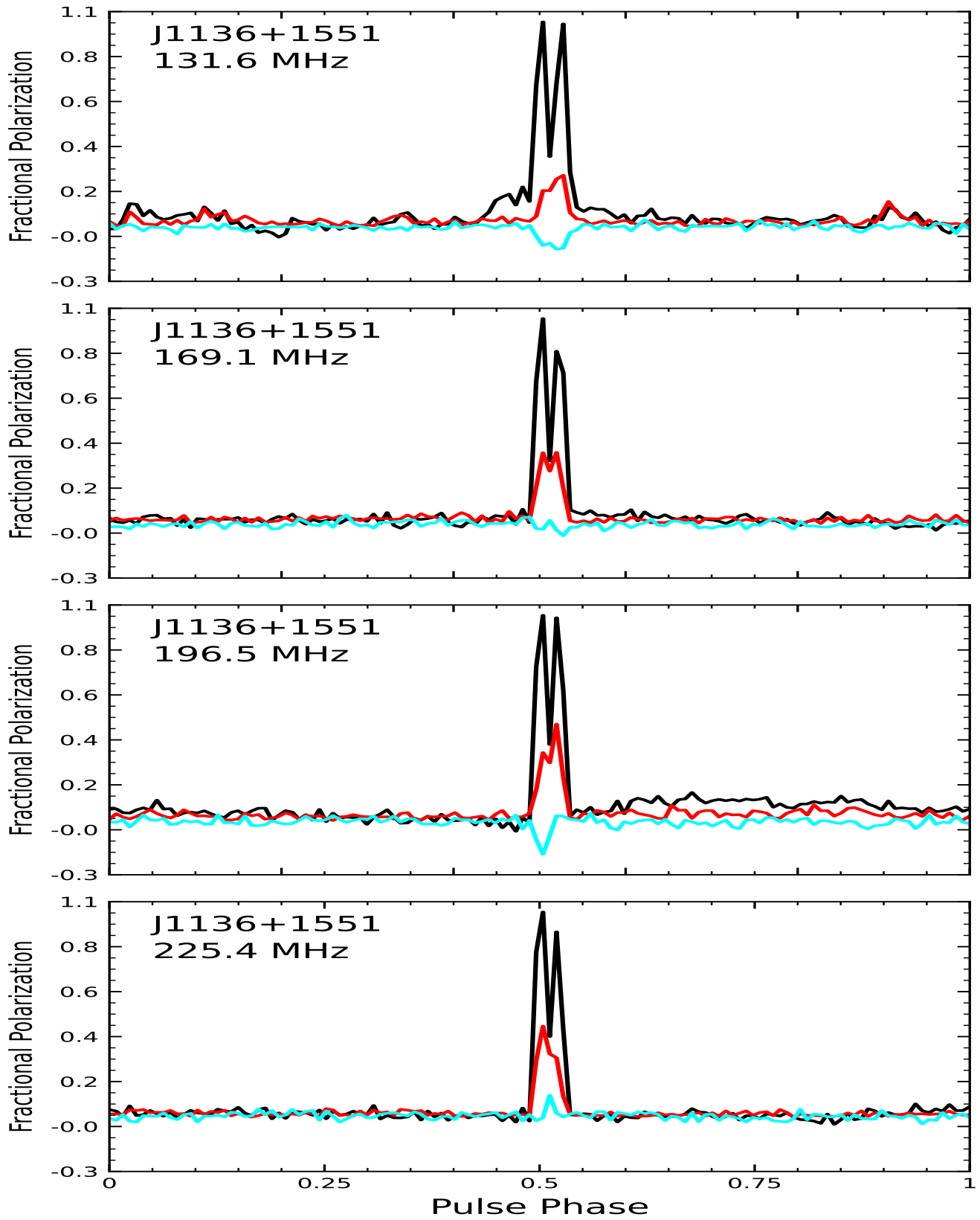


Figure H42. Fig H34 Continued

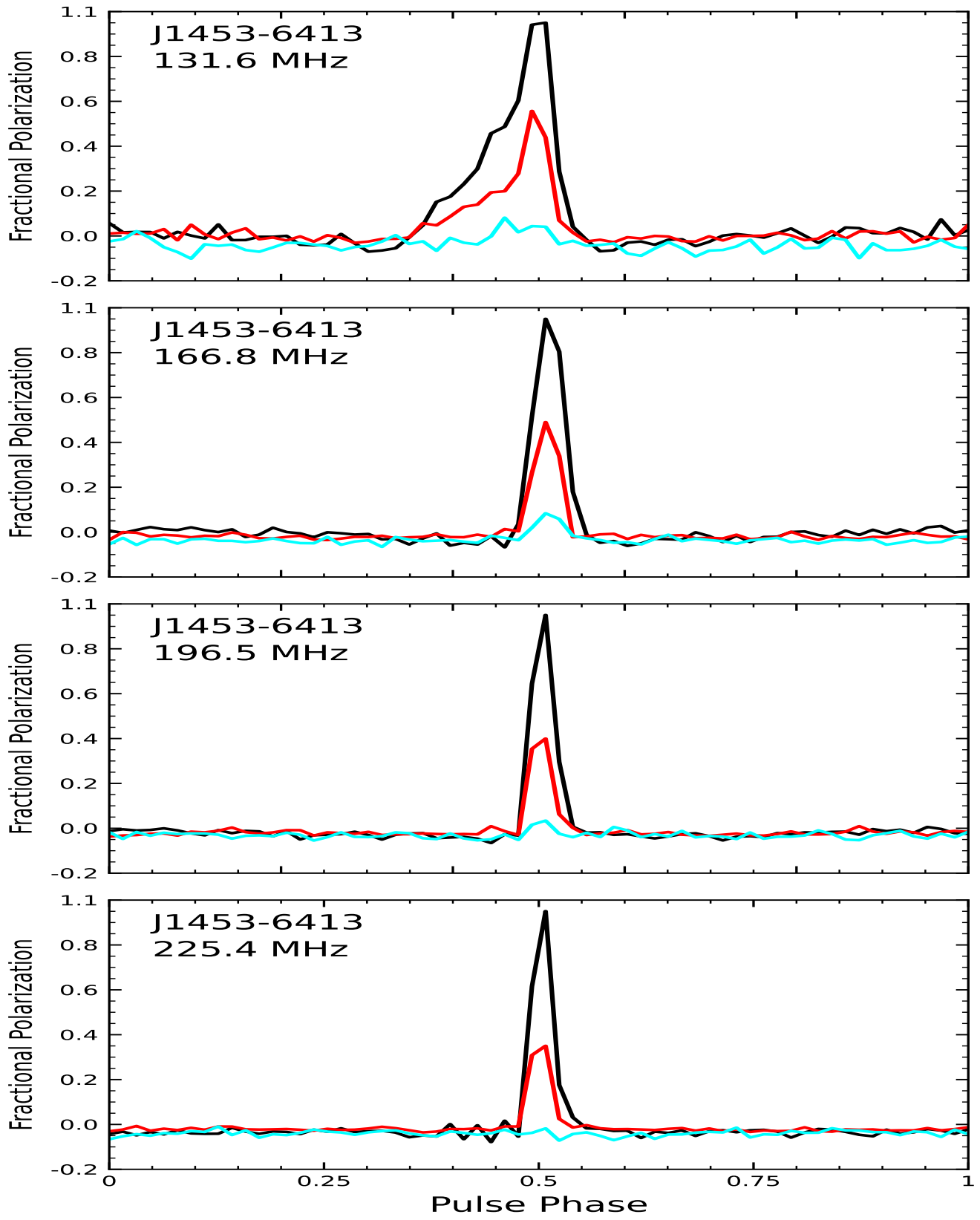


Figure H43. Fig H34 Continued

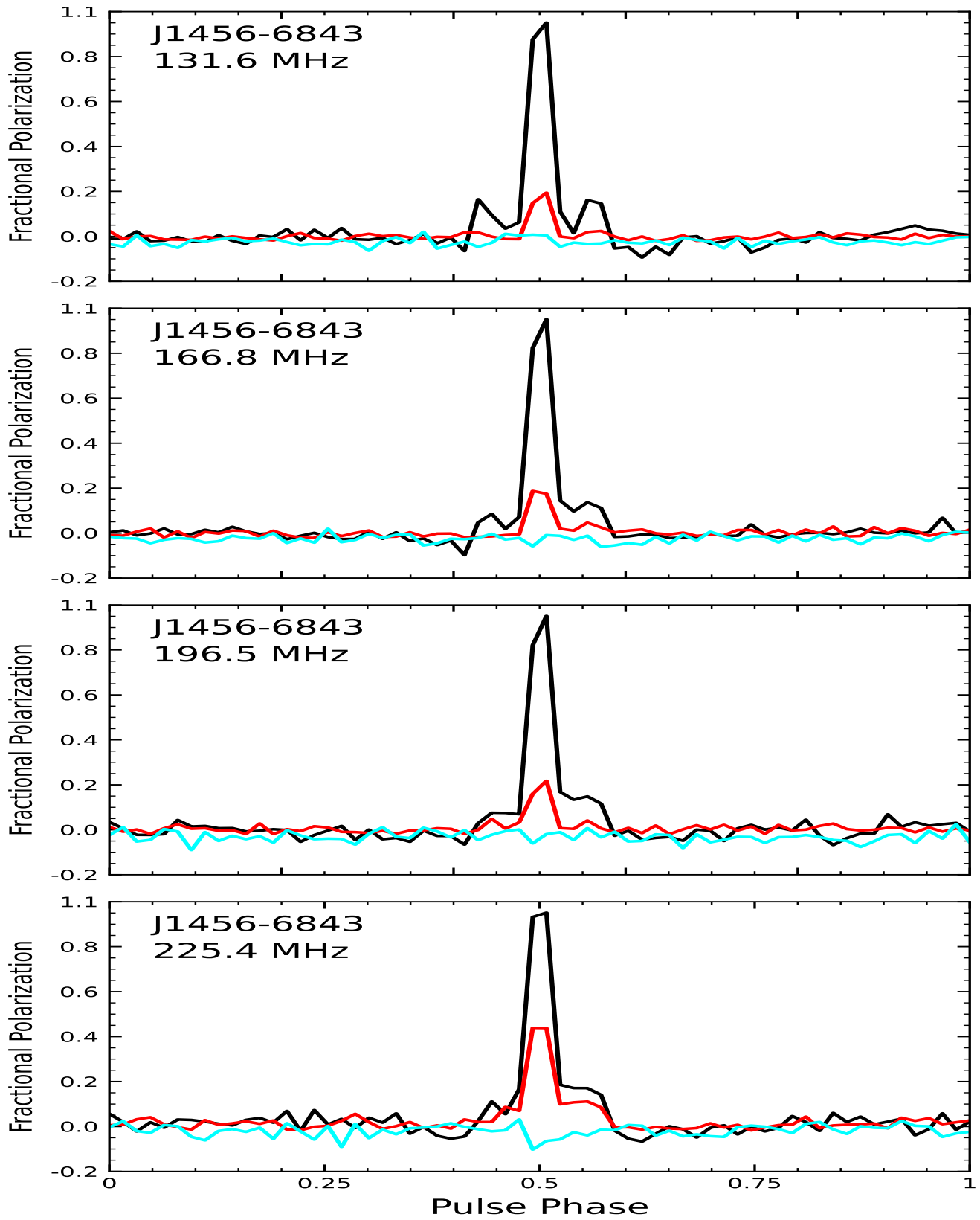


Figure H44. Fig H34 Continued

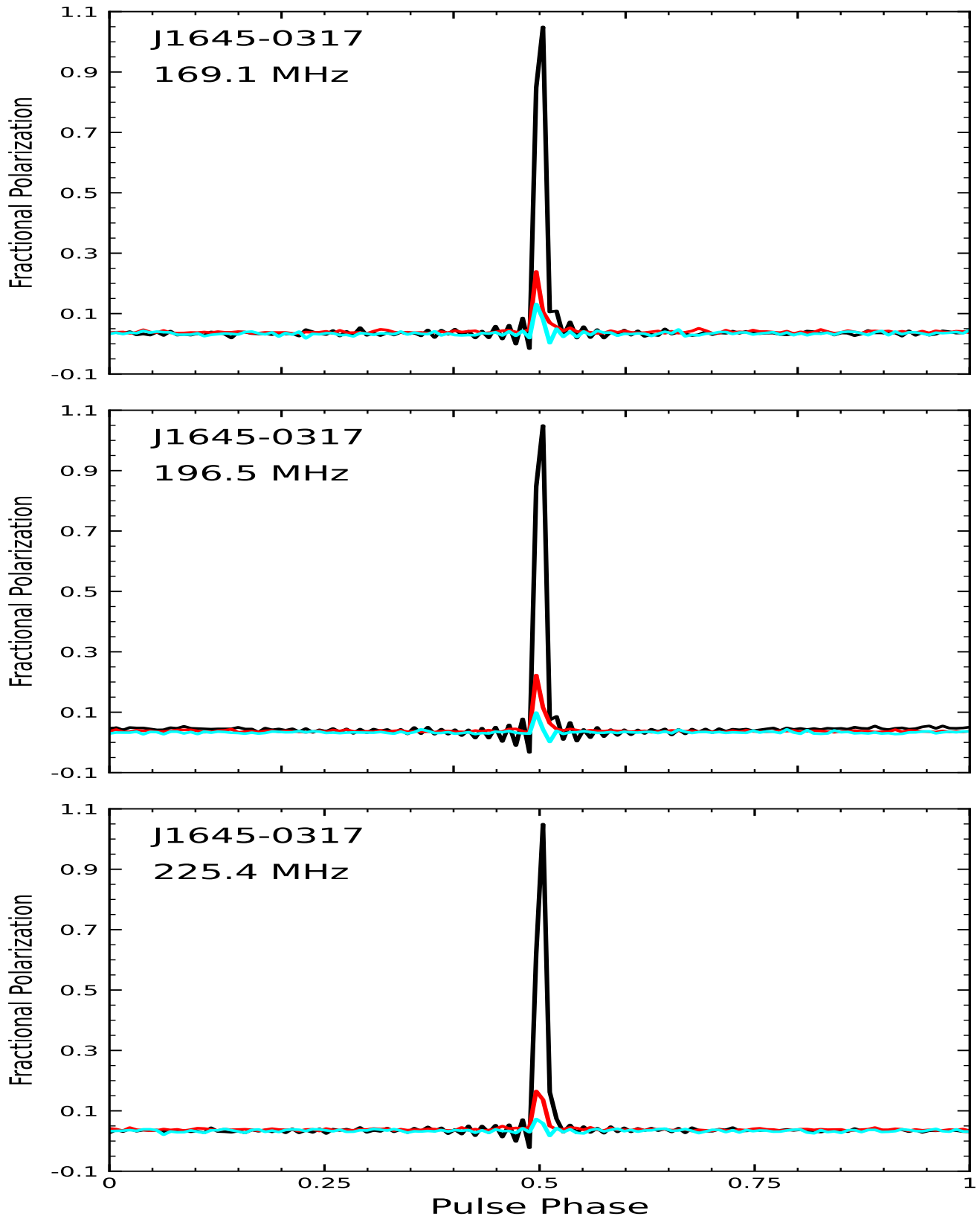


Figure H45. Fig H34 Continued

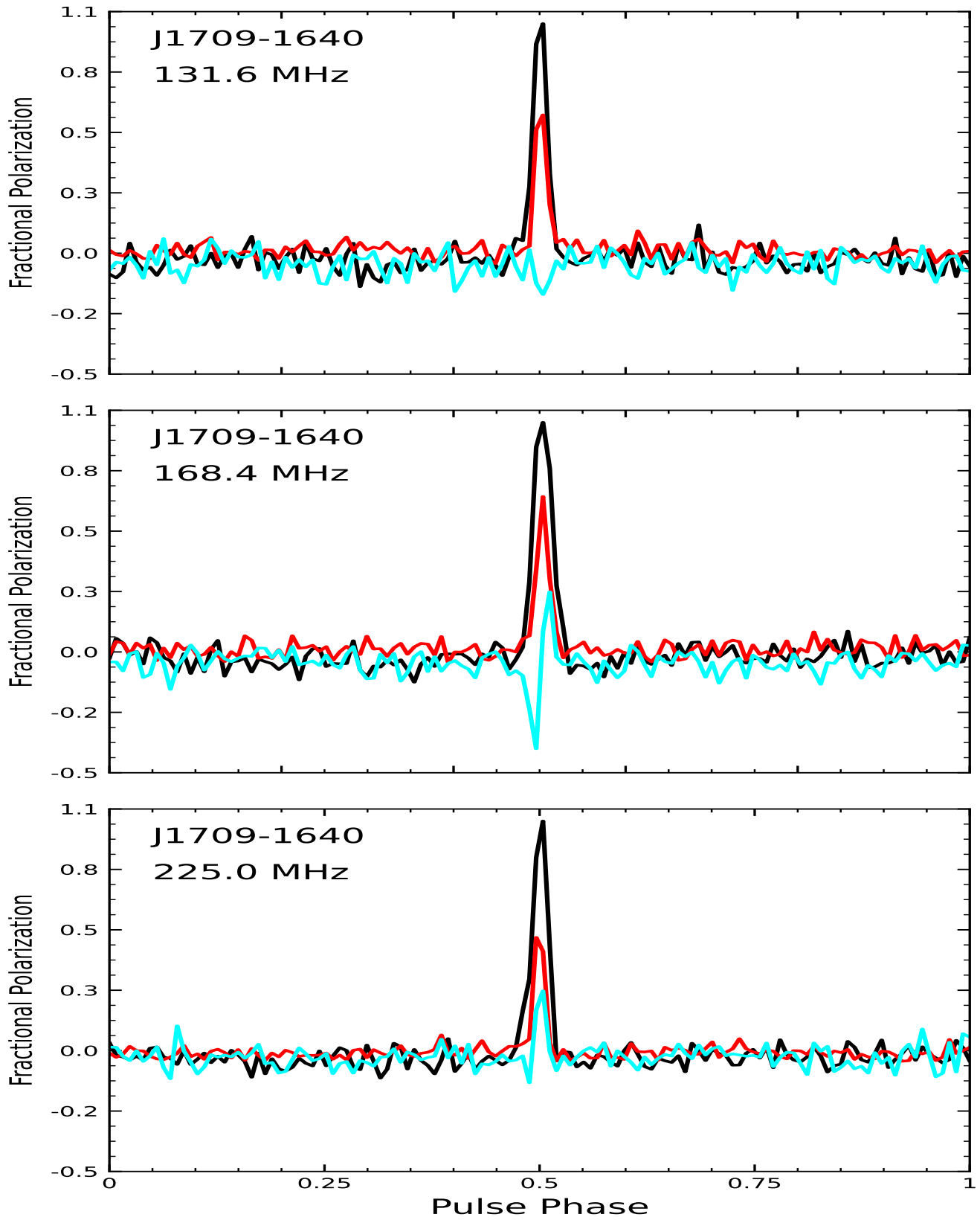


Figure H46. Fig H34 Continued

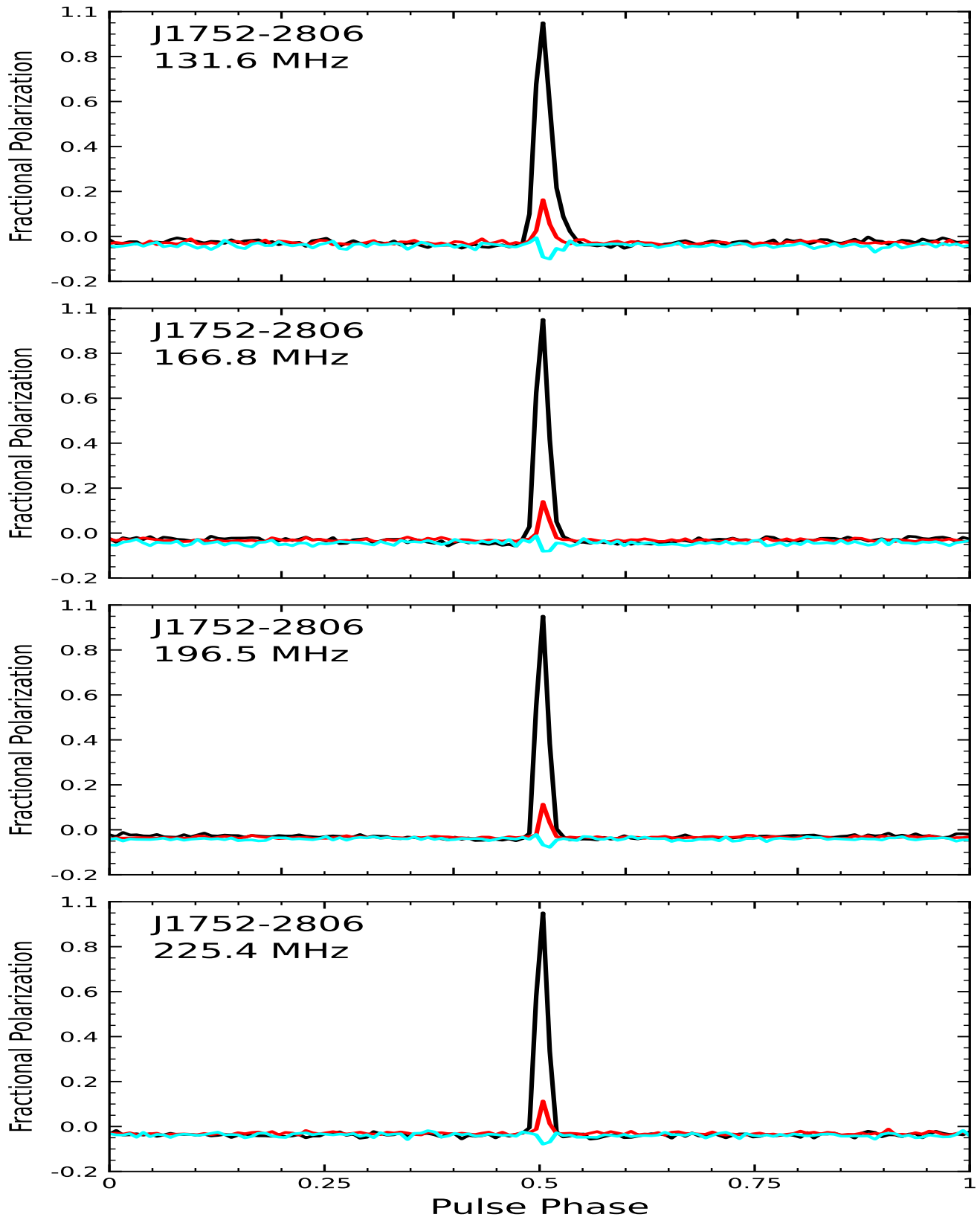


Figure H47. Fig H34 Continued

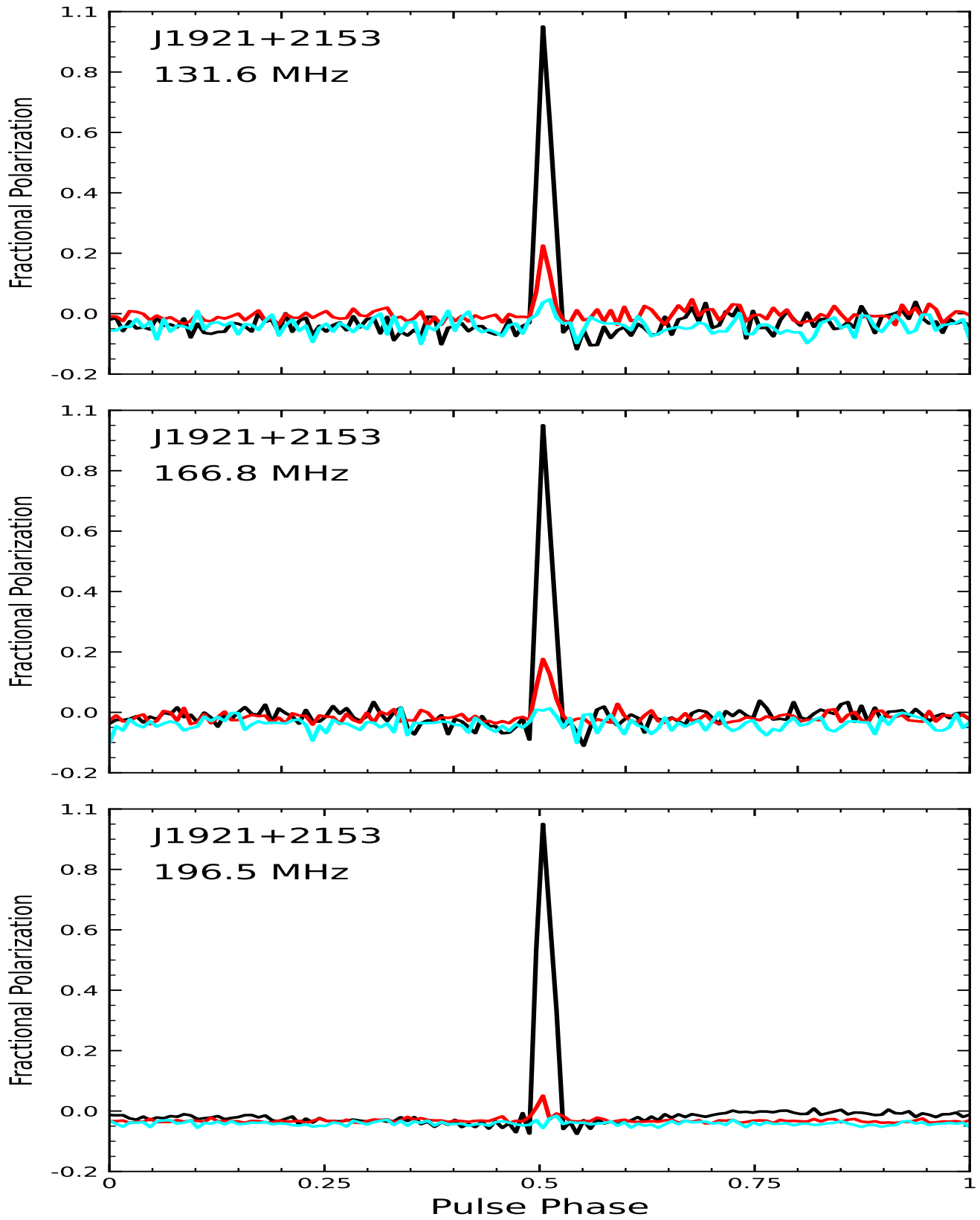


Figure H48. Fig H34 Continued

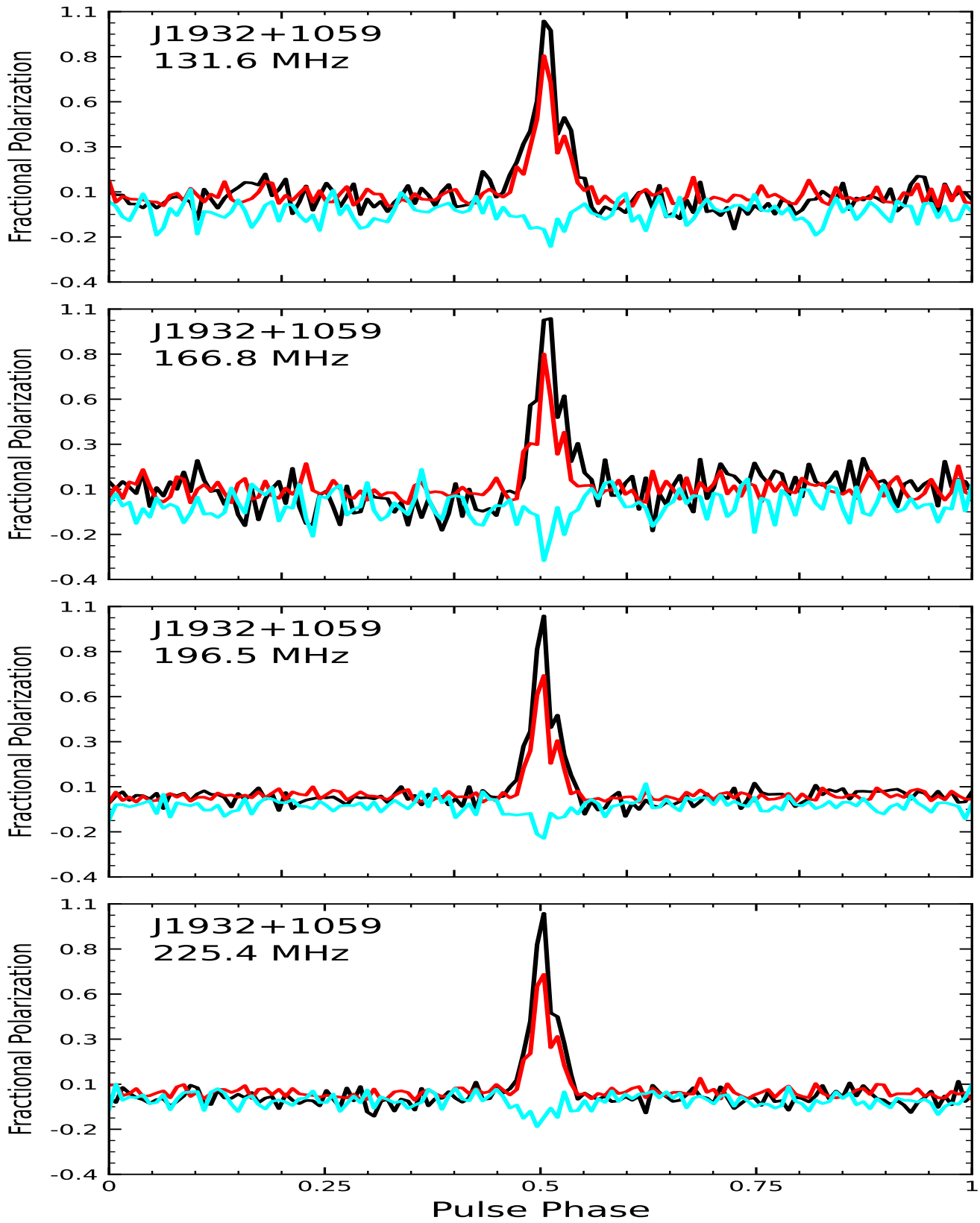


Figure H49. Fig H34 Continued

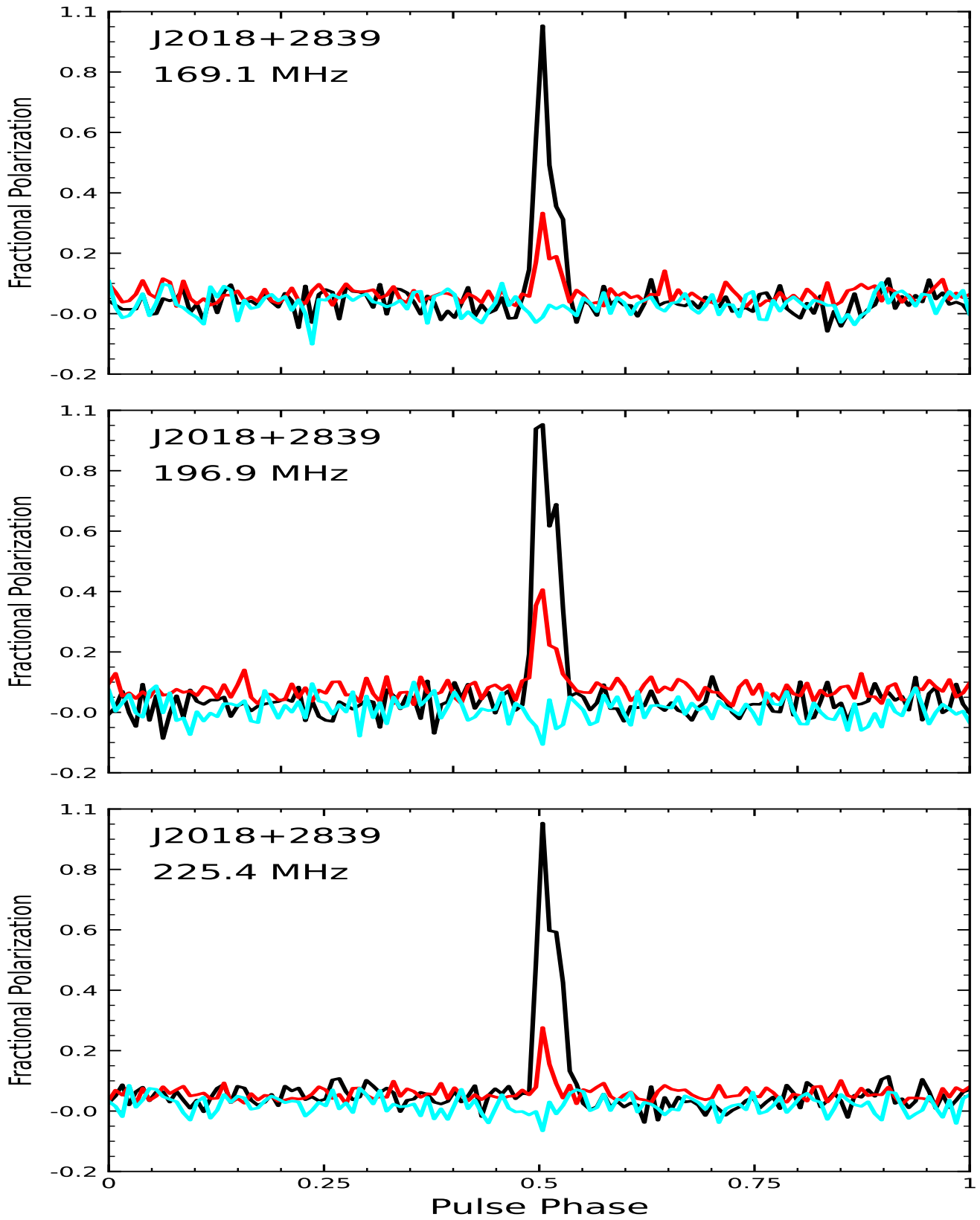


Figure H50. Fig H34 Continued

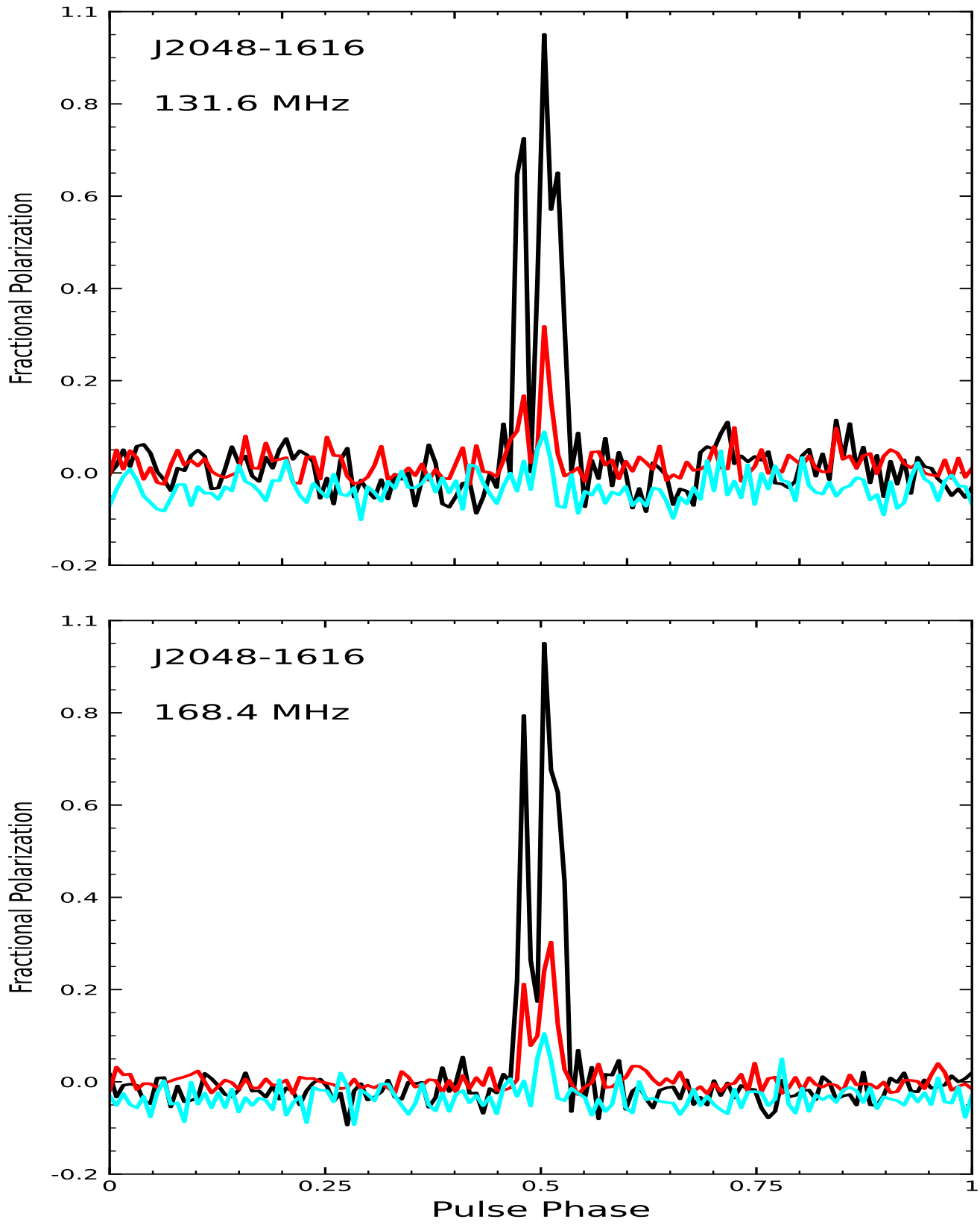


Figure H51. Fig H34 Continued

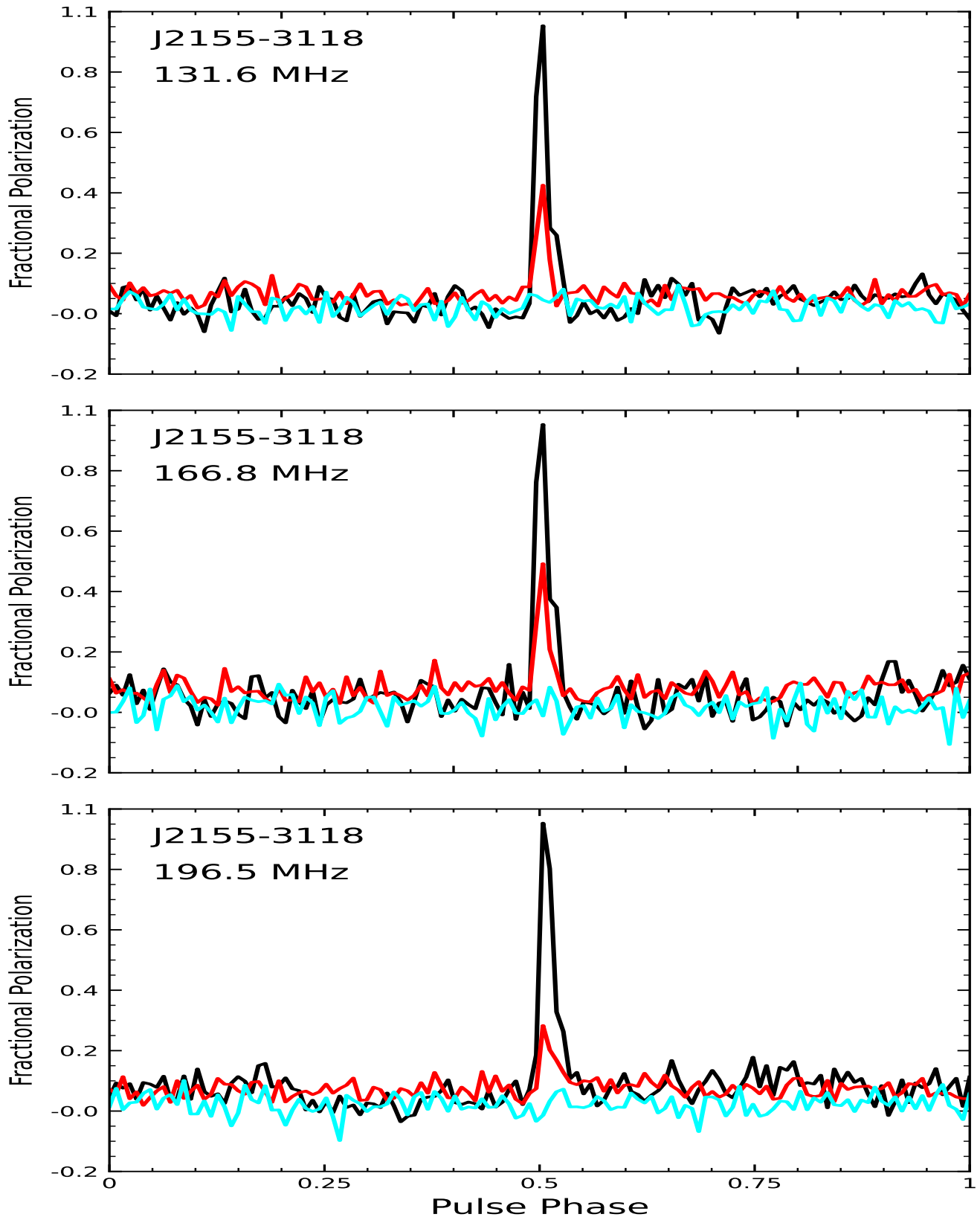


Figure H52. Fig H34 Continued

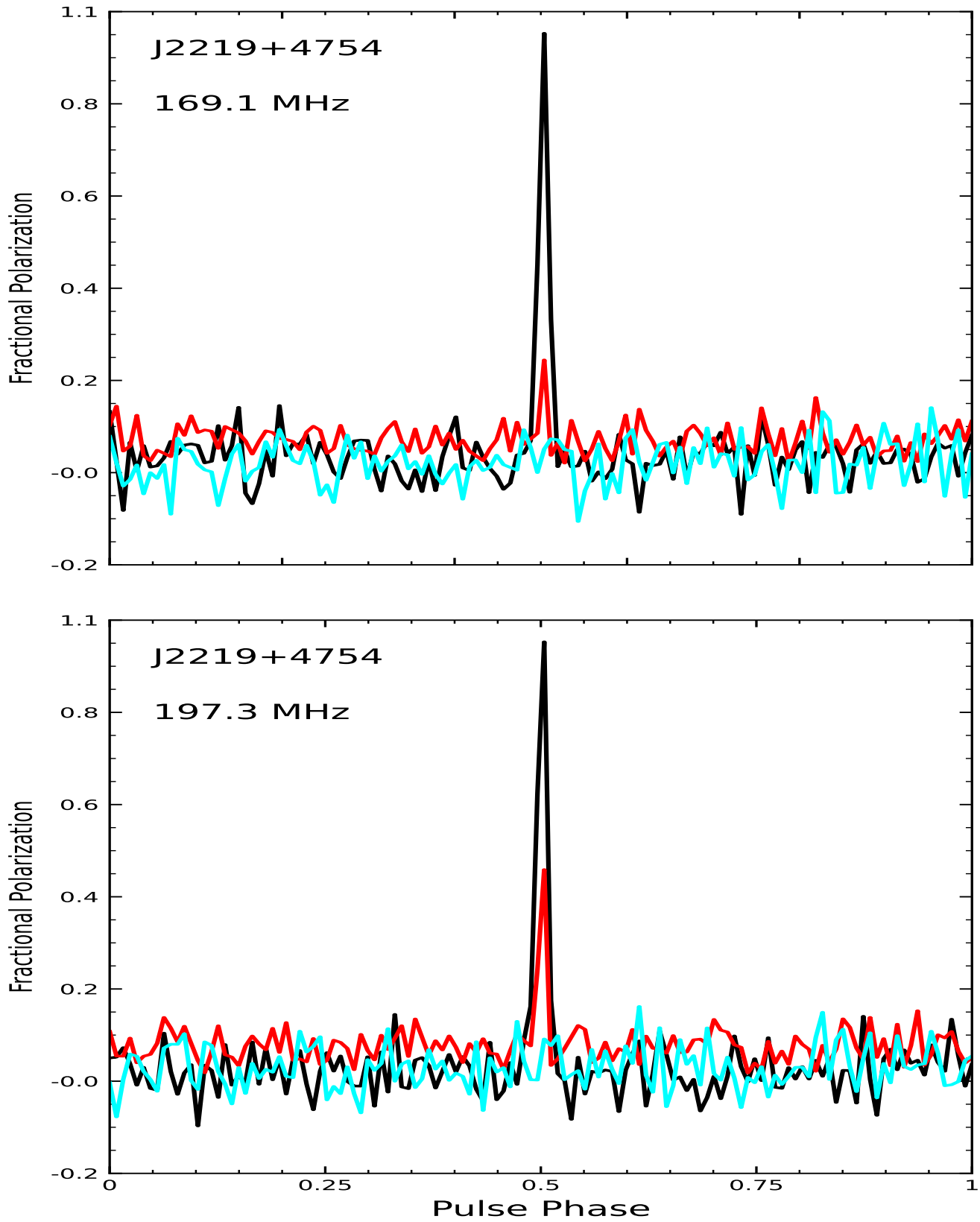


Figure H53. Fig H34 Continued